

**DESIGN AND DEVELOPMENT OF A ROBOTIC
PLATFORM FOR GENERAL NEUROSURGICAL
PROCEDURES**

AMIR HOSSEIN MEHBODNIYA

**FACULTY OF ENGINEERING
UNIVERSITY OF MALAYA
KUALA LUMPUR**

2020

**DESIGN AND DEVELOPMENT OF A ROBOTIC
PLATFORM FOR GENERAL NEUROSURGICAL
PROCEDURES**

AMIR HOSSEIN MEHBODNIYA

**THESIS SUBMITTED IN PARTIAL FULFILMENT OF
THE REQUIREMENTS FOR THE DEGREE OF DOCTOR
OF PHILOSOPHY**

**FACULTY OF ENGINEERING
UNIVERSITY OF MALAYA
KUALA LUMPUR**

2020

UNIVERSITY OF MALAYA
ORIGINAL LITERARY WORK DECLARATION

Name of Candidate: Amirhossein Mehbodniya

Matric No: KHA120075

Name of Degree: Doctor of Philosophy

Title of Project Paper/Research Report/Dissertation/Thesis (“this Work”):

DESIGN AND DEVELOPMENT OF A ROBOTIC PLATFORM FOR GENERAL
NEUROSURGICAL PROCEDURES

Field of Study:

Electrical Engineering

I do solemnly and sincerely declare that:

- (1) I am the sole author/writer of this Work;
- (2) This Work is original;
- (3) Any use of any work in which copyright exists was done by way of fair dealing and for permitted purposes and any excerpt or extract from, or reference to or reproduction of any copyright work has been disclosed expressly and sufficiently and the title of the Work and its authorship have been acknowledged in this Work;
- (4) I do not have any actual knowledge nor do I ought reasonably to know that the making of this work constitutes an infringement of any copyright work;
- (5) I hereby assign all and every rights in the copyright to this Work to the University of Malaya (“UM”), who henceforth shall be owner of the copyright in this Work and that any reproduction or use in any form or by any means whatsoever is prohibited without the written consent of UM having been first had and obtained;
- (6) I am fully aware that if in the course of making this Work I have infringed any copyright whether intentionally or otherwise, I may be subject to legal action or any other action as may be determined by UM.

Candidate’s Signature

Date:

Subscribed and solemnly declared before,

Witness’s Signature

Date:

Name:

Designation:

DESIGN AND DEVELOPMENT OF A ROBOTIC PLATFORM FOR GENERAL NEUROSURGICAL PROCEDURES

ABSTRACT

For the first time in 1985, robots were introduced to the neurosurgical operating rooms. Since then this field of robotics have advanced with new technologies with better accuracy and safety. However, developing robots for neurosurgery is a challenging task due to the sensitive nature of these applications and additionally their high cost of development. A typical neurosurgical robot costs millions of dollars in 2018, even though the costs of components and calculations have been lowered tremendously. This is mainly due to focus of current neurosurgical robots on few highly precise and specific surgical tasks which makes their use limited. In this thesis, development of a neurosurgical robot with a focus on more general surgical tasks related to surgical navigation is investigated, and its design and development are reported. Using this platform to develop more general surgical applications brings down the cost. Furthermore, this system has been developed using open source platforms that continually updates new features and technologies, helping this platform to stay up to date with current science of the day. To have a unified approach, three key phases had to be included. The first was the data collection and analysis, which involved collecting actual surgical data from live surgeries to analyze the workspace of the targeted surgical tasks which helped in structural design of the robot. The second was the design and development of the actual robot based on the initial analysis of the surgeries. In this work, the robot was designed to be small and dexterously suited to neurosurgical operating rooms. The third phase was the assessment of the robot's function. Using any new device in actual surgeries requires a long track record of fault free operations. Therefore, the robot had to be validated using cadavers or animal subjects however, these methods also bring ethical, logistics and cost issues. So, a new approach

was designed for assessment of the robot. This method involves using rapid prototyping techniques and actual patient data. In the process of this work, robotic applications had to be developed from scratch to enable the robot to perform surgical tasks and applications such as semi-automated patient-image registration, biopsy needle guidance and endoscope manipulation. Patient-image registration function matches the physical coordinates of the patient with medical image coordinates autonomously. Furthermore, biopsy needle guidance for brain tissue sampling is a common feature in neurosurgical robots, which enables a suitable benchmark for a robot's accuracy. Endoscope manipulation is also a topic of interest in neurosurgery as it introduces different challenges compared to Laparoscopic surgeries. The robot performed with adequate accuracy for general surgical tasks, however, it showed some limitations in the endoscope manipulation features.

Keywords: Robotic surgery, robot assisted neurosurgery, Computer aided neurosurgery

REKA BENTUK DAN PEMBANGUNAN PLATFORM ROBOTIK UNTUK PROSEDUR NEUROSURGIKAL UMUM

ABSTRAK

Untuk kali pertama pada tahun 1985, robot telah diperkenalkan ke bilik operasi neurosurgeri. Sejak itu, bidang robotik ini telah berkembang maju dengan teknologi baru dari segi ketepatan dan keselamatan yang lebih baik. Walau bagaimanapun, pembangunan robot untuk pembedahan saraf adalah tugas yang mencabar kerana sifat sensitif aplikasi ini serta kos pembangunan yang tinggi. Robot neurosurgeri yang biasa menelan kos berjuta-juta dolar pada 2018, walaupun kos komponen dan pengiraan telah diturunkan dengan ketara. Hal ini disebabkan terutama oleh tumpuan robot neurosurgeri semasa tugas pembedahan yang hendaklah sangat tepat dan spesifik yang menjadikan penggunaannya terhad. Dalam tesis ini, perkembangan robot neurosurgeri adalah tertumpu kepada tugas pembedahan yang lebih umum berkaitan dengan navigasi pembedahan yang diselidik, serta laporan reka bentuk dan perkembangannya. Penggunaan platform ini untuk membangunkan lebih banyak aplikasi pembedahan umum boleh menurunkan kos. Selain itu, sistem ini telah dibangunkan menggunakan platform sumber terbuka yang sentiasa mengemaskini ciri-ciri dan teknologi baru, dan secara langsung membantu platform ini untuk sentiasa selaras dengan pengajian sains yang paling baru dan terkini. Untuk mempunyai pendekatan bersatu, tiga fasa utama perlu dimasukkan. Yang pertama adalah pengumpulan dan analisis data, di mana pengumpulan data dilakukan pada masa pembedahan sebenar untuk menganalisis ruang kerja tugas bagi pembedahan yang disasarkan untuk membantu dalam reka bentuk struktur robot. Yang kedua adalah reka bentuk dan pembangunan robot yang sebenar berdasarkan analisis pembedahan awal. Dalam karya ini, robot yang direka bentuk hendaklah cukup kecil dan mempunyai kecekapan yang sesuai dalam bilik pembedahan neurosurgeri. Tahap ketiga adalah penilaian fungsi robot. Dengan menggunakan mana-mana peranti baru dalam

pembedahan sebenar, rekod jangka panjang adalah diperlukan yang menunjukkan operasi bebas kesalahan. Oleh itu, robot perlu disahkan menggunakan bangkai atau subjek haiwan, namun kaedah ini juga membawa masalah etika, logistik dan kos. Oleh itu, satu pendekatan baru telah direka untuk menilai aplikasi robot. Kaedah ini melibatkan teknik prototaip pantas dan data pesakit sebenar. Dalam proses kerja ini, aplikasi robotik perlu dibangunkan dari dasar asas untuk membolehkan robot melakukan tugas pembedahan dan aplikasi seperti pendaftaran imej pesakit separuh automatik, bimbingan jarum biopsi dan manipulasi endoskop. Fungsi pendaftaran imej pesakit mestilah sepadan dengan koordinat fizikal pesakit serta koordinat imej medikal secara autonomi. Selain itu, panduan jarum biopsi untuk pengsampelan tisu otak adalah ciri umum dalam robot neurosurgeri, yang membolehkan penanda aras yang sesuai untuk menunjukkan ketepatan robot. Manipulasi endoskop juga menjadi topik minat dalam bidang bedah saraf kerana ia memperkenalkan cabaran yang berbeza berbanding dengan pembedahan laparoskopik. Robot yang berfungsi dengan ketepatan adalah memadai untuk tugas pembedahan am. Walau bagaimanapun, ia menunjukkan beberapa batasan dalam ciri-ciri manipulasi endoskopi.

Keywords: Pembedahan Robotik, pembedahan saraf dengan bantuan robotik, Pembedahan saraf dengan bantuan komputer.

ACKNOWLEDGEMENTS

Foremost, I would like to express my sincere gratitude to my engineering supervisor Prof. Dr. Mahmoud Moghavvemi for his continuous support of my research, for his patience, motivation, enthusiasm, and immense knowledge. I could not have imagined having better advisor and mentors for my PhD research.

I would like to specially thank my surgery supervisor Prof. Dr. Vickneswaran who as the head of this research did not spare any help and support for me. Despite his busy schedule and massive responsibilities, he always made time to push the boundaries of this research further together with me like a true leader. My sincere thanks also go to other members of neurosurgery division in University of Malaya for their help and guidance through this research.

I thank my great friends and colleagues Isobel, Yuwaraj and Su Tung for all the discussions, for the long days we were working together, and for all the fun we have had in the last few years, you have been very good and supportive friends through these years. Also, I want to show my gratitude to the administration offices involved, department of surgery and faculty of engineering for their help and support.

Special thanks to Malaysia's Ministry of Science, technology and innovation for financially supporting this research through scienceFund grant (03-01-03-SF1219).

Last but not the least; I would like to thank my lovely family: my parents and my brother Abolfazl for supporting me in every way they could throughout my life. And my aunt Tahereh and my Uncle Jafar for showing me how lovely and beautiful the life can be.

TABLE OF CONTENTS

Abstract	iii
Abstrak	v
Acknowledgements	vii
Table of Contents	viii
List of Figures	xii
List of Tables.....	xvii
List of Symbols and Abbreviations.....	xviii
List of Appendices	xix
CHAPTER 1: INTRODUCTION.....	1
1.1 The mechanics of Neurosurgery.....	3
1.2 Image Guided Surgery	8
1.3 Problem statement	14
1.4 Objectives	16
CHAPTER 2: LITERATURE REVIEW.....	20
2.1 The targeted surgical tasks and kinematic structure in neurosurgical robots	21
2.1.1 Stereotactic robots with serial kinematic chain.....	22
2.1.2 Stereotactic robots with parallel kinematic chain.....	26
2.1.3 Unusual approaches to stereotactic neurosurgical tasks.....	27
2.1.4 Radio-surgical robots	29
2.1.5 Microsurgical robots.....	30
2.1.6 Robots for general and assistive neurosurgery	36
2.2 The methods of patient registration in neurosurgical robots	41
2.2.1 Frame based registration	42

2.2.2	Anatomical landmark registration	42
2.2.3	Fiducial based registration.....	43
2.2.4	Surface matching registration.....	44
2.2.5	Frame-based versus Frameless registration.....	44
CHAPTER 3: METHODOLOGY		50
3.1	Task space analysis.....	54
3.1.1	Methods used for a detailed analysis on Line-of-sight issue.....	63
3.2	Validation	67
3.2.1	Validation of endoscope manipulation application.....	68
3.2.2	Biopsy and Accuracy assessment.....	69
3.3	Software.....	76
CHAPTER 4: DESIGN AND DEVELOPMENT		80
4.1	Hardware.....	80
4.1.1	Design problem identification and analysis	80
4.1.2	Kinematic analysis	82
4.1.3	Kinematic optimization	95
4.1.4	Dynamic simulation	101
4.1.5	Pre-Alfa prototypes	106
4.1.6	Alfa prototype.....	112
4.2	Assistive tasks applications	116
4.2.1	Registration	116
4.2.2	Biopsy.....	118
4.2.3	Endoscope manipulation in transsphenoidal surgeries.....	119
4.3	Software.....	127
4.3.1	Robot low-level communication	130

4.3.2	ROS-Robot controller.....	131
4.3.3	ROS-Moveit	132
4.3.4	ROS-medical trajectory planner	133
4.3.5	ROS-Joystick interface.....	134
4.3.6	ROS-Registration Module.....	134
4.3.7	ROS-Joint state publisher.....	135
4.3.8	ROS-Transfer function publisher	135
4.3.9	ROS-facial detection	136
4.3.10	ROS-3D camera controller.....	141
4.3.11	ROS-simulation.....	142
4.3.12	ROS-visualization	142
4.3.13	ROS-Calibration.....	142
4.3.14	3D slicer-main modules.....	144
4.3.15	3D slicer-Slicer IGT	145
4.3.16	3D slicer-User Interface	145
CHAPTER 5: RESULTS.....		148
5.1	Size and workspace.....	148
5.2	Results observed from line of sight analysis	150
5.3	Registration, biopsy and accuracy	155
5.3.1	Models' accuracy	156
5.3.2	Repeatability.....	162
5.3.3	Movement accuracy	165
5.3.4	Registration and Biopsy	167
5.4	Endoscope manipulation.....	171
CHAPTER 6: DISCUSSION		174

CHAPTER 7: CONCLUSION AND RECOMMENDATIONS	181
References	185
List of Publications and Papers Presented	198
Appendix	199

University of Malaya

LIST OF FIGURES

Figure 1.1 Anatomy of brain and skull.	4
Figure 1.2 In neurosurgery operating area is usually small. Having several instruments in this area allows for limited movements.	5
Figure 1.3 A stereotactic frame. From left base, which fixes to patient's head. CT localizer, the N shaped rods are visible in CT scan and their distance from each other and also from a specific lesion is the reference in stereotactic calculations. Last piece is CRW frame, the arc is an adjustable arm that holds a cannula in a desired position.....	8
Figure 1.4 Stereovision camera and the reference point with reflective markers.....	9
Figure 1.5 Patient's head is fixed using a clamp. The incision marks are visible on the scalp.....	11
Figure 3.1 The flow chart describing steps taken for this project.....	50
Figure 3.2 Task space of the manipulator from [a] top view and [b] side view	54
Figure 3.3 The process of registering a dissector and an endoscope to the IGS system. Using the registering tool, the IGS can calibrate the new tool by calculating the length and thickness of it.....	59
Figure 3.4 The recorded data in tumor resection surgery, to compare the actual data if it falls into cone shaped workspace.	60
Figure 3.5 Top: an example of a situation in which the surgeon is using the tracking instrument, but the camera could not detect it. Bottom: The surgeon is using the tracking instrument and image guidance could detect it.	64
Figure 3.6 Diagram of the process performed for each operation to calculate the Line of sight error.	65
Figure 3.7 The image guidance optical tracker and the attached video camera.	66
Figure 3.8 Pituitary model used for endoscope application.....	69
Figure 3.9 Three of 24 reference points incorporated inside the CT Image of the patient to be printed.....	70
Figure 3.10 Left: The 24 markers and the support structure holding them in place. Right: The design of each pile structure.	72
Figure 3.11 The two models are shown side by side. First model on the left, with 24 marker points. Second model on the right provided with 12 marker points.....	73

Figure 3.12 The setup with the first model	75
Figure 4.1 In this picture the surgeon is marking the incision on scalp of the patient. The tool's movement is illustrated on the left, the movement is small and does not move deep inside the head which indicates category 1 of assistive tasks.	83
Figure 4.2 The endoscope movements in an ETV operation, the movement along the operating area is significant. This type of tasks helped to determine the size and shape of operating area in these operations.	84
Figure 4.3 A full observation of the surgery as far as the IGS camera range could allow. Matching this data with video recordings of the operation provided data on positions of Operating area and its surroundings.	85
Figure 4.4 The recording of an endoscope movement during transsphenoidal surgery. A) the movements as recorded from IGS system. B) while the endoscope is in nasal canal (operating area). C) The endoscope is out for cleaning. D) the endoscope is out for adjustments.	86
Figure 4.5 the task space needed to be covered by the robot is a spherical cone with patient's head at bottom and center of it.	87
Figure 4.6 The task space when the base is positioned at the side, white area is the task space the robot needs to cover (while positioned on the right side). the grey area is the area the robot cannot cover with full dexterity.	90
Figure 4.7 Position of the microscope and it's field of view.	92
Figure 4.8 The wrist consists of two actuated axes, Z4 and Z5 and a passive axis Z6. This arrangement is smaller than normal 3 actuated axes.	93
Figure 4.9 The two kinematic topology considered for the manipulator, 3R on the left and 4R on the right.	94
Figure 4.10 Normal path planned for test 1. The tip point of SAD (UP) should touch the numbered points, not necessarily in that order.	98
Figure 4.11 The path for collision detection. The simulation calculates how much of the SAD body is in the grey area while it is performing the designated maneuvers.	99
Figure 4.12 The 2D eyesight plane changes with the progression of viewing direction.	99
Figure 4.13 The output torque for actuated axes of each joint in 5DOF structure with bases at B1.	102
Figure 4.14 The output torque for actuated axes of each joint in 5DOF structure with bases at B2.	103

Figure 4.15 The output torque for actuated axes of each joint in 6DOF structure.	104
Figure 4.16 Force and torque effects on the joint one of the two main structures, 3R and 4R. this shows stress on this joint as the robot is moving.....	105
Figure 4.17 The tool's location and orientation are being tracked by the algorithm. The slices shown based on the tool's location.	107
Figure 4.18 a) The designed structure is touching a point on a head model with the tip point (universal probe). b) This 3D model has a slot that can accept replaceable cartridges. These cartridges mimic different pathological characteristics. c) The small wrist of the robot and the attachment of universal probe to the wrist.	108
Figure 4.19 The second prototype uses electromagnetic brakes to keep the joints rigidly when it is needed. The joints were load balanced to put less pressure on the servo motors, at joint 2 two synchronized servo motors were used to handle the needed torque.	109
Figure 4.20 The third prototype was developed using more accurate and powerful servo motors, all the attachments were made using metal. the picture on the right shows the point indication feature of this prototype.	110
Figure 4.21 The moving base of the Alfa prototype. the base slides on two parallel rails, the movement is controlled by a servo motor which can provide position feedback for the controller.	112
Figure 4.22 The Alfa prototype holding a pencil as a pointer on a selected point from tumor model's medical image.	114
Figure 4.23 A bracket for the robot, designed to house a 3D camera and a cannula housing for needle placements.	115
Figure 4.24 The biopsy trajectory in software and robot's spaces.	119
Figure 4.25 The summation of recorded endoscope positions in a transsphenoidal surgery.	122
Figure 4.26 A pivot plane for transsphenoidal surgery based on boundaries defined by nasal bone.	123
Figure 4.27 cross section of nasal cavity and the suggested position of endoscope compares to pivot plane.	124
Figure 4.28 Steps of the designed endoscope manipulation application.	125
Figure 4.29 Software diagram of the Alfa prototype.	128

Figure 4.30 Modified 31 mark-up points for facial landmarks excluding the unused points	139
Figure 4.31: Detection of the trained model on the right vs normal face model on the left, normal face model fails to detect landmarks while the mouth is covered or blocked. .	140
Figure 4.32 The algorithm used in this module to detect the faces and facial landmark uses the trained facial landmark detection algorithm. On the left the image shows a typical output of the Dlib facial landmark detection and on the right the output of a ROS wrapper written for this algorithm is shown, this image shows the facial landmark points in different colors (for example green for the nose area).	141
Figure 4.33 During the calibration procedure the robot points the camera to a circle pattern from different directions and with different poses.	143
Figure 5.1 Overall dimensions of the robot	149
Figure 5.2 The bottom picture shows a scenario were the nurse was blocking the IGS camera. The scrub nurse had to move away from the patient so that the image guidance camera can see the instrument in the top picture.	154
Figure 5.3 Box plot for error deviation among the three registration methods for first model.	157
Figure 5.4 Box plot for error deviation among the three registration methods for second model.	157
Figure 5.5 using a dial indicator with 0.01mm resolution to calculate repeatability in X,Y and Z at one point of the robot's workspace.	164
Figure 5.6 movement accuracy is tested using the dial indicator which has 1cm range. The robot was commanded to change the tool position along the indicator's plunger. The differences between the calculated forward kinematics and the indicator showed the error value. The camera and laser pointer are to measure the flex in the tip point.	166
Figure 5.7 Left the needle hits the colored circle which means the error was recorded as 1.5 mm and on the right a caliper had to be used to measure the error.	167
Figure 5.8 biopsy error recorded for manual registration on the two accuracy models. Paediatric models mean error is 3.36mm and 3.38mm for tumour model.	168
Figure 5.9 while the head was tilted the facial landmark algorithm hardly could align the facial landmark to the model's face however, the direction of the head estimated correctly.	169
Figure 5.10 the recorded point cloud vs registered point cloud.	170

Figure 5.11 represented error in biopsy operation using semi-auto registration. Mean error for paediatric model was 4.85mm and for tumour model it was 4.51mm. 170

Figure 5.12 Setup for endoscope manipulating application..... 172

University of Malaya

LIST OF TABLES

Table 2.1 list of neurosurgical robots introduced in this chapter.....	47
Table 3.1 The steps performed in the mock surgeries and the instruments used in each step.	59
Table 4.1 Optimization results for test 1 without considering the obstacle avoidance feature.....	100
Table 4.2 Results for Test 2.	100
Table 4.3 Frequency of endoscope removed from nasal cavity for cleaning and changing of nasal canal.....	127
Table 4.4 A comparison between two facial landmark detection methods used.	138
Table 5.1 The frequency and period of line of sight error for the observed operations.	151
Table 5.2 the total lasted time of error during each operation compare to the total use of image guidance.....	152
Table 5.3 Summarised reasons of line of sight errors.....	153
Table 5.4 the calculated error between the IGS based coordinates and original imaging coordinates utilizing the 3 different methods of registration.	156
Table 5.5 distance of the tool point from a desired position attempted 7 times after taking few random pose and the whole process was repeated every 2 hours for 4 times.....	165

LIST OF SYMBOLS AND ABBREVIATIONS

DOF	:	Degrees Of Freedom
OR	:	Operating Room
CT	:	Computed Tomography
MRI	:	Magnetic Resonance Imaging
N.M	:	Newton Meter
DICOM	:	Digital Imaging and Communications in Medicine
SVD	:	Singular Value Decomposition
ICP	:	Iterative Closest Point
3D	:	Three Dimensional
STL	:	Stereolithography
IGS	:	Image Guided Surgery

LIST OF APPENDICES

Appendix A: Ethics approval letter

199

.....

University of Malaya

CHAPTER 1: INTRODUCTION

Technology and computer advancements have vastly improved practice of medicine. These improvements affect a range of areas from diagnostic sciences to surgical interventions. Medical imaging techniques have benefited from new technologies in magnetic resonance imaging (MRI), Digital Imaging and Communications in Medicine (DICOM) and computer tomography (CT). Not only diagnostics, but also Surgical intervention have been revolutionized by technology, technologies such as image guided surgery (IGS) and surgical robotics have also vastly improved the practice of surgery.

The techniques and procedures that use computer technology in surgery are called computer aided surgery (also called computer-assisted surgery). Computer aided surgery technologies are currently being used in different aspects of surgery such as surgical planning and guidance in surgical interventions. A very well established technique in computer aided surgery is image guided surgery (also called surgical navigation and image guided therapy). IGS systems use the medical image of a patient in digital form to render and create a 3D model of the patient body and organs. Using this model, surgeons can plan the surgery according to specific anatomy of each patient and then use this plan during surgery while their movements are tracked by IGS. Inside the operating room (OR), the rendered model will be registered to the patient's actual body by matching samples position of physical points on the patient's head to their corresponding point in the medical image. To scan these points' positions on patient's head a tracking system is used, after the patient-image registration this tracking system is used to track the surgical instruments' position during the surgery. Basically, the IGS works similar to a car navigation system that lets surgeons know where their instruments are inside a patient's body. Using this technology rather than blindly approaching a surgical problem, the surgeons can perform more accurate and less invasive operations which leads to less

complications and better outcome for the patient. The advancements in computer-aided surgery and IGS technologies have laid the foundation of surgical robotics.

The term surgical robotics embodies the use of any electro-mechanical device (usually in the form of an arm) in conjunction with the medical images (live or scanned images) to perform a surgical procedure on a patient. This can be done with the assistance of a surgeon or remotely by a surgeon who is not in the same room. The surgical robotics field has witnessed immense growth in recent history to the point that some of the new surgical robots such as Davinci robot (Morelli et al., 2016) are well known not only to the scientific community but also to public. And each year, more robots are set to enter the world of operating rooms ("New surgical robots are about to enter the operating theatre," Nov 16th 2017).

Surgical robots have been working in different aspects and disciplines of surgery. For example, laparoscopic surgery has benefited from using robots such as Da Vinci (Morelli et al., 2016) and Zeus (Butner & Ghodoussi, 2003). Renaissance (spineAssist) robot can be used in pedicle screws placement in spinal surgeries (Lieberman et al., 2006). Radiosurgery has been revolutionized with the introduction of Robotic systems such as CyberKnife and Novalis (Bertelsen, Melo, Sánchez, & Borro, 2013). Robodoc has been used in Orthopaedic surgeries (Bertelsen et al., 2013). Some of these systems are designed to be used in multiple disciplines of surgery (like Da Vinci) due to the structural and anatomical similarities between these disciplines, which means that the ways surgeons are approaching the anatomical problem are similar, for example using multiple entry points in different types of minimally invasive surgeries. These types of robots can be used in general cardiothoracic, gastrointestinal and spine surgery. However, for Neurosurgery discipline approaches (in this thesis neurosurgery refers to brain surgery), it is different from other disciplines. This is due to the distinct position of the brain in the

skull which makes the approach to it restricted. Furthermore, the sensitivity of the brain tissue adds on to the restraints of neurosurgical approaches (Bergman, Schulz, & Davis, 2009). Due to this contrast of approaches, it can be seen that neurosurgery robots are correspondingly designed differently than other surgical robots (Motkoski & Sutherland, 2016). To understand neurosurgical robots, the mechanics of neurosurgery approaches should be explained first.

1.1 The mechanics of Neurosurgery

Figure 1.1 shows an over simplified abstract of the head anatomy. The brain consists of four main sections, which are the cortex, cerebellum, ventricle and brain stem. The brain structure is wrapped inside a thin tissue called dura. The dura and brain are located and protected inside the bony structure of the skull called the cranium. The topmost layer is the scalp or skin covering the cranium. The brain is suspended inside cerebrospinal fluid (CSF) outlined by dura. They are not attached to the cranium, but if small movements of brain (brain shift) is ignored they are considered to be in constant position compared to the cranium.

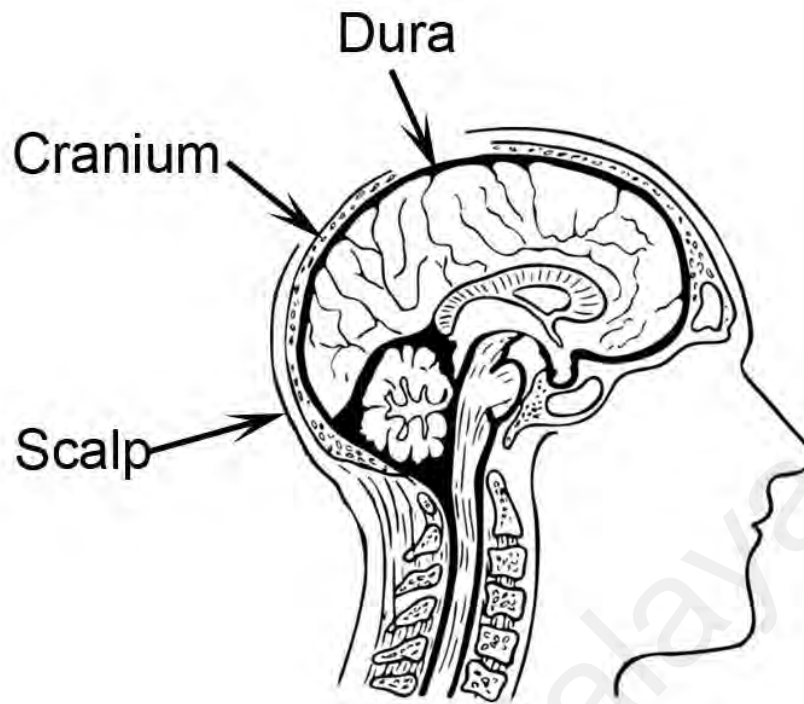


Figure 1.1 Anatomy of brain and skull.

To get access to the brain tissue, the scalp, cranium and dura should be opened. This means making an incision on scalp, drilling and/or removing part of the bone on cranium (craniotomy) and making an incision on the dura. The opening and incisions in neurosurgery should be as small as possible to minimize infection possibility and CSF leaks. In most cases, the tendency is to have only one opening. But, in other types of surgeries such as general surgery, bigger and multiple entry incisions are common.

Neurosurgical operations can be divided into three different categories by their approach to the brain opening and access. The first type are operations that only use small holes (burr hole) on the skull such as brain biopsies, Deep Brain Stimulation (DBS) electrode placement and removing a hematoma. During these surgeries small amount of brain tissue is exposed, and the surgeon doesn't have a big field of view over the surgery. Therefore, sometimes these surgeries are called semi-blind surgeries. The second type of approach is craniotomy in which part of the cranium is removed to gain access to a bigger area of the brain such as big tumour resections (these openings are still considered small

compared to other open surgeries). The third type is the approaches that starts from other organs like ear, throat or nose such as acoustic neuroma and pituitary gland tumour resection. The third category is usually employed during base of skull surgery where the tumour is in hard to reach spaces, on the base of the skull.

Sometimes in craniotomies only access to the surface of brain (motor cortex) is needed, but in most operations the surgeon must go deeper into the brain tissue. This means the very sensitive and delicate brain fibers must be pushed away gently with minimum possible manipulation. Unnecessary pressure and damaging of the brain tissue affect the patient's body and life quality or in severe cases can end up in patient mortality. This limitation causes a very small and cramped operating area to work with. Therefore, compared to other disciplines the neurosurgeon is very limited in freedom of movements. In this thesis, operating area refers to the area inside and immediate surroundings of the entry incision which exposes the internal body tissue, as shown in Figure 1.2. The arrangement of equipment and staff is usually around the operating area (in an open tumour resection operation).

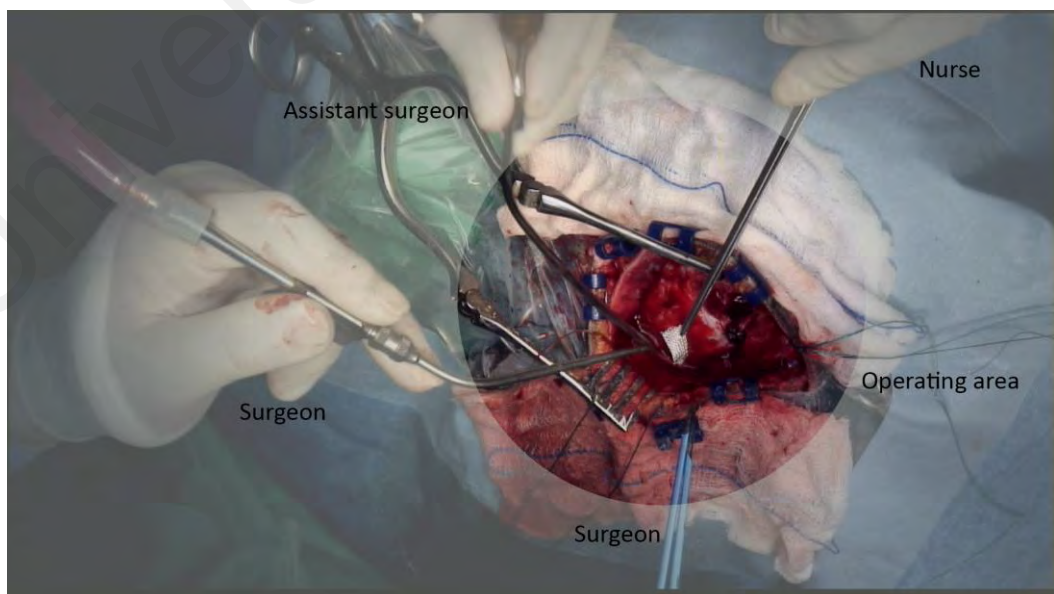


Figure 1.2 In neurosurgery operating area is usually small. Having several instruments in this area allows for limited movements.

In the third category, the characteristics of the operating area are same as normal craniotomy but with more space restriction. Additionally, in some cases like transsphenoidal surgeries the operating area is deeper inside the head and more restricted. These types of operations are done using surgical endoscopy techniques, which in neurosurgery is different from laparoscopic surgery. The operating area is smaller compared to laparoscopic surgery which has an advantage due to the big space in the abdominal cavity. Furthermore, in laparoscopic surgery the entry incision for the endoscope and instruments acts as a pivot point as well. This suggests that the entry point acts as a four-axis passive joint for the instruments (3 rotational and 1 prismatic). However, in transsphenoidal endoscopy the endoscope and instruments pass through one small canal and it is not possible to rest the endoscope or instruments on any point of this canal. This worsens the limited space problem in neurosurgery.

So far it is mentioned that in neurosurgery compared to other surgical disciplines, the entry incision should be small and usually only one is possible. The space in operating area is limited and, there is no pivot point in neuro-endoscopic surgery. These restrictions have led to the invention of new and smaller surgical instruments as well as new surgical methods in neurosurgery such as stereotactic surgery.

A very big concern in neurosurgical procedures is if the path being taken by the surgeon is the correct one, will it end up in the proper location inside the brain? This is due to a small operating area in combination with the lack of sufficient anatomical landmarks, so it is hard for the surgeon to easily recognize the position of the operating area. In semi-blind operations such as brain biopsy, the trajectory and target of the biopsy needle have to be precisely assigned before the operation. There is no room for trial and error to see if the biopsy needle going in the right direction or for sampling the correct

tissue (usually the brain tissue is not clear in live X-ray scanner images). This concern has given birth to a surgical method called stereotactic surgery.

Stereotactic surgery is the surgical intervention in which the spatial location of the desired pathology or tissue is calculated using a constant landmark. In Neurosurgery this constant landmark is usually the bone (cranium). As mentioned before the brain and bone are in constant spatial relation to each other, so by measuring the coordinates of the desired location in the brain in relation to a known bone landmark it is possible to calculate the proper trajectory from the cranium to the desired location.

A very good example of stereotactic surgery is a traditional method of brain biopsy procedure, which is using a stereotactic frame. The stereotactic frame consists of a base, a localizer unit and an adjustable frame (usually an arch) the adjustable unit has a guidance arm that can be positioned based on the accurate rulers on the frame. First the base is fixed to the patient's head (with screws gripping the skull bone) and the localizer unit is attached to the base. Then the patient's head with the attached frame is scanned in CT scanner or MRI scanner (the frame should be compatible to be used in CT and if needed MRI scanner). The localizer unit has reference points that are visible in the medical image and because the frame is attached to the cranium, these reference points always maintain the same location in relation to the brain. With the localizer unit and target lesion visible in the medical image, the surgeon then calculates the entry point and trajectory of the biopsy needle. In the next step, the localizer unit is removed. The guidance arm on the moveable frame would be set to proper coordinate values and attached to the base unit. The guidance on the moveable frame indicates the trajectory and entry point of the biopsy needle. The base of the frame remains fixed to the head; therefore, it always provides the constant frame of reference for the needle coordinates.

Figure 1.3 Shows a typical stereotactic frame.

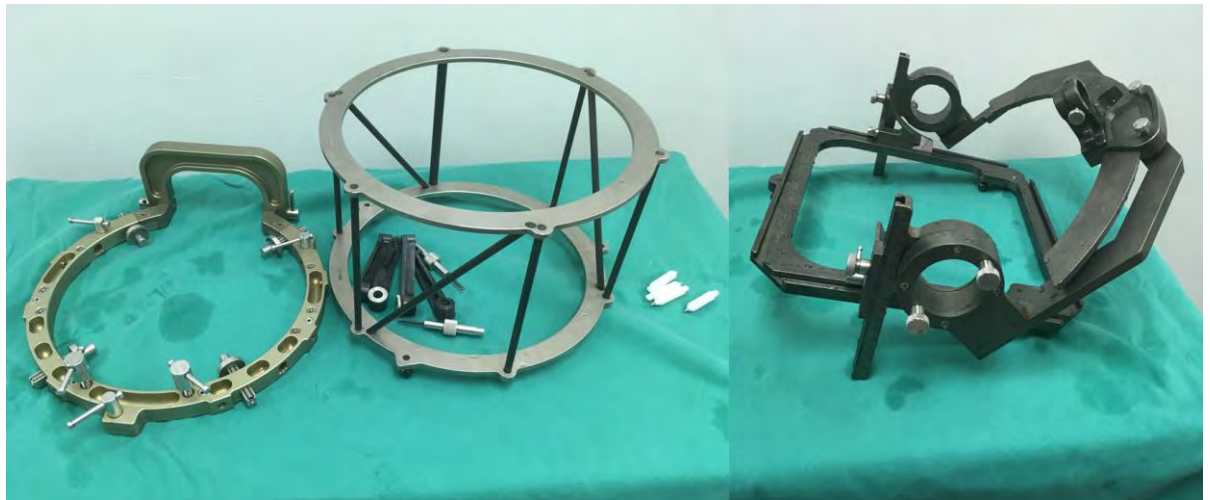


Figure 1.3 A stereotactic frame. From left base, which fixes to patient's head. CT localizer, the N shaped rods are visible in CT scan and their distance from each other and also from a specific lesion is the reference in stereotactic calculations. Last piece is CRW frame, the arc is an adjustable arm that holds a cannula in a desired position.

Stereotactic frames are very accurate and reliable. However, they are not perfect. Setting them is time consuming and because of their bulky structure it is hard and cumbersome to use them in most neurosurgery cases such as craniotomies for tumour resection. Image guided surgical systems use similar principals without using a big frame fixed to the patient's head. Advances in IGS technology has been a key factor in developing neurosurgical robotics, in continue IGS systems, their flaws and improvements hoping to achieve by surgical robots are discussed.

1.2 Image Guided Surgery

IGS has been used in neurosurgery for more than 30 years. It is easier to use and offers more functionality than stereotactic frames. Its effective implementation has made it a standard device in neurosurgical cases (however, it is less accurate than stereotactic frames).

IGS consists of two main components, which are software and tracking system. An IGS software imports medical images (MRI, CT, Ultrasound, ...) and position information from the tracking system and combines them together. The main function of

the software is to process the images and coordinates and visualize the live location of the instruments in relation to the patient's brain or targeted pathology (navigating). In addition, the software can have additional features (different in each commercial system), features such as rendering a 3D model of a segmented part of an image, importing video images from other sources like endoscopes and communicating with surgical microscopes to induce a virtual reality image into the microscope image. Using the IGS software, surgeons can plan the operation and later use the planned data in the live navigation images to verify their actions.

The tracking system or localizer (also called digitizer) is the system which tracks the surgical instruments in relation to the patient's head (IGS can be used for other organs but as this thesis focus on brain surgeries, the targeted organ is head). Therefore, it can provide the software with the location of the instrument inside the brain. There are different types of localizers, but the most used system is optical tracking cameras. These systems perform stereoscopy using a stereovision camera and infrared reflective markers on the instruments.

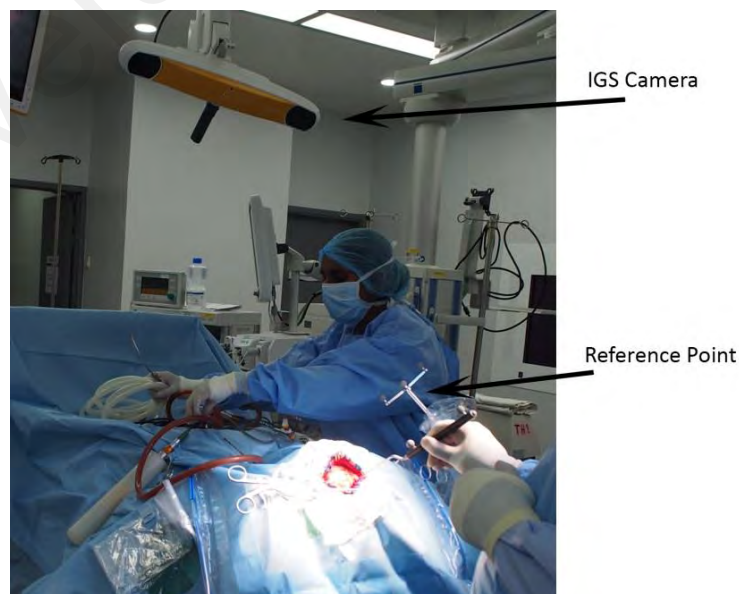


Figure 1.4 Stereovision camera and the reference point with reflective markers.

Describing a typical workflow in an image guided tumour resection surgery would further clarify the technology and usage of these systems. The events, in order of occurrence are as follows:

1. Preoperative image scanning.

Patient's image is obtained via CT or MRI images in DICOM format. The type of medical image depends on the case. Sometimes both MRI and CT scans are used, sometimes other type of scans such as PET (Positron Emission Tomography) are acquired. Whatever the image it should be in a format that is importable by the IGS system. DICOM is one digital format well-accepted by medical image scanners, hospital information systems and IGS systems.

2. Patient's head is fixed to the surgery table using special head clamps.

This is to avoid unwanted movements of the head and keep it in a constant frame of reference with the instruments. Similar to base part of the stereotaxic frame, the head clamp provides a constant reference frame for the IGS and the head is not able to move freely during the operation.



Figure 1.5 Patient's head is fixed using a clamp. The incision marks are visible on the scalp.

3. A reference frame is fixed to the head clamp.

The reference frame provides the stereovision camera with reference to measure the coordinates of instruments. This reference frame (also called reference star) contains infrared reflective markers (ball markers) in a pattern recognizable by IGS tracker. As it is fixed to the head clamp its location is always constant in relation to the patient's head. So, other tracked instruments' location is always compared to this reference frame by the IGS tracker. Its visibility is important to the tracking process and it should always be in the field view of the IGS camera.

The primary function of the head clamp is to keep the patient's head from moving by the forces exerted on it from operation. it is possible to refrain from using a head clamp but instead, the IGS reference frame should be attached to the patient's head so the head and reference frame move as one.

4. The head is registered to the images.

Registration basically refers to the act of matching the medical image coordinates to the patient's anatomical coordinates on the surgical table. It is done with scanning the coordinates of sample points on the patient's head before the IGS software compares these coordinates with the coordinates of respected points in the medical image. A transform function is then produced to place two coordinate systems in the same frame. This transform function is used throughout the operation to convert positions between the two coordinate systems. Scanning the coordinates of sample points can be done in different ways. Surface scanning is a common method to scan the sample points. Surface refers to the patient's face as it has enough distinct points thus, it provides the IGS software with a big enough sample to match the point on the face surface of the rendered medical image. When the patient's face surface is not available for scanning (for example patient is positioned in prone) the surface scanning cannot provide the IGS software with a big enough sample so, fiducial registration is used. Fiducials are markers placed on the patient's head, where these markers are visible on the medical scans therefor on IGS software as well. So, coordinates of these markers are used as sample points for registration by the IGS software

5. Checking the registration accuracy.

This is done by placing a tracked instrument on a known point of the patient's head such as tip of the nose, side of the eyelids and ears. If the IGS shows the instrument is in the correct place that means the registration is done successfully.

6. Mark the entry incision and start of surgery.

The surgeon uses a tracked instrument to locate the tumour under the scalp. He then finds the proper incision location and marks it using a normal marker. After draping

the patient and making sure everything is sterile around the operating area the surgeon starts the surgery.

7. Finding the opening location of bone and craniotomy.

Similar to marking the entry incision, the surgeon uses IGS to mark the bone area that needs to be opened and continues with drilling.

8. Using IGS during surgery.

After opening the bone and dura, IGS is used by surgeons to know where they are and to make sure they are going in the right direction. For example, some surgeons use IGS pointers to find the outlines of the tumour before progressing with resecting it. Steps 7 and 8 are considered as intraoperative steps as the surgery is started and patient is covered with sterile drapes.

This is a common workflow for an optical IGS and may differ in other types of IGS. For example, in IGS systems with electromagnetic tracker the patient head is not fixed to the head clamp and a reference marker is attached to patient's head with an antenna array placed beside the head. But as optical trackers are the mainstream in IGS systems and usually all navigation systems are equipped with optical trackers the standard here considered to be optical trackers.

While IGS is a necessity in neurosurgical OR these systems suffer from some shortcomings as well. The registration is not always very accurate, thus, for precise operations (for example Deep Brain Stimulation) surgeons still tend to use stereotactic frames (Matias, Frizon, Nagel, Lobel, & Machado, 2018). Using optical cameras in IGS means the camera must have a direct line of sight with the reference frame and

instruments in order to track the instrument (more detail on the line of sight issue has been given in the methodology chapter).

Another shortcoming, or to put in better words a lack of feature, is that IGS does not provide any feedback other than visual. For example, in a biopsy operation using IGS the surgeon plans the target and trajectory in an IGS software. However, to perform the biopsy the surgeon must attach an articulated arm and fix it to the surgery table to perform the biopsy. In each step of fixing the arm the surgeon needs to visually verify the location on the IGS software. This may take a long time to set especially if the surgeon is not experienced. In a tumour resection operation, the surgeon may advance in a wrong path and unless a tracked instrument is used the potential mistake cannot be discovered. Not all surgical instruments are tracked during an IGS surgery however, almost all instruments can be registered to the IGS to be tracked using attachments with reflective balls.

This requirement has been answered by neurosurgical robots. Robots can perform biopsies with the least amount of human intervention (Faria et al., 2015) or perform surgeries while patient is in the MRI scanner with the surgeon controlling it from another room (Sutherland, Wolfsberger, Lama, & Zarei-nia, 2013). Lots of general and specialised neurosurgical robots have been and are being developed.

1.3 Problem statement

Commercial neurosurgical robots, like many other robotic systems, are designed to shine where the human is weak. They can help surgeons to perform highly precise operations that are challenging without the utilization of robots. They can operate in constrained and hazardous locations where the human surgeon cannot. Their rigidity and robustness have made them very reliable to perform various surgical interventions. However, neurosurgery also usually requires the use of microsurgical techniques that involve dissecting and/or elevating the overlying brain or dissection through the brain

parenchyma. This requires delicate and special techniques and, as neurosurgical robotics is considered to be young, surgeons may be reluctant to hand over these techniques to a machine presently (Sloan et al., 2013). Therefore, the use of robotics in neurosurgery is limited to specific procedures, for example performing deep brain biopsies, Deep Brain Stimulation (DBS) and stereo electroencephalography (SEEG). This makes these machines costly as their use is limited. Even systems with a broader application range, like ROSA (ROSA.) can perform only few specific procedures. Additionally, these systems are not considered to be portable as they are relatively bulky. Lack of portability and limited use, has made these systems costly for hospitals and medical centres especially in third world countries (Smith, Jivraj, Wong, & Yang, 2016). This has resulted in a small market penetration of these systems compared to IGS systems.

Neurosurgical robots are often used in combination with IGS systems. However, their application is narrower than what a surgeon can use the IGS for. There are different applications in general neurosurgery that in contrast with deep biopsies and DBS surgeries, demand smaller positioning accuracies. Applications such as handling an endoscope in the operating area, marking the scalp for entry incision, using a pointer connected to a robot to show pre-planned boundaries of operating area or for virtual reality applications. This list can continue for a few pages. The goal to develop a robotic system which can be used in combination with an IGS software to perform multiple types of general non-invasive neurosurgical applications is the motivation of this thesis. In this thesis these tasks are called assistive neurosurgical tasks or, in short, assistive tasks.

Assistive tasks are tasks which provide the surgeon with guidance and support and not invasive tasks such as cutting the skin or craniotomy. The term guidance refers to providing the surgeon with any additional information that helps the process of surgery and trajectory guidance. For example, ways to show pre-planned targets to surgeon (for

example pointing a laser to location of an artery or nerve). Support refers to handling and manipulating instruments in or near the operating area such as handling an endoscope or exoscope (this is a viewing camera which is positioned on top of the operating area to provide visual feedback as clear as surgical endoscope for surgeons) (Nishiyama, 2017).

Based on a target in or near an operating area, different robot tool positioning accuracies could be needed, and it often depends on size of the target and length of trajectory. Small angular deflection in long trajectory means much higher deflection at the target and clearly smaller targets need higher accuracies to reach. There are plenty of stereotactic robots that have the accuracy and rigidity to reach these targets. Therefore, in this thesis the goal is to have a robot which can be used as an assistant inside neurosurgical OR. It will not be targeting high accurate needle placements. However, this robot is targeting tasks in neurosurgical operations and naturally a reasonable amount of accuracy is demanded in these applications. The necessary calculations for assistive tasks are achieved in an IGS software, therefore an accuracy near to clinical IGS systems is considered reasonable. This will help to develop more assistive applications in neurosurgery and to further advance the use of IGS in neurosurgery. Hopefully, this will help in better acceptance of robotic systems in neurosurgery.

1.4 Objectives

As discussed, neurosurgical operations impose some ergonomic limitations. Firstly, the space in and around the operating area is very limited. Furthermore, the area around the surgery table in neurosurgical ORs are usually cramped with different big and bulky equipment such as an IGS and microscope. It is also mentioned that portability is an important factor for surgical robots (and any surgical device). Therefore, it is important for a neurosurgical robot to be relatively small. This allows it to be moved to another location and its size would not occupy big spaces in the operating area and around the

patient. Working as an extension of the IGS system, the robot should be able to communicate with the IGS and accomplish necessary procedures for the IGS system with a comparable accuracy. Basically, the robot acts as a high-end localizer. So, to sum up, the objective of this thesis is:

To design and develop a robotic system that have the following characteristics:

- It should be small enough to be portable between ORs and medical centres. So, a single person can carry the robot.
- It should be able to register the patient's head to the medical images. So, it can act as a standalone IGS system without the need for external IGS.
- It should be able to perform assistive tasks. Such as biopsy and endoscope manipulation.
- It should have good enough accuracy for assistive tasks. Below 5mm considered good enough for assistive tasks.

Being portable refers to the size of this system and means that the robot should be small enough that the user can put it in a box and carry to another medical centre rather than being big and bulky on wheels and only able to be pushed around in one centre. In this way, the surgeon can take this device to remote places if needed. Additionally, a portable device can be rented to clinical centres if demanded and the medical centre does not necessarily have to purchase it.

The ability to register the patient refers to the need for the software to be able to handle image guided applications. As image patient registration is the most basic important function in IGS the robot must be able to perform it. This implies a robust communication between the robot's controller software and an IGS compatible software to handle the surgical navigation duties such as registration and image guidance.

As discussed, assistive tasks are tasks that do not handle invasive tasks but helps the surgeon in the process of surgery. The two tasks that are chosen to be performed by the robot are brain biopsy and endoscope handling in transsphenoidal surgery. Brain biopsy has been chosen for two reasons. Firstly, it is a good measurement of the robot's accuracy. With some predetermined targets, mock biopsy procedures can be performed using the robot and a clinical IGS system. The error to targets can indicate the accuracy of the robot compared to the IGS system. Second, in the current clinical IGS systems setting a biopsy arm takes a long time (especially if the surgeon is not experienced). Using the robot for biopsy gives a good indication of how fast a biopsy can be done when using a robotic arm.

The task of handling the endoscope has been chosen because of the special characteristics of this task. First, compared to other neurosurgical instruments the endoscope is heavy so, handling it with the robot is a good measure of robot's load handling in neurosurgical environment. Second, handling an endoscope during a transsphenoidal surgery is usually done by an assistant surgeon or a passive endoscope holder. It is done so the surgeon has both hands free in the operation. Having the robot handle the endoscope can show if using a robotic arm would improve this task and, as a result, the surgical operation itself. Third, as mentioned in transsphenoidal surgery, the operating area is deep inside the nasal canal where the endoscope should always be present. If the robot is successful in manipulating the endoscope, it will be able to manipulate other instruments inside the nasal canal as well.

As mentioned, the robot should have accuracy comparable to IGS systems. The tracker systems of current clinical IGS systems have very high accuracy (submillimeter) but, when IGS systems are put to test in surgeries their accuracies are far from a submillimeter. It can reach up to $2\pm$ mm (in some case to 5 mm) (Vercruyssen et al., 2014). the

inaccuracy is due to other errors like patient image registration error and brain shift. The registration can be reduced by using different methods of registration such as auto-registration in an OR with an integrated MRI scanner but, it will not be zero. Brain shift is the change in brain position between the image scanning and operation. As mentioned, the brain is not attached to the cranium bone and moves according to head movement. Experienced neurosurgeons always keep that in mind as a patient position in the OT is different from the position the patient was scanned in. In this work the robot was used to perform mock biopsy procedures the same way that an IGS was used. Then the errors obtained from both experiments were analyzed to show how accurate the robot is.

Achieving these objectives helps in creating a robotic system which when compared to other neurosurgical robots, is small hence more portable. This robot is a standalone IGS system without the need for an external IGS system. This will result in a robot which can be used in wider range of neurosurgical tasks (assistive tasks) and therefore can cost less for medical centers to obtain.

CHAPTER 2: LITERATURE REVIEW

The first neurosurgical robot was introduced to the world in the year 1985 which in fact was an industrial robot, Programmable Universal Machine for Assembly (PUMA) (Kwoh, Hou, Jonckheere, & Hayati, 1988). A cannula was connected to the end effector of a PUMA 200 robot and CT images were used to position the canula in proper position and orientation for surgeon to perform a brain biopsy. PUMA 200 is a 6-axis arm developed in early 1980s. It is a desktop size serial manipulator with all revolute joints. The arm was equipped with locking mechanism to stop it from drifting away from the correct position and orientation as well as stopping it in case of emergency. Later in 1987 researchers from University of Toronto and Hospital for Sick Children coupled the same model of industrial robot with a stereotactic head frame and performed five cases of astrocytoma tumors removal on pediatric patients with success (Benabid et al., 1987). In 1991 same robot model was used with some modifications, a retractor was used as tool for resection of multiple pediatric thalamic astrocytoma (Drake, Joy, Goldenberg, & Kreindler, 1991). These systems proved that robots can be used in neurosurgery. They basically jump-started research and development in neurosurgical robots. Since then the number of surgical cases performed using robots around the world reaches millions (including radiosurgeries). This is due to the precision and reliability of neurosurgical robots. Furthermore, some of them are matured enough to be accepted as a standard tool in neurosurgery (radiosurgery robots).

This chapter reviews the past and current trends in neurosurgical robots. These robots were reviewed based on the objectives of this thesis which are robot's main task, their structure (structure defines the size of the robot) and their method of registration. In this review the effort was to include any robot which is designed (partially or in whole) for neurosurgical applications. So, the systems not included are systems which are only

created for surgical simulation, for surgical data collection or entirely designed for other disciplines of surgery.

2.1 The targeted surgical tasks and kinematic structure in neurosurgical robots

Targeted tasks for neurosurgical robots can be divided in three categories, stereotactic surgery, microsurgery and general neurosurgery (for assistive tasks). Since the beginning, neurosurgical robots have pursued surgical tasks and goals which are hard to improve further manually by surgeons. These tasks are mainly involved around stereotactic operations which need high precision and microsurgery which requires very fine tool movements. Comparatively, general neurosurgery has received less focus in the early researches however, in recent years more neurosurgical robots have started to focus on a range of assistive tasks instead of targeting invasive stereotaxy or microsurgery. Stereotactic surgical tasks can be considered assistive task when there is no invasive action (drilling or needle insertion) done by a robot. On the other hand, assistive tasks that require robot to position tools in relation to patient's medical images must follow stereotactic principals. So, both categories are intertwined. In this thesis the goal is to develop a robot that can perform tasks from both categories, however as robot assisted stereotactic tasks have received lots of attention in literature (robots that focus entirely on stereotaxy), it is decoupled from other assistive tasks.

These robots have achieved their intended goal by various kinematic designs and structures. The kinematic structure refers to different mechanical characteristics of a manipulator such as Degrees of freedom (DOF), type of kinematic chain (serial or parallel), location of the base and size of the structure. Intended tasks of a robotic manipulator extremely influence the design and these characteristics in a robot. Nevertheless, there can be different design approaches to a similar task. And different

structural design lead to different sizes of robots. Therefore, in this section kinematic structures are reviewed side by side with the robots' tasks.

In stereotactic operations there is a frame of reference to calculate target's position and a trajectory to reach it. In a stereotactic operation using a head frame, the frame of reference is provided by the base unit of the frame. Similarly, the position of the robotic manipulators tool point is calculated in relation to a world frame using kinematic chain theory. So, the idea of using manipulators in neurosurgery started with suggesting that if both the head and the manipulator's base are kept in constant relation to each other the position of the target can be calculated with a simple conversion from head to robot's coordinates. This is the main concept that drives stereotactic neurosurgical robots till today.

Researches have performed various experiments with different approaches to the robot assisted stereotactic surgeries. systems such as MARS and iSYS use uncommon kinematic structures while systems such as Neuromate, ROSA, Pathfinder and Remebot developed on more common structures such as typical multipurpose serial and parallel manipulators.

2.1.1 Stereotactic robots with serial kinematic chain

In 1994 researchers at E' cole Polytechnique Fe'de' rale de Lausanne (EPFL) suggested that using general purpose industrial robots in surgery impose limitations and constraints on surgery. Therefore, they developed a new robotic platform for neurosurgery, neurosurgical robot **MINEVERA** (Fankhauser et al., 1994). It was a robot designed to work inside CT scanner, it was connected to a stereotaxy frame to provide rigidity for the patient's head. Using MINEVERA surgeons could perform live CT guided brain biopsies. However, its usage was limited as it could only be used together with a CT scanner.

The **Pathfinder** was a 6 DOF serial manipulator which was mounted on a mobile cart (M. Eljamel, 2007). It could carry a needle guide for surgical applications such as biopsies and electrode placement. Patient's head was fixed using a Mayfield head clamp. After registration, the system aligned the needle guide according to the preplanned trajectories. The needle was then inserted inside needle guide by surgeon and followed the trajectory to reach the target. This system increased precision of needle insertion compared to the conventional approach (M. S. Eljamel, 2008). Pathfinder has been discontinued because of lack of commercial interest.

Among stereotactic surgical robots the most utilized and probably the most well-known is **Neuromate**. Its development started in 1989 in Grenoble France (then owned by Integrated Surgical Systems LLC and now by Renishaw PLC) as a semi-autonomous system. This means, it is not designed to perform autonomous functions, but to improve a surgeon's movements. Neuromate was the first stereotactic neurosurgery robot to achieve FDA approval in the US and CE certification in Europe (in 1997) (Motkoski & Sutherland, 2016; Smith et al., 2016). Neuromate consists of a five DOF manipulator, it is an image-guided computer-controlled robotic system (Beasley, 2012; Cardinale et al., 2012). This system can be used in basically any stereotactic approach. The system is marketed for deep brain stimulation, stereotactic electroencephalography, transcranial magnetic stimulation, radiosurgery, neuroendoscopy and biopsies (Li, Zamorano, Pandya, & Gong, 2012; Xia et al., 2008).

The **ROSA Brain** (Medtech, France) is a 6 DOF robot mounted on a mobile chart. Like pathfinder the arm carries a needle guide. It is a stereotaxy robot and can perform precise needle and electrode placements such as brain biopsy, DBS and SEEG surgeries. ROSA has cooperative control over the needle and allows the surgeon to place the guide in desired position by manually moving the tool mount. The ROSA system can limit the

movements of the needles based on predefined limits (Virtual Fixtures) and therefore increase the precision of the needle placement (ROSA.). In 2011 Medtech surgical started the development of ROSA spine. ROSA spine is the spinal surgery version of ROSA which both have been used more than 1200 procedures. ROSA has received US FDA, EU CE and Health Canada approval.

Development of **Remebot** was first started in 1997 as a collaboration between researchers in PLA Navy General Hospital and Beijing University of Aeronautics and Astronautics. First version was using a PUMA 262 robot as a passive arm for stereotactic. In 2007 a new version of this system was introduced (Tian et al., 2008; Wu et al., 2014), it was a five DOF manipulator mounted on a mobile cart. It consisted of three components: operation planning system, surgical localization system, and telemanipulation operation system. The operation planning system was basically the IGS software portion of the system which provided surgeons with a suitable user interface. This system planned to handle DICOM images, render 3D model of the images and visualize the navigation. The surgical localization system was basically a five DOF manipulator, which is 40 kg in weight and was actuated by PLC-controlled stepping motors. The tool point of the manipulator was equipped with a needle guide, the robot was moving the guide to the correct position with correct orientation. After the guide moved to the correct location the surgeon performed the needle placement. The telemanipulation system is the system that facilitate the communication with the robot and consists of expected components such as network communication and video transmission. this system was used by a surgeon to remotely perform brain biopsies in 10 cases. The latest version of this system is called Remebot and is awarded the CFDA (China Food and Drug Administration) in 2015. The latest version uses a similar approach to the explained prototype but with a six DOF general purpose manipulator (the connection between CAS-BHD and Remebot is a conclusion driven by this thesis' author

based on the shared similarities in design and the team. No official document has been found to connect these two).

NeuRobot was introduced in 2002 by researchers in Imperial College of London, it is a 4 DOF manipulator to manipulate an instrument around a pivot point which is usually a burr hole on patient's skull (Auer, Starkie, Auer, & Davies, 2002). This system was developed mainly for manipulating an endoscope in neuroendoscopy. The 4 joints control the rotation of a cannula around the pivot point as well as a depth position. NeuRobot controller was developed based on a flight-simulator from Fokker control systems b. v. which enables the surgeon to control the manipulator with high precision and safety. For registration NeuRobot must be attached to a stereotactic frame. This also means if more than one trajectory for endoscopy is desired or the surgeon has to change the trajectory, the manipulator has to be repositioned again (Davies et al., 2000).

Ronna System was introduced in 2014. This system used a novel dual manipulators approach, master robot which was a 6 DOF manipulator and a 7 DOF manipulator as an assistant robot (Jerbic, Nikolic, Chudy, Svaco, & Sekoranja, 2015). Master robot holds a cannula in direction of a preplanned entry point in patient's head while the assistant robot or a surgeon perform the needle insertion. The surgeon could guide the assistant robot by hand while the system restricts the movements of the robot based on the operation restrictions. New version of this robot was used on real patient for a brain tumor biopsy with success (Dlaka et al., 2018).

Serial robots are easy to control, have excellent repeatability and their workspace is large compared to parallel robots. The robots introduced here are big and bulky while mounted on a cart. Their size is mainly due to the use of bulky industrial solutions as they traditionally offered the accuracy and rigidity needed for accurate stereotactic surgeries.

They are usually mounted on carts as their weight often prevents them from other mounting options, surgery table mount ceiling boom mount.

2.1.2 Stereotactic robots with parallel kinematic chain

iSYS is a needle guidance robot for biopsies on different parts of the body. It is a developed version of B-ROB or biopsy robot. B-ROB was developed for CT and ultrasound-guided biopsies, it was a 7 DOF manipulator which was mounted on a cart. The positioning structure which had 4 DOF was used to position the needle to the biopsy entry point (Cleary, Melzer, Watson, Kronreif, & Stoianovici, 2006; systems, 2019). B-ROB used a parallel structure for accuracy and modularity, and it can be used for biopsies on different tissues. The robot was equipped with a Needle Positioning Unit (NPU) for fine orientation. It has been tested on gel phantom with accuracy of 0.66 ± 0.27 mm in image guided positioning. This prototype was also tested for ultrasound guided biopsy, where the mean error (deviation of the needle tip from the target) was 1.1 ± 0.8 mm.

The **Renaissance** system was released in 2011 by Mazor Robotics (originally SpineAssist 2006 (Devito et al., 2010; Lieberman et al., 2006)). It was originally designed for spine surgeries (Hu, Ohnmeiss, & Lieberman, 2013; Ringel et al., 2012) however it was adopted to be used for neurosurgeries such as biopsies, minimally invasive surgeries, and electrode placement procedures. It consists of two different parts: a guide frame and a tool positioning robot. The tool guide is fixed onto the patient's spine or cranium in order to prevent any relative movement between the robot and patient. The robot is a six DOF parallel (hexapod) small manipulator (2.5 in diameter; 250 g) (Barzilay, Liebergall, Fridlander, & Knoller, 2006). Additionally, this robot can be mounted on a typical Mayfield frame if necessary. First using CT or MRI surgeon chooses the entry and target points and type of the robot mount (guide frame or Mayfield frame) (Joskowicz et al., 2006), then guide frame is fixed to the patient and registered via a registration jig. After

registration the manipulator guides the tools onto the right trajectory. Mazor Robotics published a minimum positioning accuracy of 1.5 mm ("Mazor Robotics Ltd. Renaissance," 2018) in a phantom study (Joskowicz, Shamir, Israel, Shoshan, & Shoham, 2011) which makes this robot an accurate biopsy tool.

Evolution 1 which was introduced in 2004, is a 4 DOF parallel manipulator (hexapod) mounted on a cart. Benefiting from the parallel manipulator features, Evolution 1 is a very precise robot with high payload, with reported absolute positioning accuracy of 20 μm (Nimsky, Rachinger, Iro, & Fahlbusch, 2004; Zimmermann, Krishnan, Raabe, & Seifert, 2004). Its high payload and the design of its tool holder allow this robot to incorporate different types of tools such as endoscope and surgical drill. This robot was controlled by a joystick while its infrared surface scanner allowed the system to register the patient using facial surface registration. This robot has high precision and payload and the ability of fine movements (10 μm motion resolution), however, hexapods are big and bulky, and it limits the surgeon's movements around the operating area.

Parallel robots are very accurate; however, they offer small workspace compared to their base footprint. Their target operating area should be planned carefully before starting the operation, as any additional target or bigger movements demand moving of the robot and reregistration.

2.1.3 Unusual approaches to stereotactic neurosurgical tasks

NeuroBlate project started in 1999 as a MRI compatible robot (Mohammadi & Schroeder, 2014; Voigt & Torchia, 2014). NeuroBlate is a two DOF manipulator that mounts on a stereotactic frame and has the ability to emit laser beam as commanded by a surgeon. Surgeon remotely controls the robot while it is inside MRI scanner bore. The stereotactic frame and the robot are MRI compatible and are visible in MRI image. This

system is only capable of working in a small workspace and changing operating area demands manual replacement of the robot.

The **ROBOCAST** project-an acronym of “Robot and Sensor integration for Computer Assisted Surgery and Therapy”- (FP7 ICT-2007-215190), started in 2008 aiming to resolve some mentioned issues with robotic neurosurgery, this project was aiming to develop a keyhole neurosurgical robot. ROBOCAST is a master-slave robot consists of a parallel kinematic structure with haptic feedback as master and a manipulator which is a chain of 3 different manipulators which in total delivers 13 DOF (Comparetti, De Momi, Vaccarella, Riechmann, & Ferrigno, 2011; De Momi, Cerveri, & Ferrigno, 2009). The three manipulators are: 1) Positioning arm (PathFinder) serial six DOF arm, which is used to position the tool point and therefor the connected 2 robots in a desired position; 2) Fine Positioner (Renaissance from Mazor robotics), a parallel six DOF as a fine positioner; 3) Linear Actuator with a on translational axes with piezo-actuator, which acts as needle insertion actuator with controllable depth. The system’s tool position was being tracked by an optical tracker (stereovision camera similar to what is being used in IGS systems) using optical tracking system as an external sensor allows the system to correct the position and orientation of the robots in case of error occurrence. ROBOCAST’s software consists of several subsystems such as preoperative planning, human computer interface, sensor manager, high level controller, haptic controller and safety check (De Momi & Ferrigno, 2010). The preoperative planning is able to plan the needle’s trajectory automatically based on information provided by the surgeon. Human computer interface system facilitates the interaction between surgeon and the system. Sensor manager gather and manage the data from ultrasound and tracking subsystems as an input to the controller. The controller receive all the information for other subsystems and calculates the kinematic positions for each part of the robot (Comparetti et al., 2012). The haptic controller facilitate the haptic interaction between robot and surgeon, system can send

haptic feedback to surgeon's hand based on the force applied to the linear actuator from brain tissue (De Lorenzo et al., 2011). This is done by a force calculation based on the velocity of the needle penetration. The safety check subsystem runs verifications on the other subsystems states and stops the probe in case of emergency (Comparetti, Vaccarella, De Lorenzo, Ferrigno, & De Momi, 2011). ROBOCAST system was tested on different models made from gelatin with largest position error of 0.6mm (Comparetti et al., 2012). The ROBOCAST project ended in 2011.

Mars is a stereotactic robot which uses an arc shaped arm to move a needle guide around patient's head. the arc is connected to a head ring which attaches to patient's head and provide rigid coordinates for needle placement (Heinig et al., 2011b).

These systems offer novel methods to problems however, their use is limited due to targeting only certain tasks.

2.1.4 Radio-surgical robots

Among all the aspects of robotics in neurosurgery, radiosurgery is the most matured aspect. Radio surgery follows the concepts of stereotactic surgery in which high dose of radiation is delivered to a precise target in the brain without any skull openings and incisions. Robotic radiosurgery has recorded millions of treatments with systems such as GammaKnife, CyberKnife and Novalis. GammaKnife is not considered a robot, however it uses robotic techniques to focus several beams of radiation on the tumor tissue to kill its cells (Bertelsen et al., 2013; Smith et al., 2016). Each individual beam is not strong to damage the healthy cells on the way but, when all focused at one point and on the tumor, they have enough power to damage the tumor. **CyberKnife** however uses an industrial multipurpose manipulator to deliver the radioactive beams to the desired tissue (Adler Jr et al., 1997; Iwata et al., 2011). CyberKnife is more precise than GammaKnife and it can be used for other parts of body as well. Novalis system uses a L shaped arm to deliver the

beams, this arm rotates around the patient while the patient is on an articulated table (J. C. Chen, Rahimian, Girvigian, & Miller, 2007; Sung, Song, & Kim, 2016; Teh et al., 2007). These robots have a unique task which demands special structures, which is out of aspects of this thesis.

2.1.5 Microsurgical robots

Usually microsurgery refers to surgical operations in which the targeted tissues (small vessels and nerves) are so small that for operating on them a surgical microscope is needed. These surgical techniques are being used in neurosurgery as well as other surgical disciplines. The challenge that surgeons are facing in microsurgeries is the fine and precise maneuvers they have to perform. Microsurgical robots use the manipulators abilities to perform these tasks more reliably than human surgeons. These systems are designed to follow surgeons hand movement, (often in master-slave system) correct them and then replicate them on the brain tissue. Usually in other disciplines of surgery the microsurgery techniques follow similar patterns. Therefore, some of the systems introduced here are able to perform more than neurosurgery.

Steady-Hand robotic system was developed in 1999 to enhance surgeon's abilities in microsurgery (Taylor et al., 1999). This system introduced a shared control over surgical tool between robot and surgeon. The robot could sense the forces imposed by surgeon's hand and the environment, using them to calculate the smooth action. Basically, smooth action means to actuate the instrument tremor free, precise and down-scaled force compared to surgeon's hand. The same team improved the design of Steady-Hand for a new microsurgical retinal surgery robot. The new system is called EyeRobot, a manipulator with three prismatic joints and two revolute joints ("Steady-Hand Eye Robot,").

The Robot Assisted Microsurgical System (RAMS) was introduced in 2001, a system by the Jet Propulsion Laboratory and MicroDexterity Systems, Inc (Le Roux, Das, Esquenazi, & J. Kelly, 2001). A master-slave system for microdexterity enhancement in microsurgery. It consisted of a master handle that can sense operator's commands in 6 dofs and a slave robotic arm with 6 dof dexterity. This system senses the hand movements of surgeon with 30 μm accuracy and position the robot with an accuracy of 10 μm .

In 2002 the microsurgical robot **Neurobot** (not to be confused with the neurobot in stereotaxy section) was introduced (Hongo et al., 2002; Takasuna et al., 2012). It is a master slave system with teleoperation capability. The surgeon can perform an operation remotely by controlling the slave manipulator with an input system (master manipulator). The slave manipulator is a tube shape consists of three sets of 3 DOFs micro manipulators and a rigid 3D endoscope, each micromanipulator can handle an instrument with minimum actuation of 20 μm . The slave manipulator outer diameter is 10 mm, the three micromanipulators each has 1 mm thickness and the endoscope has a 4 mm thickness. Slave manipulator is attached to a 6 DOFs supporting structure. Using simple directional switches, the surgeon controls the supporting structure to position the slave manipulator in a desired position. The master manipulator has the same 3DOFs configuration as micromanipulators and conducts the surgeon's hand input to the micromanipulators.

MM-1 is a microsurgical robot introduced in 2005 by researchers in University of Tokyo (Morita et al., 2005). MM-1 (Micromanipulator prototype 1) is a master-slave system with teleoperation capability. The slave system consists of two manipulators each with 6 DOF (Asai et al., 2004). The slave system is connected to a base which itself has six DOF. The master-system has two hand control manipulators with seven DOF control. This master-system also includes three footswitches to control the speed of the manipulator and the combinations of manipulator motions. The visual system for the

surgeon includes a HD video-camera system attached to a 300-mm microscope lens and a 3D display for surgeon.

In 2002, researchers at the University of Calgary (Calgary, Alberta, Canada), in collaboration with MacDonald, Dettweiller and Associates, began the development of a **Neuroarm (Symbis)**(Sutherland et al., 2013). Neuroarm is a robotic system capable of both microsurgery and stereotaxy surgery (Louw et al., 2004). Neuroarm is designed to be MR compatible so the surgeons can operate while the patient is in MRI scanner bore (Sutherland, Latour, & Greer, 2008) . Neuroarm consists of two 7 DOF manipulators, six spatial and one for tool actuation (Sutherland, Latour, Greer, et al., 2008). Because the size of the system is large, and it cannot entirely fit inside an MRI bore, image-guided microsurgery would be performed outside of the bore with the two manipulators, and stereotaxy operations by using a single arm, inside the bore of MRI magnet. The manipulators are mounted on a mobile base, the mobile base has height adjustment ability to accommodate the height of the surgery table. The manipulators are equipped with force sensors to measure forces applied onto tissue; this force information is relayed back to the surgeon's hand through the surgeon's remote station. As the surgeon operates the machine remotely there was a need for a 3D display which can relay 3D visual information acquired by the intraoperative MRI and other methods (such as stereovision cameras mounted on the system) to the surgeon. Neuroarm is also equipped with tremor filtering features which removes low-frequency tremors induces by surgeon's hands. The integrated motion scaling feature scales down the surgeon's movement in case it is needed (Pandya et al., 2009; Sutherland, Latour, & Greer, 2008). In 2010 Neuroarm was acquired by IMRIS a biomedical company which later in 2015 filed for bankruptcy which put Neuroarm's fate in jeopardy.

Raven project was introduced in 2005 by the BioRobotics Laboratory at the University of Washington (USA). They have designed this system aiming for a lightweight tele operative minimally invasive surgical robot (Rosen & Hannaford, 2006). The RAVEN II has a workspace design optimized through an observation of the kinematics and dynamics of surgical tools acquired from 30 surgeons who performed seven different surgical tasks (Hannaford et al., 2013) these tasks were performed while a passive manipulator was attached to the surgical tool. Using this passive manipulator (it is named blue dragon) and the embedded sensors in it the researcher has recorded the workspace characteristics of different surgical tasks. Raven II (the current version) consists of two seven DOF cable driven manipulators, the manipulators has a fixed base. Each joint of the manipulators is actuated by a DC motor mounted on the base of each manipulator, moving the motors to the base makes the arms small and light so actuation can be smoother. The RAVEN is controlled by a standard PC that runs the controller software on top of ROS (robot operating system). The surgeon console is equipped with commercial haptic controllers (from Geomagic Technologies) to control the two manipulators and also send haptic feedback to surgeon. This system has been tested in a transatlantic experiment, in which surgeons at Imperial College in London successfully controlled a RAVEN robot in Seattle using a regular internet connection. Off-the shelf technology used for this experiment, haptic controllers and software such as Microsoft Skype. The researchers have made Raven an open source project, aiming to develop a developers' community for this system and further its goals in motion planning, computer vision, machine learning software (Hannaford et al., 2013). This system has been designed for minimally invasive surgery and mainly for laparoscopic surgeries. However, it has also been tested for brain tumor surgery using head phantom models.

Morita microsurgical is a master-slave robotic system designed for neurosurgical microsurgery (Mitsuishi et al., 2013). This system was designed based on equipment and

patient configuration in a typical neurosurgical OR. The design takes the location of patient, a surgical table, surgical microscope and OR personnel into account. So, the system was designed to be easily movable and could be placed at an optimal configuration based on surgeon's preferences. The master system consists of two manipulators each with seven DOF. The gripper on the master manipulators was designed so that it mimics a pair of tweezers while surgeon is holding it. The gripper is also equipped with a small DC motor to apply a force mimicking the tension on a tweezers jaw. The slave system consists of two separate identical manipulators. These manipulators each have two kinematic structure, translation section to position the tool point in a desired position and an orientation component and place the tool in the right orientation. The orientation and translation of the tool was controlled independently from each other. The orientation structure has an arc shape with a remote center of motion (RCM). The mechanical decoupling of position and structure and the arch shape of the system helps to achieve a precise dexterous motion needed for robotic microsurgery. This system also has custom designed forceps to be used as the robot's tool.

The **ACTIVE** project (FP7 ICT-2007-270460) -acronym for “Active Constraints Technologies for Ill-defined or Volatile Environments” (The DG Information Society & Media)- is a project aiming to solve the problems with neurosurgical robots of the time namely the lack of touch feedback, the need for rigid frames of reference, difficulties with soft tissue manipulation (De Momi et al., 2014). It would tackle the traditional drawbacks of robotic systems which enter the operating room (e.g. encumbrance, slow execution, lack of interface ability, non-real-time controllability) working in close cooperation with humans. The main objective of the ACTIVE project was to use multi manipulator arrangement to build a complete surgical robot for soft brain tissue operation. The multi robot arrangement consisted two seven DOF Light Weight Robots (LWR, KUKA LWR4+), with low inertia, wide sensing capability (force, position) and fast access

controller, increases the safety while working around human users. The ACTIVE system has three control modes: 1. autonomous; the robot autonomously moves when operating away from the operating area or can maneuver tools on the surgical field; 2. tele-operated, in which a haptic master manipulator is used to control the movements; 3. hands-on, in impedance control mode where the surgeon moves the robot by manual control. In autonomous and tele-operated modes, the ACTIVE system is provided with dexterity capability for multiple arm coordination, high level control for space conflict resolution and environmental sensors for workspace sharing among humans and robotic coworkers (Meli, Pacchierotti, & Prattichizzo, 2014). The controller in tele-operated and hands-on modes used dynamic virtual constraints to increase the safety (Nicolai, Raczowsky, & Wörn, 2015).

In 2012 researchers in University of Maryland introduced a 3D printed spring-based continuum robot for MRI based neurosurgery this system is called **MINIR** (Minimally Invasive Neurosurgical Intracranial Robot). This is a maggot like robot with six DOF consists of three segments is developed consisting of three segments. This robot is actuated by tendons connected to actuators placed away from the robot. This robot has been tested in mock operations using dead animal tissues (e.g. cow brain) under MRI. The researchers are working on this project to develop an entire robotic system to be able to place MINIR on the skull and make it easier to use in an actual neurosurgery operation, and the possibility of using non-magnetic piezoelectric motors for enhanced reliability (Ho, Kim, Cheng, Gullapalli, & Desai, 2015).

2.1.6 Robots for general and assistive neurosurgery

Because of advancements in robotics and IGS technologies in recent years, researchers and medical companies have focused on robots with bigger range of applications and better adaptability to existing procedures, the newer systems offer more flexibility to accommodate different features as the researches advance. In the new trend of neurosurgical robots, we can see creation of robotic Microscopes such as **Modus** and light weight robotic systems with better adaptability such as **LWR** and **Medineering** arm.

TMS or Transcranial Magnetic Stimulation is a non-invasive operation in which a small part of brain is stimulated by inducing small electrical current in it, using electromagnetic field. This is done using a coil and electromagnetic induction principals. Axilum Robotics TMS-Robot is the first robot developed specifically to assist researchers and health care professionals for the positioning of a Transcranial Magnetic Stimulation coil. It includes a 7 DOF robotic arm and a 2 DOF, computer-controlled patient seat. Axilum Robotics has introduced the first robot for TMS. TMS-Robot helps doctors in positioning of Transcranial Magnetic Stimulation coil ("Robotic Assistant for Transcranial Magnetic Stimulation (TMS)"). It consists of a seven DOF robotic manipulator and a two DOF patient seat. The coil is mounted on the tool point of the manipulator with a contact sensor. The contact sensor determines if the coil is touching the patient's head before the stimulation starts. To position the coil in the correct position an IGS system is used to track the coil's position as well as the movements of patient's head. The coil is connected to a stimulator, which can be commanded using the controller software. The operation can be done automatically using preplanned simulation targets defined by the doctor. Once these targets have been defined in the IGS software the

system positions the manipulator tool point (thus the coil) in the correct positions, after ensuring that coil is touching the head the stimulation starts. During stimulation the system senses the movements of the head compensates the position and orientation of the manipulator for it. This system has been used in a brain to brain communication experiment in (Grau et al., 2015).

SemiAuto trepanation is smart craniotomy handheld device which can control the depth of a drill in a burr hole or craniotomy operation (Fontana, Korff, Follmann, Radermacher, & Schmieder, 2014). This is to protect the dura mater and reduce the bone gap compared to a traditional operation. This system is small, so it can be used without changing the existing surgical workflow. This system accepts a preoperative CT images together with the current position of the system as inputs and based on them adjusts the depth of drill penetration. This system can be registered to a standard optical tracking system to be provided with its relative position.

Modus is a robotically operated digital surgical microscope ("MODUS V, Fully-automated, robotic digital microscope," ; Waqas, Enam, Hashmi, Mubarak, & Arain, 2017). This system consists of a robotic arm which carries optical equipment attached to its tool point. This system has two visual modes, classical microscope which shows the zoomed in view of operating area and wide camera which can show a bigger portion of the operating area. This helps surgeon during the operation when they need a wide view of operating area without zooming out or moving the microscope away. Modus has two modes of control, manual mode which surgeon can move the tool point of the robot by hand and automatic guide in which the robot moves based on the predetermined positions. Modus can be integrated with an IGS system to track its position relative to operating area. In the automatic control mode modus can be set to position itself based on the location of IGS probe.

In 2011 DLR Germany introduced a light weight robot LWR, with goals to perform different types of surgeries such as cranial neurosurgery and laparoscopy (Hagn et al., 2008). The new version is named **MIRO** and is based on older version KINEMEDIC. MIRO has six DOF. As the design approach in MIRO was focused on weight, the accelerated masses are relatively low, this improves the safety of the system while in operation. As MIRO was designed to be compact, it is possible to use multiple MIRO robots in one operating room. Similar to DLR light weight robot (Albu-Schäffer, Ott, & Hirzinger, 2007), MIRO uses torque sensors for a human-robot collaborative environment. However, compared to LWR, MIRO uses a slimmer design with dedicated groups of joints with intersecting axes. The MIRO robot has two main control modes, which can be selected by the application. The first one is position control mode, in which the robot is commanded by the software to follow a certain trajectory. In neurosurgical applications this mode is required for stereotaxy operations like needle placement. The second mode is called the compliant mode, in which the robot follows the users command induced manually on the robot. In this mode, the surgeon can move the robot to a desired position and orientation by hand. In this mode the manipulator follows the manual command unless the commanded position and orientation is restricted by the controller software. These restrictions can be defined based on the application for example the sensitive areas in brain like blood vessels can be used as restrictions in a biopsy application. This manipulator has not been used in neurosurgical head models and not yet on real patients Medtronic company is working with DLR to release their version of surgical robot in 2018.

Medineering positioning arm is a robotic manipulator designed for surgical applications. It is designed with a modular tool point which can receive different types of surgical mechatronic devices and position them in a desired position. It has 7 DOF. Currently Medineering is collaborating with BrainLab in their **Cirq** system (BrainLab,

2018). Cirq is a neurosurgical system based on Medineering positioning arm that can perform needle guidance, drill depth control and guidance. Because of the modular design of this system, it is considered to be future proof if new applications have been developed. Medineering also offers a research version of their positioning arm in which researchers have access to all sensors and interaction modalities of the Intelligent Positioning Device. An example of applications and modularity of this arm is the Medineering endoscope Guidance Robot which is a compact robot that can hold and orient during transsphenoidal surgeries. This compact robot should be connected to the tip point of the Medineering positioning arm and using the modular connection it can power up and communicate with controller software. The positioning arm keeps the endoscope holder in place.

Looking at stereotaxy robots it can be concluded that they have the following common features (Understandably, the radiosurgery robots are not considered in this comparison as they are not used in open surgeries):

- They are using image guided techniques either live images or pre-operation images.
- The tool is usually a needle guide without any actuation.
- They use stereotactic approaches frame-based or frameless.
- It is usually the surgeon that perform the operation and the robot is for support and guidance.

These robots have proven their ability in stereotaxy operations. They are accurate, and they have features to make stereotaxy easier such as frameless registration. They introduce features to make stereotaxy more reliable such as being able to operate inside medical scanners. However, their functionality is narrowed down to stereotactic surgery and this makes them not cost efficient enough for smaller medical centers to afford. In this list only, few such as Neuromate and ROSA are considered commercially successful,

many were just one-off projects or are considered costly as well. Clearly, these robots have been created to answer a demand, which is the need for a faster, accurate and reliable method for needle placement to replace stereotactic frames, and they have. However, IGS systems to a great deal have been replaced stereotactic frames and only for very accurate procedures (for example DBS and deep brain biopsies) the frames are still being used. Therefore, the stereotactic robots have started to include more autonomous features to prove their necessity in neurosurgical operating room as the IGS systems have done (Smith et al., 2016). With slight difference, this has been the trend in microsurgical robots as well.

Microsurgical robots focus on fine movements of the tool inside operating area and:

- The surgeon is controlling the robot using another articulated arm (slave arm).
- Usually equipped with force feedback from the operating area.
- The robot is performing the invasive task
- Usually teleoperated with movement correction ability

Compared to stereotaxy robots, microsurgical robots are more complex, and it can be observed that they possess (or they have aimed to) stereotaxy features as well. Microsurgical robots are beneficial for hard to reach areas or very delicate operations which is impossible to achieve by human hand. For other disciplines of surgery, the microsurgical robots such as Da Vinci have been more successful in convincing surgeons to perform the operation robotically, the neurosurgeons on the other hand are hesitant to leave these tasks to robots as currently it increases the time of operation, alters flow of surgery and brings up the cost for patients. This will be changed as neurosurgical robots are introducing more features to widen their range of applications and robots' structures are getting smaller.

From early basic systems such as MINEVERA to more complex systems such as Neuroarm the focus has been on developing a robot surgeon which removes the surgeons out of surgical field and grab the invasive task from them this has caused in having systems with big footprints. However, starting from 2013 there was a shift in neurosurgical robots' innovation, focus is shifted towards general neurosurgery and assistive tasks. Companies and researchers have started to design more general-purpose robotic systems such as Modus, a robotic microscope that can be used for many neurosurgical operations or Medineering arm which acts as a holding platform for robots and surgical tools. This is a trend indicating cooperative robotic surgery and more robots which enhance surgeon's ability and not replacing it. This does not mean the stereotactic and microsurgical robots will disappear but an increasing trend in the assistive robots.

The robot in this thesis is an example of this trend which contributes to the goal of having a robot for general neurosurgery. This robot makes robotic more accessible to neurosurgeons by first, being smaller and portable, second, being a standalone IGS system which widens the range of applications it can be used for. Portability with wider range makes the return of investment faster therefor, brings the overall cost of the robot lower.

2.2 The methods of patient registration in neurosurgical robots

As mentioned, image-patient registration refers to calculating the transformation conversion between patient's physical coordinates and patient's image coordinates. Different techniques have been used to achieve this (Eggers, Mühlhling, & Marmulla, 2006; Woerdeman, Willems, Noordmans, Tulleken, & van der Sprenkel, 2007). Technology has moved from early frame-based registration approaches to modern auto-registration using intraoperative imaging. In the early days of neurosurgical robots, frame-based registration was the reliable registration method. As the IGS technology advanced the frameless techniques also gained more attentions. IGS systems are usually packed with multiple

registration capabilities to accommodate different surgical scenarios. As robots started to merge with IGs software, they also benefited from several registration capabilities.

Neurosurgical robots as an extension of IGS systems have incorporated variety of this techniques. These techniques are reviewed in this section. It should be noted that most microsurgical robots are based on microscopic vision control and usually do not need position feedback in relation to patient's head therefore, no registration was needed for them.

2.2.1 Frame based registration

The frame is attached to patient's head and the robot rigidly, so it can be used as a registration tool. This way the patient's head will be in constant relation to the robot during the surgery. This method is arguably the most precise registration method; however, it is proved to be cumbersome for bigger operating areas.

The robots that use only frame-based technique are Minevera, NeuRobot and Neuroplate. Minevera manipulator had CT visible markers which provided position feedback for the surgeon while targeting a lesion or pathology. Neuroplate is mounted on an MRI compatible frame (AXII frame).

2.2.2 Anatomical landmark registration

In this method few distinct anatomical landmarks on patient's head such as the tip of the nose, the angulus oculi, the tragus on the skin surface or the spina nasalis are identified and marked in the image same set of points are located on patient's body (usually by touching them using a tracked instrument). The software then calculates the transform between the two (usually using a numerical method such as least square). This method is one of simplest registration methods as there is no need of markers attached to patient.

However, it is not as accurate as other frameless techniques, the landmarks are usually located on soft tissue which can be shifted during the surgery.

2.2.3 Fiducial based registration

Fiducials are usually referring to markers which are visible both in medical scanners and normal vision. Fiducials are attached to patient's body before patient going through scanning procedure, they are kept in their place and later their location are recorded by an IGS system (either manually or automatically) for registration (Mani & rivazhagan, 2013). Fiducials can be attached to skin and bone (Salma, Makiese, Sammet, & Ammirati, 2012). Skin fiducials pose bigger error compared to bone and mask fiducials mainly due to skin shift and higher probability of fiducials changing their original position. Bone fiducials are very accurate however, putting them is often invasive as access to bone tissue is needed (Widmann et al., 2010). There have been attempts to rigidly attach fiducials to patient's head without invasive approaches such as

Neuroarm and Pathfinder are reported to use this method of registration. In Neuroarm system registration of patient is done using MR visible fiducials on the IGS level and touching these fiducials with a digitizing arm (an articulated arm which is attached to same platform as the Neuroarm). A very distinct feature of Pathfinder is the use of fiducial markers on patient's scalp or skull to track the head movements in real-time (Deacon et al., 2010). These markers are reflective to be visible by the camera system attached to the robot and also visible in CT scans (M. Eljamel, 2007; Morgan et al., 2003). These markers allow the robot to be moved inside the OR without the need of reregistration (Sivakumar, Smith, Morgan, & Byrne, 2003).

In the **Renaissance** system fiducial markers are located on a registration jig. Registration is performed by scanning of point cloud containing the registration jig and patient's ears and forehead by a laser scanner (Joskowicz et al., 2005; Ruby Shamir et al.,

2005; R Shamir et al., 2006). Using x-ray image and the attached markers the patient-image registration is performed.

2.2.4 Surface matching registration

Surface matching refers to scanning patient's facial surface and match it with the same surface in the 3D render of medical image. In fiducial based registration there have to be two sets of paired points in other words, each point in physical coordinates has to correspond to one point in image coordinates. This is done by rescanning the patient with attached fiducials. In surface matching, rescanning is not necessary as there are no paired points. The two set of points go through optimization algorithm which calculate the closest conversion between the two and use it as registration transform. The most common algorithm to do this is ICP (Iterative Closest Point)(Besl & McKay, 1992).

There are various methods on scanning the physical surface. Scanning using contact tools such as an IGS probe, scanning using noncontact methods such as using laser pointers to scan the face and using combination of laser projector and stereoscopic camera for scanning (X. Chen, Song, & Wang, 2014; Raabe et al., 2002; Zhou et al., 2016). Robots have been used to perform surface scan as well by using force sensors connected to tool point as scanner (Glozman, Shoham, & Fischer, 2001), however, contact scanning poses issues such as being slow and in case of skin scanning it may coz skin to move therefor, a wrong position may be recorded.

2.2.5 Frame-based versus Frameless registration

Neuromate has two modes of operation, the conventional frame-based systems and a frameless mode (Varma & Eldridge, 2006). In frameless mode, a reference frame is fixed onto the patient cranium. Using this reference frame CT and MRI localization markers are mapped to physical space. The robot then moves the mounted guide into position which has been determined by the surgeon. Then the robot is fixed so it provides the

rigidity for the surgeon while a surgical tool (such as a probe or drill) is guided through the mounted guide. Neuromate delivers sub-millimeter accuracy (0.86 mm) in a frame-based configuration and millimeter accuracy (1.95 mm) in a frameless configuration (Cardinale et al., 2013; Li et al., 2002; von Langsdorff, Paquis, & Fontaine, 2015).

ROSA also benefits from having two modes of operation with stereotaxy frame and frameless operations. For planning purposes, patient undergoes MRI scan, which helps the surgeons to plan the trajectories for needle or electrode placement (Gonzalez-Martinez et al., 2014; Serletis, Bulacio, Bingaman, Najm, & González-Martínez, 2014). The MRI image is then registered to a CT scan image (pre-op or intra-op) to have a better geometrical accuracy. It is recommended (Michel Lefranc et al., 2015; M Lefranc & Le Gars, 2012) that for a better registration accuracy, an intraoperative Flat-Panel CT can be used. Using the MRI/CT merged image the robot performs registration based on the chosen approach, frame-based or frameless. In the frameless mode ROSA scans for fiducial markers attached to patient's scalp or skull (Michel Lefranc et al., 2014; Medtech, 2010). ROSA's accuracy is reported to be below 1mm for frame-based fiducial registration and a 1.22mm for frameless surface registration (Michel Lefranc et al., 2014). ROSA is praised for its flexibility to integrate with existing surgical workflow in many institutions and, it's variety of options for patient registration.

Table 2.1 shows registration method used in each neurosurgical robot introduced here. There are many associated with IGS registration. This refers to the use of an external IGS system (software and tracker) for registration and surgical navigation features. The robot is usually registered to the IGS tracker and when image-patient registration performed the robot would also be considered registered to the patient. Using robots in conjunction with an external IGS has advantages. IGS acts as external position tracker for the robot to

improve tool positioning error, an approved clinical IGS system can also help in clinical certifications approval as the tracking system already fits the specification guidelines.

When an external tracker is used in combination with a surgical robot, they usually have a detached stereo vision camera that is movable around the OR for better view over operating area or it is another type of tracker, such as the mechanical tracker in Neuroarm, which is connected to same platform as the robot. Using a detached camera for a moveable robotic system suggests separate boom and trolley, this leads to bigger footprint of the robot, even when it is connected to same platform as the robot it still needs a bigger footprint as it can be seen in Neuroarm and the camera in Remebot system. In Remebot robot, a stereovision camera was used to perform stereoscopic localization as external position sensor for the manipulator, using additional markers attached to surgical tools and patient's head. This camera is connected to same trolley as the robot is.

As the most common tracker (digitizer) used in IGS systems are optical trackers. And as mentioned before, they suffer from line of sight issue which may limit robots' movements and its positioning as the camera always needs a direct line of sight to robot's tool point. Using electromagnetic trackers solves the line of sight problem however, it may cause interference when it is used near to robot's metal body and DC motors.

Table 2.1 list of neurosurgical robots introduced in this chapter

Project	Main task	Size and Structure	Year of introduction/development	Control	Registration Method
Minevera	CT compatible for live CT operations	Big 6 DOF manipulator attached to a stereotactic frame	1989	Image (CT) guided	Live fiducials reading by intra-op Ct scanner/frame attached
cyberKnife	Stereotactic image guided radiotherapy	6DOF industrial manipulator	1997	Image guided	Registration using IGS with live imaging.
CAS-BH5/ Remebot	Stereotactic	5 DOF manipulator	1997	Image guided	IGS optical registration
NeuroBlate	MRI compatible stereotactic laser surgery	Small 2 DOF head frame mounted	1999	Surgeon	No registration- the robot's frame is visible in MRI/ Frame attached
Eye Robot/ steadyhand	Micromanipulation for Microsurgery and needle placement	Small kinematically decoupled robot, separate XYZ, orientation and RCM structures.	1999	Shared control	No registration, robot corrects surgeons hand movement.
NeuroBot (Imperial college of London)	Neuroendoscopy and Stereotaxy	Cart mounted 4 DOF, 3 Revolutions and 1 prismatic plus passive xyz	2000	Surgeon and Image guided	Frame based registration
Symbis/ neuroarm	Microsurgery and Intra-op stereotactic surgery	Two MRI compatible big manipulators with seven DOF each	2001	Surgeon and image guided	IGS registration based on MR visible fiducials and digitizing arm connected to the robot
Neuromate	Stereotactic surgery and target guidance (drill, endoscope, etc)	Highly accurate 5 DOF manipulator with big footprint.	2002	Image-guided	Two modes, frame based and frameless. Using IGS techniques to register in frameless mode
RAMS	Study of microsurgery on rats	Master-slave small and accurate (10 μ m) six DOF manipulator controlled	2002	Surgeon	No registration control solely by vision
Neurobot(Shinshu University, Japan)	Microsurgery	Three micro manipulators each three DOF. Small robot but the supporting structure is big.	2002	Surgeon	No registration, surgeon control the micromanipulators remotely.

Novalis	Stereotactic image guided radiotherapy	Big L shaped rotating arm	2004	Image guided	Registration using IGS with live imaging.
Evolution 1	Neuroendoscopy and Stereotaxy	4 active DOF parallel Manipulator	2004	surgeon	IGS registration
MM-1 and MM-2	Microsurgery	6 DOF Master-slave manipulator with 2 micromanipulators	2005	Surgeon	Not registered
Raven 1 and 2	Microsurgery and telesurgery	Two 7 DOF cable driven table mounted manipulators	2005	surgeon	Not registered
iSYS	Needle placement	Parallel manipulator held by holders on top of the operating area.	2006	surgeon	IGS auto registration using intra-op CT
Pathfinder	Stereotaxy	6 DOF serial manipulator on a cart with big footprint	2006	Image guided	Fiducial marker-based registration
ROBOCAST	Research in Stereotaxy	13 DOF chained robots	2008	Image guided	IGS registration
Active	Research in surgical robot interactions and safety	Two seven DOF manipulators	2008	Surgeon guided	Not registered
MIRO	Stereotaxy and general surgery	Six DOF table mount manipulator	2008	N/A	Not specified
Renaissance (based on spineassist)	Stereotaxy needle placement	6 DOT hexapod parallel manipulator, small structure but small workspace as well.	2011	Image guided	Registration is done with scanning patient's face and a registration jig which robot attach to
Rosa	Stereotaxy, precise needle placement	6 DOF cart mounted robot with big footprint	2011	Image guided/surgeon	Frame based and frameless registration
MARS	stereotaxy	Six DOF with an arc	2011	Image guided	IGS registered
MINIR	Research on MRI compatible microsurgery	Maggot like 3D oriented 6 DOF robot	2012	surgeon	Not registered
MORITA microsurgical	Microsurgery	Two 7 DOF decoupled cart mounted manipulator	2013	Surgeon	Not registered
SemiAuto Trepanation	Safe Trepanation	One DOF Handheld tracked drill	2014	Surgeon/Image guided	IGS registration
Ronna	Stereotactic surgery	master, 6 DOF and assistant 6DOF manipulators	2014	Image guided	IGS registration

TMS robot	TMS	7 DOF manipulator and 2 DOF seat	2015	Image guided	IGS registration
Synaptive modus	Robotic microscope	6 DOF cart mounted manipulator	2016	Image guided/surgeon	IGS registration
Medineering positioning arm	Multipurpose	7 DOF table mounted lockable arm	2017	Image guided	IGS registration

University of Malaya

CHAPTER 3: METHODOLOGY

Manipulator design has been a topic of research for decades, literature is rich with different methods of designing a robot. There is no unified method to address questions in robot design problems. Every author had their method to answer questions regarding kinematic structures and dynamic performance of a design (Jain, 2010; Martínez Verdú, María Sabater Navarro, José González Penella, Manuel García Aracil, & Miguel López Buendía, 2013). This is mainly due to huge differences in applications and requirements of robots. Even in neurosurgery, which is a much narrower subject of robot design, it could be observed from the literature review that the approaches to this subject are vastly diverse. In this thesis the methodology for design and development of this robot, has been chosen to use computer aided design, simulations and physical prototyping. Figure 3.1 shows flow chart describing the methodology of this project.

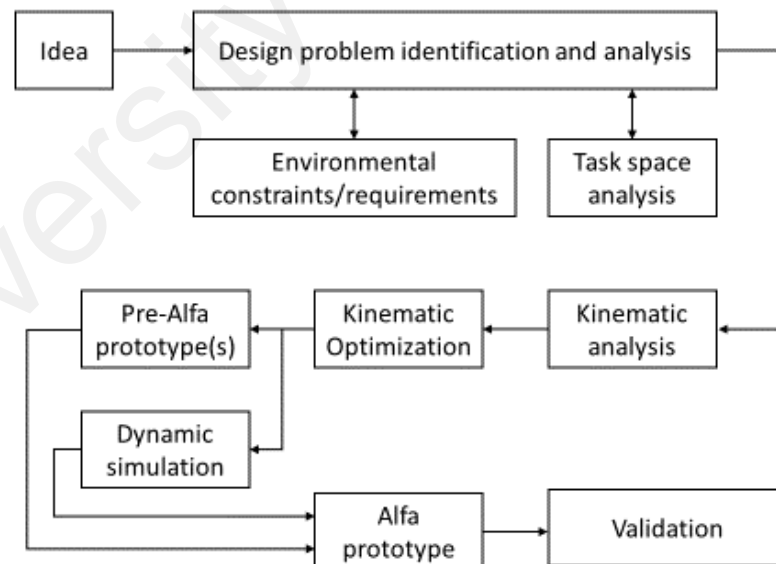


Figure 3.1 The flow chart describing steps taken for this project.

The first step was to identify the design problem requirements and constraints, such as size of the robot, the objectives to be achieved and the safety concerns. The objectives have been discussed in the introduction chapter and are analyzed and translated into

design requirements in the design and development chapter (Chapter 4). The physical problems analysis was done using task space analysis and observing the environment in which the robot is intended to work. Task space analysis carried out with observing and recording position of selected instruments during live surgeries. Methods regarding task space analysis has been discussed in next section of this chapter. Each step mentioned in Figure 3.1 has been introduced in this chapter.

Kinematic analysis- Designing a robot involves answering technical questions about kinematics of the robot. Questions such as, how many degrees of freedom (DOF) the robot needs, what topology is suitable for the targeted tasks and the details about mounting of the robot. Answering these questions demands details about the tasks which robot is going to perform and the specifications of the task space, which was concluded in the first step. DOF determines the level of dexterity a robot has, higher numbers mean the robot can reach more positions and orientations, and it also means more complexity both in mechanical and controlling aspect of the robot. Topology of a robot refers to the structure of the robot, is it a parallel or a serial manipulator? How many of the joints are revolute and how many are prismatic? And how all these joints are connected to each other. Finally, the mounting dictates the origin of the kinematic chain, its position dictates shape and size of the robot's workspace and links.

Kinematic optimization- Based on the answers obtained from the kinematic analysis, the kinematic chain must go through an optimization to find the most optimum design. Some of the kinematic parameters have been optimized based on the defined requirements and constraints. Due to the importance of manipulator's size in this project, the parameters that are used for optimization are lengths of the robot's links. In this thesis the kinematic optimization produced three different kinematic structures with different size and topology to be chosen so, further analysis was required.

Pre-Alfa prototypes- based on the results of kinematic optimization of the three structures three early prototypes were developed and tested. These prototypes were used to test the kinematic design's workspace, functionality and rigidity. Besides design and functionality, different hardware was also needed to be tested therefore, each of these prototypes have been carefully planned to use different hardware such as body, brakes and servo motors. These prototypes are named pre-Alfa as their sole purpose was to enable the decisions for the design and hardware of the Alfa prototype.

These prototypes were also used as a proof of concept which were capable of registering head models to their medical images, which was done using landmark registration. As mentioned in the introduction chapter patient-image registration depends on scanning the sample points. Different types of scanning methods are being used by clinical IGS systems. Methods such as scanning patient's facial surface with IGS probe or laser pointer (in a sweeping motion). Instead of a sweeping action IGS probe can be used to touch known landmarks on the face. Basically, any method that can provide IGS software with position information from points on patient's head can be used as point scanning method. There are automatic methods in use as well. These automatic methods use integrated medical scanners to scan a reference array (reference star or additional array) together with patient's head. The medical image contains the reference array in relation to the brain image which means the registration transform function can be calculated without manual facial scanning. The concept of automatic registration without using medical scanners and using a 3D camera attached to the robot's body, is explored later in this thesis. Although, the method developed in this thesis is considered semi-auto registration as it need input from user on the IGS software side.

Dynamic simulation- the dynamics characteristics of the three optimized kinematic chains were tested using software simulation. Dynamic analysis usually deals with the

tool and joints velocity, acceleration and torques. The needed speed for the surgical tasks are not a topic of great importance and they can be performed with low speed and no acceleration (this is preferred because of safety concerns as low speed means smaller impact force) so, in the dynamic simulation the torques imposed on the joints were recorded while the simulated manipulators were performing maneuvers in low speed. The stall torque was also another topic of interest in these simulations and the value needed in each joint of the manipulators to keep a load in steady position. Later, during the development stage to ensure a low impact force the torques, velocities and accelerations of the servo motors were limited to low values inside the internal controllers of the servo motors.

Alfa Prototype- this prototype was developed based on the results obtained from previous design steps taken in this project, it is the first fully functioning prototype which was used for validating the objectives of this thesis. This prototype has not been used (or intended to) in any clinical trial, the results delivered by this prototype or any flaw founded in the design will be used in developing a clinical trial prototype (Beta prototype), which is out of the scopes of this thesis. This prototype was used in different experiments using 3D printed anatomical models which their details are presented in the results section of this thesis. The details of methods used for validation and to obtain results are presented later in this chapter in the validation section.

3.1 Task space analysis

Task space is the summation of positions and orientations the robot's end effector must take in order to perform the required tasks. In contrast, the workspace of the robot is the total of all positions and orientations the robot can take. So, in other words, the robot should be designed so that its workspace contains and covers the full task space. The workspace can be bigger than the task space as long as it covers the task space but, cannot be smaller.

Based on early observations from real surgeries it was hypothesized that in neurosurgery the targeted task space is a cone shape containing the operating area. The operating area is usually positioned upwards or tilted sideways (to provide better access to the surgeon). Which means, the workspace does not need to cover the bottom area (under the patient's head). The patient's head is placed in the center and bottom of the cone (Figure 3.2).

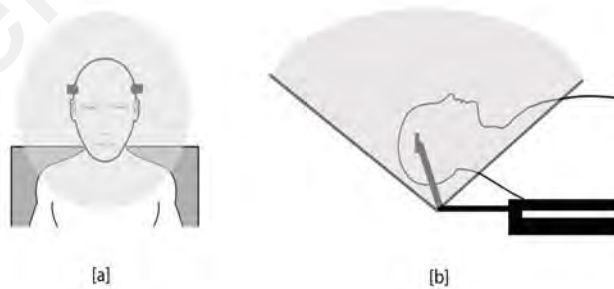


Figure 3.2 Task space of the manipulator from [a] top view and [b] side view

The exact dimensions of this cone vary and depends on the tasks targeted by the manipulator. For example, the cone can be small if the manipulator is only targeting endoscope handling, or large if the manipulator is designed to place Stereo-electroencephalography (SEEG) probes in the brain. The orientation of the tool is

predicted to be in line with the depth of operating area but again, the exact values can vary, exact dimensions are very unlikely to be found as this cone also depends on the patient's anatomy, which is different for each patient. Therefore, a proper method had to be used to measure the task space in multiple operations on different patients to have a more comprehensive understanding of the task space.

A method had to be used to map the movements of surgical instruments in a 3D space while they are being used by a surgeon. This could be accomplished using many devices such as a multi axis articulated arm or a stereoscopic camera (optical tracking). An excellent example of workspace study is the Blue Dragon system (Rosen et al., 2002). It is a passive articulated arm with position, force, and torque sensors that can record the desired data in a laparoscopic surgery. This system is used in dry labs and animal experiments. With the data gathered from this system, researchers developed Raven, which is an open source robotic system for research in surgical robotics (Hannaford et al., 2013). While the method used in Blue Dragon is very effective in determining the task space of robots in laparoscopic surgery, it is not suitable for neurosurgical surgeries. This, and many other similar works, are designed for use in laparoscopic surgery (Smith et al., 2016), making it unsuitable for neurosurgery. As mentioned, neurosurgery is structurally different from laparoscopic surgery for several reasons. First, the field of view in neurosurgery is generally smaller, as surgeons work through small openings in the skull (craniotomies) or in areas of endoscopy in the brain where the working area is limited to a single port. This changes in abdominal or thoracic surgery, as the organ of interest is contained in an open cavity (Peritoneum and Thoracic Cavity) that allows a wider field of approach and endoscopic surgery in these areas to be carried out via multiple ports of entry. This creates enough free space around the tools and the surgeon's hand so that it can move freely, making it easier to attach an articulated arm such as Blue dragon to the laparoscopy tools. Second, in laparoscopy, the entry point is used as a passive spherical

joint for the tools, while in neurosurgery (and neuro-endoscopy) there is no location for such a joint.

Another problem with systems such as Blue dragon is their usage in real-time surgeries. Introducing a new instrument to a real surgical operation presents ethical challenges, such as issues regarding the contamination of the instrument, danger to the patient, and maybe the most important one, possible interference with the operation. It is possible to design and develop an articulated arm to rectify these problems but, it can be costly and time consuming. However, an alternative approach is to use non-contact methods. Methods such as optical tracking to track the surgical instruments. Using non-contact methods solves the ethical issues associated with the articulated arm method and delivers six axes of measurements in the limited space of Neurosurgical operations.

IGS trackers (localizers) are usually non-contact trackers (Cleary & Peters, 2010; Keereweer et al., 2011) and they are being used in real neurosurgeries, using them as trackers for task space analysis, was not going to cause any interference with any surgery. So, a method was developed to use the data from the IGS system inside OR to quantify a desired task space. The open source software library IGTLINK (Lasso et al., 2014; Tokuda et al., 2009) was used for this purpose. This library facilitates the communication between medical image scanners, IGS systems and robotic systems. The IGS system used in this method is BrainLab Curve. This system has the feature to connect to other devices using IGTLINK protocol. This makes it possible to read and use live surgery data without interfering with the flow of the surgery and impacting the clinical status of the IGS device¹. IGTLINK only handles the communication between devices so another program was needed to use IGTLINK protocol and record the data from BrainLab device. A Matlab

¹ The intension was not to touch any of the internal hardware or software of this clinical device.

program was developed to take care of this matter. This program could connect to BrainLab IGS and record the position data of patient, tracked instruments and reference star. The MATLAB program also recorded the time stamp of the movements to be able to recreate them if needed. The surgery would go on as planned without any interference from the researcher and the extra devices connected to the IGS system. These experiments were performed (in order of occurrence) as follow:

1. The researcher connects the computer containing the recording software to the same network as the IGS system.
2. The researcher sets network settings so that the program can connect to the IGS (IP addresses and port numbers) and starts the program.
3. The surgeon imports the patient image data in the IGS and register the patient.
4. The surgeon will be prompted to accept the new IGTLINK connection.
5. The surgeon continues the surgery as planned.
6. The IGS data is recorded as the surgery goes on.
7. After the end of surgery, the program is stopped, and the computer is disconnected.

The BrainLab system was able to provide the MATLAB program with tracking data of different surgical instruments such as IGS probe (pointer). The IGS probe is the standard tool of any IGS system, and usually, surgeons use it like a pointer in surgeries. However, if tracking extra instruments are needed, the surgeon can configure the system, so the extra instruments can be tracked by the IGS. The IGS probe was a suitable instrument for this task space analysis as it was being used in various stages through the whole process of surgery from beginning to end. However, to have better understanding

of the task space, in addition to the probe, usage of other instruments has also been recorded through the progression of this study.

Before experimenting on real surgeries, basic studies were conducted to fine-tune the programs and algorithms. These basic studies were conducted in dry lab conditions. A series of experiments on surgical models were then conducted. These models are anatomically precise, and mimic brain tissue and pathologies (Waran, Narayanan, Karupiah, Owen, & Aziz, 2014; Waran, Narayanan, Karupiah, Pancharatnam, et al., 2014).

Three instruments were used in the dry lab experiments; namely the IGS probe, a dissector, and an endoscope. As the dissector and endoscope are not standard IGS instruments, they needed to be registered (calibrated) to the system before the system could track them. Registering an instrument to an IGS with an optical tracker is done using the provided attachments. These attachments have a known geometrical shape (to the IGS system) with infrared reflecting markers (in this case the markers are reflective balls) to allow the IGS to recognize them. Figure 3.3 shows the process.

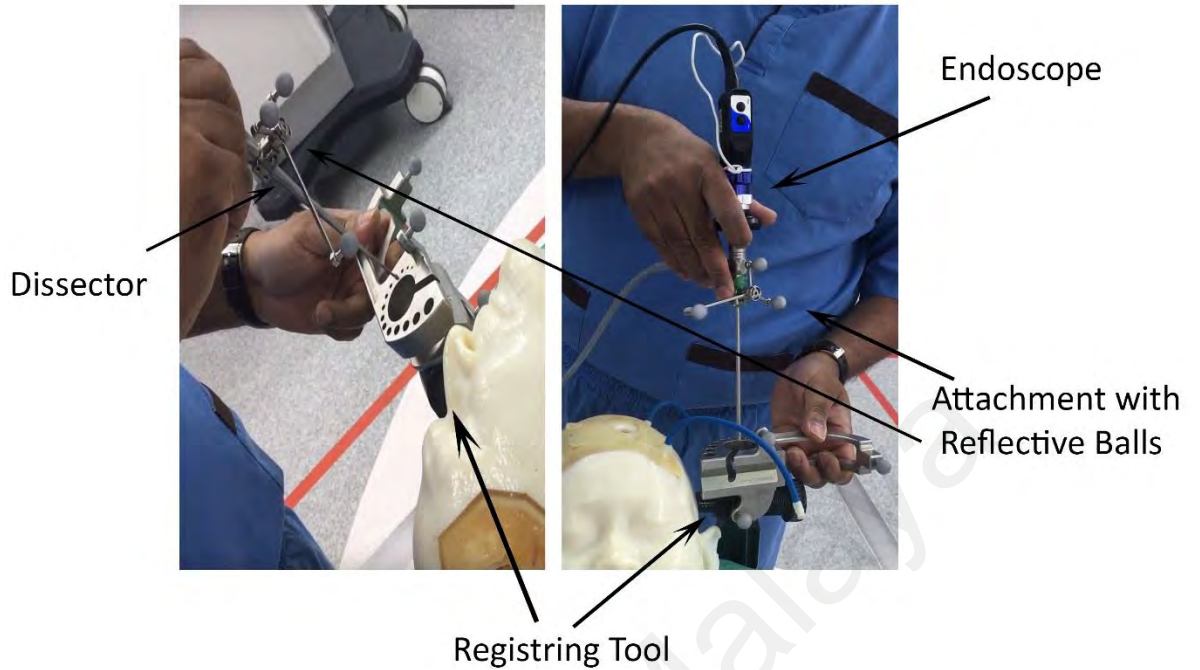


Figure 3.3 The process of registering a dissector and an endoscope to the IGS system. Using the registering tool, the IGS can calibrate the new tool by calculating the length and thickness of it.

Two types of mock surgeries were conducted during the dry lab experience. One was performed as a tumor resection, while the other for brain endoscopy intervention. The mock surgeries were carried out in different steps, with the details of used instruments presented in Table 3.1. During each step, the position and orientation of the instruments were recorded using the program developed for this experiment.

Table 3.1 The steps performed in the mock surgeries and the instruments used in each step.

	IGS Probe	Dissector	Endoscope
Marking the Skin	✓		
Marking the bone	✓		
Check the entry on Dura	✓		
Finding the edge of the tumor	✓		
Removing the tumor		✓	
Endoscope assisted intervention			✓

Figure 3.4 shows a sample diagram for combined position data acquired from the tumor resection mock surgery. The virtual cone shape workspace is marked. Most of the points are above the surgery table level. Few points are outside the cone and under the surgery table level. These points are recorded while surgeon was handing over the instrument to assistant or putting them down on the instrument table. As expected, the operating area shows concentration of activity.

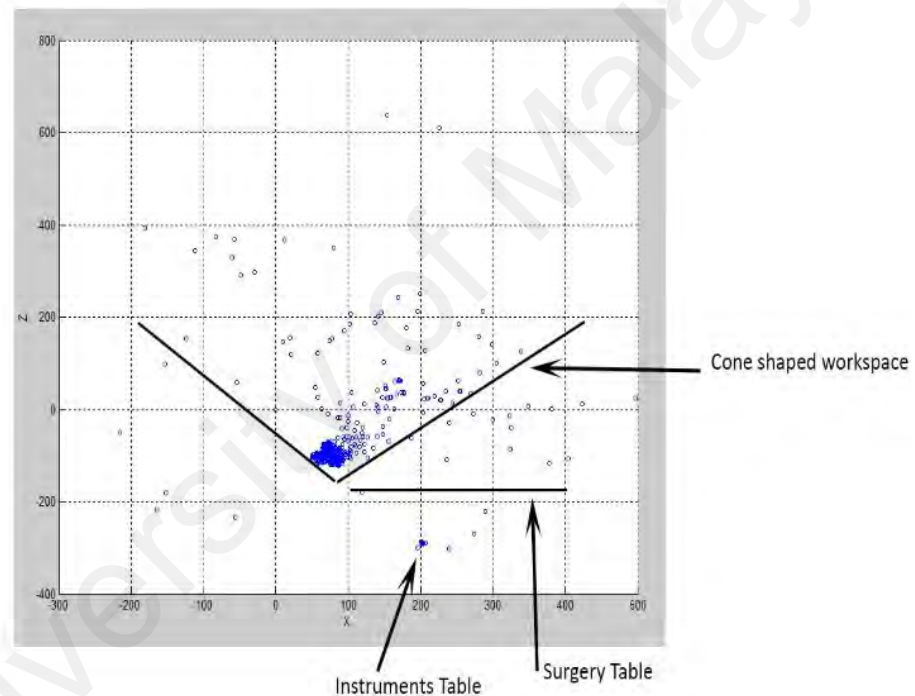


Figure 3.4 The recorded data in tumor resection surgery, to compare the actual data if it falls into cone shaped workspace.

The data capturing on the mock surgeries were successful. The positions of the instruments were successfully recorded, and no major issue had occurred. However, it was clarified from the data that each different registered instrument has its stamped data stream from BrainLab system, which means that BrainLab software differentiates

between what type of instrument is being tracked and identify that in the position data sending through OpenIGTLink. While prior to this the MATLAB program would record all positions from all instruments under the same name. This means that the tracking data delivered by BrainLab system for each instrument has unique name and time. The data stream consists of data packs, each pack contains the transformation matrix (a 4x4 matrix with the tool's position and orientation data), name of the instrument and milliseconds passed from start of the surgery. Start of the surgery is when patient-image registration completed successfully. BrainLab system only delivers one stream at a time so if the surgeon is using multiple tracked instruments, only one is navigated by BrainLab. The Matlab program was improved, so that user can choose which instrument to record and accommodate different data streams (with different name stamp) from the BrainLab system.

To get the permission to conduct the data acquisition in real surgeries, the preliminary data and method was presented to the research ethics committee of University of Malaya Medical Centre. The ethics approval letter is included in the appendix A.

A second round of trial experiments were conducted for three live surgeries. These surgeries include two craniotomies (tumor resection) and a transsphenoidal pituitary tumor resection. The observed instruments include IGS probe, Surgical endoscope and microscope. IGS probe and endoscope provided data on the location, orientation and size of the operating area, position and orientation of the patient's head and location of the surgeon, assistant surgeon and scrub nurse. The surgical microscope was chosen to be tracked because its position provides data about the obstacles near the operating area that the robot has to avoid. Surgical microscopes are usually big and bulky and if the robot is going to work near the operating area it needs to avoid crashing into microscope.

A secondary goal of task space analysis using IGS, was to evaluate the IGS performance as an external position tracker for the robot. Relying only on mechanical sensors can lead to less accuracy than optical trackers as mechanical systems suffer from physical effects such as gear backlash and temperature fluctuations. However, the optical trackers used in IGS systems are precise and robust without much sensitivity towards physical effects, they have been used in some neurosurgical robots as external sensors (BrainLab, 2018; "MODUS V, Fully-automated, robotic digital microscope,"). On the other hand, using IGS optical trackers imposes other issues to the robot's design, they increase the robot's footprint (the stereoscopic camera is relatively large compared to the size robot is aimed for), they escalate the cost and they may cause interruption in tracking while their line of sight is blocked. The first two issues may be less relevant with the improvement of technology, but line of sight issue depends on the OR set up and the nature of the surgeries. The line of sight issue in the optical trackers is a well-known fact. But this problem has not been quantified to know how severe it is. So, the decision of considering it in the design process of this thesis needed more information on the severity of line of sight issue.

After the second round of dry lab trials it was concluded that the OR events should be recorded during the surgery by a video recorder. This is beneficial for two reasons, first the researcher has an idea of how the OR was setup (location of surgeon, nurse, microscope, instrument table, etc.) in the surgery so, he/she can correlate the IGS data to real setup faster and more efficient. Second reason is to research the Line of Sight problem. Consequently, the MATLAB program has been altered to help with quantifying line of sight issue. The changes and process of detecting line of sight issue is discussed independently in next section.

The task space study continued with 15 more real life surgeries. 15 consecutive patients undergoing image guided neurological procedures were identified. The patients underwent standard surgical procedure, with the addition of IGS data acquisition and video recording of the entire surgery from the perspective of the optical tracker. The detailed analysis of the task space and how they have been used is discussed in the design and development chapter (Chapter 4).

3.1.1 Methods used for a detailed analysis on Line-of-sight issue

The analysis showed this issue happened in almost all the observed surgeries and as it is discussed later in chapter 4 the use of external cameras was avoided. In this section methods used for analysis of line-of-sight issue is discussed and corresponding results for this analysis is delivered later in end of chapter 5.

There are 2 main scenarios where the system cannot detect the instruments during the surgery. First, the instrument is not being used or is out of the optical tracker's field of view. The second situation is when the instrument is being used but the optical tracker's line of sight is blocked. The latter is the line of sight error identified and investigated in this analysis.

The data for this study was collected from 2 main sources. The first source is raw data from the IGS which documented the number and duration of time periods the image guidance system was unable to detect the tracking instrument while in use. The second source of data was the video recording during surgery, which recorded the entire surgery from an external camera attached to the optical tracker. The Matlab program analysed the recorded image guidance data and assigned the time period when the image guidance system could not detect the tracking instruments. The two datasets were synchronised to generate a merged video clip based on the recorded data.

The software added a green rectangle to each of the video frames in which the image guidance system could detect the instrument and a red rectangle to frames in which the instrument could not be detected. Figure 3.5 shows snapshots of clips created of merged data in two separate situations.



Figure 3.5 Top: an example of a situation in which the surgeon is using the tracking instrument, but the camera could not detect it. Bottom: The surgeon is using the tracking instrument and image guidance could detect it.

The generated clips were then analysed by two blinded neurosurgeons to determine if the situation with red rectangle (when the image guidance cannot detect the instrument) was considered a line of sight error. The criteria used to consider a situation as line of sight error are as follow:

- The tracking instrument is in the surgeon's hand
- The image guidance system cannot see the instrument (red rectangle)
- The tracking instrument is being used within the area of surgery

If the situation met these criteria, it was recorded as a line of sight error. The duration of error was measured based on the number of frames where line of sight error lasted. The videos were recorded at 60 frames per second, allowing for accurate calculation of the time, based on the number of red frames (i.e. 240 frames equal 4 seconds). The suspected cause of line of sight error was recorded by the neurosurgeons based on the video recording.

A total of 5 surgeons (with average of 10 years of experience) were involved in the observed surgeries. Before starting the surgery, the room setup and patient registration process was confirmed by the surgeons to make sure the surgical equipment and the image guidance camera were in best possible positions. Figure 3.6 shows the diagram of the data collection and analysis algorithm.

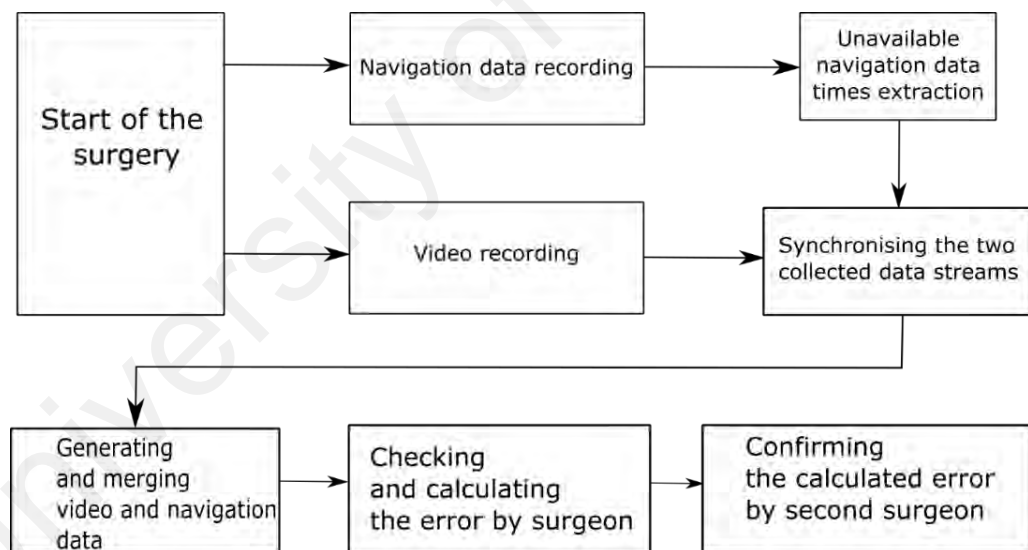


Figure 3.6 Diagram of the process performed for each operation to calculate the Line of sight error.

The IGS stereoscopic camera boom was ceiling mounted and could be moved within the surgical field without limitation. The video camera was battery powered and small enough to mount on the hand holder of the optical tracker, thereby directly viewing and capturing any line of sight errors. The camera used wide angle view lens to ensure a

wider area was captured on video compared to the image guidance coverage. The camera recording is synchronised by the software to ensure simultaneous recording of the video and image guidance data stream. Figure 3.7 shows the image guidance optical tracker with video camera attached to the hand holder.



Figure 3.7 The image guidance optical tracker and the attached video camera.

It should be mentioned that the surgical and operating room personnel who participated in this study are highly experienced in using optical tracking image guidance systems, having used similar systems regularly for more than 15 years. New surgical or operating personnel would probably be facing a much higher rate of line of sight issues than has been documented in this study due to their inexperience.

3.2 Validation

The perfect way to evaluate a surgical device is to use it in clinical study and on real patients. But reaching the clinical trial phase itself needs preliminary data to be presented to the ethical committee (This thesis is done as the research phase of this robotic device, so the clinical study is out of its scope). To make sure the device is safe for the patient and it will do its job safely with reliable functionality. This data has to be generated from experiments on non-human subjects, animals and/or anatomical models. To verify the design and functionality of this robot and generate the preliminary data, alternatives near to human patient anatomy had to be used. These alternatives had to be able to be used with clinical IGS systems to have a benchmark to compare with the robot's functionality. They should be able to get registered to IGS and the robotic systems. They should have valid medical image such as CT scan and MRI. For brain surgeries only monkeys and primates are anatomically close to human. Using monkeys in surgical experiments demanded to overcome lots of ethical considerations and obstacles. Additionally, because of contamination considerations the clinical IGS system could not be used on animals². Therefore, the choice for robotic surgical experiments was made to be anatomical head models.

In total three human head models have been used for performance evaluation, each representing different surgical cases. All these models are fabricated using 3D rapid prototyping (3D printing) from medical images of real patients. They mimic real patients with real pathological problems. Different surgical cases are performed with these models and the result have been presented in results and discussion chapter. These models consist of two parts, base, that mimics the face and head of the patient, this is to provide IGS

² There was only access to clinical IGS system, unfortunately an additional external coordinate measuring system was not available throughout the experiments of this thesis.

registration with face surface data. They also have a replaceable part which exactly mimics the human anatomy and hold the problematic tissue and pathology. The replaceable part has fake scalp skin, skull bone and dura, so during the mock surgery the surgeon goes through the same steps of a real surgery. These models are proven to be accurate enough to train junior neurosurgeons and to inject realism in surgical simulation (Waran, Narayanan, Karuppiah, Owen, et al., 2014; Waran, Narayanan, Karuppiah, Pancharatnam, et al., 2014). Pituitary model has been used in the same conditions they were developed in from other studies out of this thesis, however, accuracy models have been developed specifically for registration and accuracy assessment in this thesis.

3.2.1 Validation of endoscope manipulation application

The proposed validation for endoscope manipulation is a qualitative analysis in which the application is used in a mock surgery on a head model. This model (Figure 3.8) has been created to mimic a patient with pituitary adenoma tumor. It is fabricated using multi-material 3D printer that gives designers the ability to mimic soft tissues such as the skin and cartilage inside human's nasal canal. The approach to this tumor is transsphenoidal using neurosurgical endoscope. The mock surgery was carried out by an experienced neurosurgeon who has carried out numerous transsphenoidal pituitary tumor resections.



Figure 3.8 Pituitary model used for endoscope application

3.2.2 Biopsy and Accuracy assessment

Biopsy application is a good measure of a neurosurgical robot's accuracy and as real biopsies cannot be performed at this stage, head models had to be used, models that are near to real patients' anatomy and features. However, head models with real facial surface and distinct targets inside the brain area are not available. So, models should have been developed and first assessed by a clinical IGS system and then the same models had to be used to assess the robot's accuracy. This provided a benchmark for the robot's accuracy assessment.

Initial studies to assess 3D printed model accuracy has been focused on cross referencing various anatomical landmarks with imaging studies as demonstrated on the IGS system. While these studies managed to demonstrate the overall surface accuracy of the models, spatial accuracy has never been analyzed or demonstrated especially in a quantitative manner. The accuracy errors may arise from multiple sources including data conversion error, 3D printing and fabrication error and IGS registration error. These errors usually are calculated on a cumulative fashion and do not discriminate between the

largest or the avoidable sources of error. So, a new study has been conducted to demonstrate and quantify the presence and the causes of spatial accuracy errors in 3D printed models of the head. Models developed in this study are the benchmark for the robot's accuracy validity and they have been used with clinical IGS systems

In total, two 3D printed head models were fabricated. The CT images of the head of two patients (one from a paediatric patient with hydrocephalies and one adult with tumour) were pre-processed via a 3D slicer software with the addition of multiple marker points within the space of the head. After considering the available space and the printer's tray size, a total of 24 marker points for the first model (paediatric) and 12 for the second model (tumour) were incorporated in the image data. These points were scattered within the area of the estimated brain. Each of these marker points were 1mm in diameter. (Figure 3.9 shows three of the marker points on an axial view of the CT scan of the first head model). These marker points formed the base of spatial accuracy points.

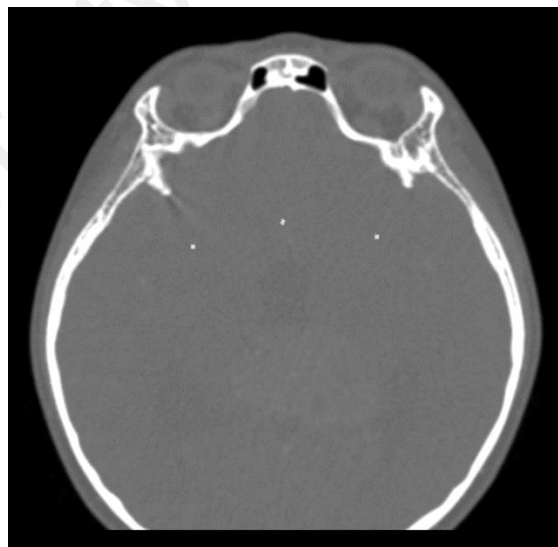


Figure 3.9 Three of 24 reference points incorporated inside the CT Image of the patient to be printed.

The resulting images were then converted from DICOM to a printable format, STL (Stereolithography) data. Each of the models were printed in two parts, a base that

consisted of the facial features that were to be used for registration purposes and an insert that contained the printed marker points

- The Bases

Using a mesh software, the skeletal head and surface area were converted to STL format and fabricated separately in a 3D printer. The parts were printed using a high accuracy printer (Stratasys Objet 500) with high precision.

- The Inserts

In the second step, images from the inner brain area with the reference markers were converted into STL format. These points were scattered within the brain space, and a support structure (cone shaped pole) was designed for each point and included in the STL file to be printed. This pole forms the support structure and base for the reference points in the defined coordinates. The reference point was designed in such a way that it has to be at the end of the pole, with a step-down design (divot), and the apex of the divot being the reference point. Due to the small diameter of the reference point, the step-down design helped stabilise and keep the IGS probe (IGS pointer) in place. Figure 3.10 shows the support structure with the reference points at the end.

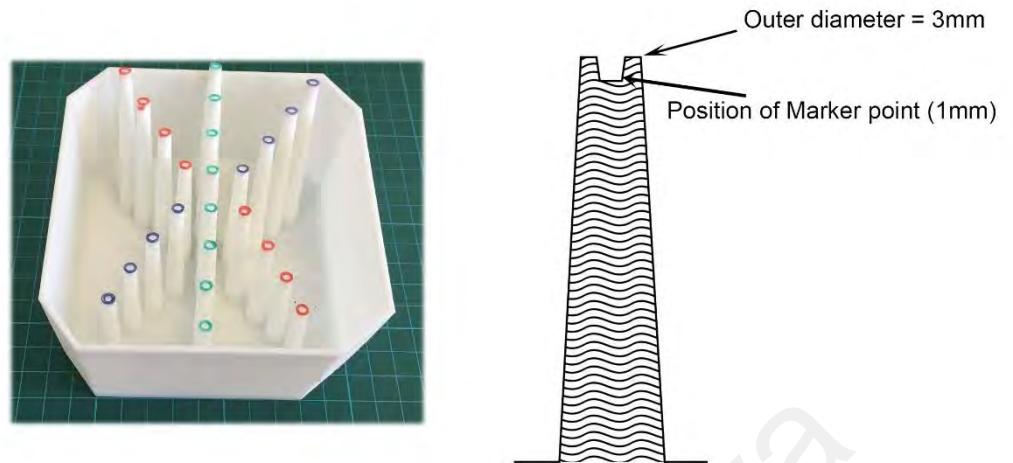


Figure 3.10 Left: The 24 markers and the support structure holding them in place. Right: The design of each pile structure.

The printed models (bases and inserts) were combined to form complete head models. These two head models then had the facial surface of the original patients with incorporated reference marker points in the brain area (Figure 3.11).

The differences between the two models were in position of the inserts and number of marker points. The first model was based on a paediatric patient with the insert covering the base of the skull to the crown. The first model had 24 marker points. The second model used a CT image of an adult with the inserts located in the right temporal region, which included 12 points arranged in 3 rows. The pole structures in the second model are designed to be parallel to printing bed, which made the printing process slightly different from the first model.

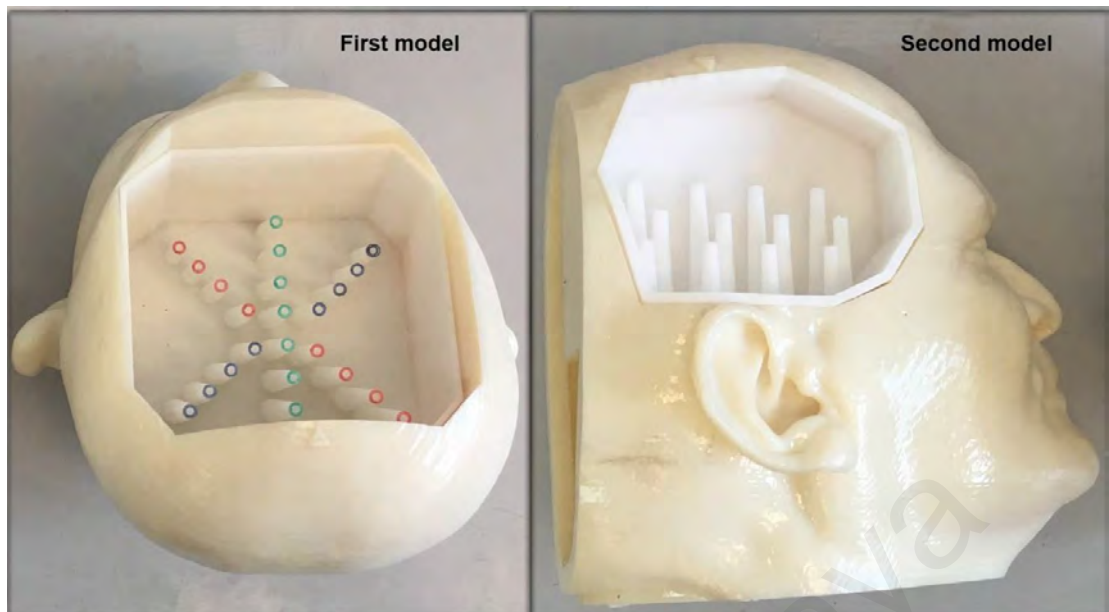


Figure 3.11 The two models are shown side by side. First model on the left, with 24 marker points. Second model on the right provided with 12 marker points.

In the next step these models were fixed to the surgical operating table inside an operating theatre via a Mayfield clamp to prevent unwanted movements (as performed on real patients). Using the Brainlab cranial navigation software, the models were then registered to the image data. The registration was conducted in 3 different ways to determine the source of possible error.

Method 1 (model based on patient and registration based on actual patient's scans)- the models were registered using a manual surface registration with the original patients' CT images. In this method, the IGS compares the scanned surface data of the model with the surface data of the original patient's scan and calculates the conversion between coordinate systems of the model and CT accordingly so that the tracking instruments such as an IGS probe can be tracked in relation to the patients' image data.

Method 2 (model based on patient's scan data and manual registration performed on data obtained after the model was rescanned), the printed models were scanned using an intraoperative CT scanner and new CT images were acquired. The models were then registered using manual surface registration with the newly acquired model CT data. In

this method, the IGS compares the scanned surface data of the model with the surface data of the newly acquired scan and changes the coordinate systems accordingly so that the tracking instruments and the head model would be in the same coordinate system based on the new scan.

Method 3 (model based on patient's scan data and automatic registration based on scan performed on data obtained after the model was rescanned), the model was automatically registered using the integrated intraoperative CT scanner, which first acquires a new scan of the model, and then registers the model to this newly acquired scan. In this way, the exact spatial position of the head model is then calculated and utilized by the IGS system. The expectation here was that the automatic registration would be highly accurate compared to the previous methods.

After confirming the registration for each experiment, the IGS system was connected to another computer with the 3D slicer software installed through IGTLINK. IGTLINK is an open source communication library which facilitates the connection of imaging devices, robots and navigation systems in a research set up (Tokuda et al., 2009). Using this set-up, the coordinates of each point was recorded inside the 3D slicer while the surgeon was holding the IGS probe on the marker points. The IGS based coordinates were compared to the original imaging coordinates and total error was thus calculated. The error is the length of the direct 3D line between the two coordinates. Figure 3.12 shows the setup with the head model clamped to the table.



Figure 3.12 The setup with the first model

These experiments were performed by a neurosurgeon with 20 years of experience and an expert in image guided neurosurgical operations. All experiments were performed in the same operating theatre using the same IGS system and intra operative CT scanner. The outcome of these experiments has been delivered in Results and Discussions chapter (Chapter 5)

3.3 Software

Several software programs have been used in the process of this work, for different purposes such as testing, prototyping and control. Various open source software programs have been used as well. The following list describe the utilised software programs and their intended use.

MATLAB (2012b and 2016a)- MATLAB is well known and easy to use software for research with numerous numbers of toolboxes to be used in different areas of science. Because programming in MATLAB is fast, it was used for the preliminary testing, analysis and prototyping. Optimisation toolbox was used for kinematic optimization, video editing toolbox was mainly used for line of sight issue analysis, image processing toolbox was used in early prototype of navigation software and robotic toolbox (Corke, 2017) have been used in the process of this work. Robotic toolbox has been created by Peter Cork and is developed for learning robotics; it is simple to use. It was used for basic kinematic calculations which is based on DH convention.

Solidworks (2014)- Solidworks was used as the main mechanical design software. It was used for designing the robot parts and testing the assembly fitting. The robot parts first designed in Solidworks for fabrication using 3D printers and metal machining process.

Meshlab (V1.3.3)- MeshLab is a powerful software to work with and edit mesh files such as STL files. STL file is combination of unit normal and vertices which form triangulated surfaces. Triangles has cartesian coordinates, MeshLab can be used for rotating, transferring, centring and removing of these triangles. Basically, MeshLab can be used for any mathematical alteration of the triangles. MeshLab was used to prepare

the designed part files for 3D printing. Beside 3D printing MeshLab was used for editing medical models. Sometimes converting the medical image to STL produces some unwanted entities such as the CT scanner table on which the patient was scanned. So, using the MeshLab software these models were cleaned.

3DSlicer(v4.6.2)- 3DSlicer or Slicer for short is an open source software developed for research in medical image visualisation and medical image computing. It is a capable software written in C++ and Python languages. It can handle DICOM images. Using volume rendering it can produce 3D representation of medical images and turn it into STL format. It can fuse and register medical images together (for example CT scan and MRI scan of the same patient). It is capable of image segmentation, which means using Slicer a medical image can be segmented into different parts (for example separating the brain from other tissues in an MRI image). Finally, the more related function to this work is that Slicer can be used for Image guided surgery.

In this work Slicer was used as the main IGS software to visualise and compute the IGS features. Furthermore, it was used for all medical related tasks such as importing DICOM images segmenting and rendering them. It was used to create STL models from the images, either the whole patient's head or portions of it.

The main reason to use Slicer was the open source nature of this software. Slicer can be heavily modified using C++ to accommodate different features. If a heavy modification is not needed, the Python API (Application Programming Interface) can be used to develop new applications. The user interface is based on Qt and it can be used to program a new console for a new application.

Using these capabilities, a new application console was developed to facilitate the developed robot's use cases.

SlicerIGT- This is an extension of 3DSlicer and a toolkit IGS applications in 3DSlicer. It has the basic functions for surgical navigation such as IGTLINK communication, image patient registration and needle navigation.

Robot Operating System (ROS Kinetic)- ROS is an open source cluster of software packages designed for robot applications. The services provided in ROS facilitates functions from low level hardware control high level visualisations. It is based on a system of topic-message communications which enable the communication between different processes and services in a robotic system. The applications in ROS ecosystem can be written using ROS client libraries, C++ (roscpp) and Python (rospy). ROS is officially supported in Ubuntu Linux operating system. Applications in ROS enjoy the big community support of ROS users which has developed many new applications as well as new bridge applications to communicate and work with other software and libraries. Bridges to work with OpenCV (image processing library/language), OpenIGTLINK and MATLAB.

The final prototype of this thesis has been designed in ROS ecosystem. It uses many available functionalities of ROS as well as new applications developed for it in the ROS ecosystem. Everything related to the final prototype is developed with C++ to maintain a uniform coding platform in this prototype. All are explained in the Design and development chapter. Some of the major ROS applications that are used for the final prototype are mentioned in the following of this software list.

MoveIt- MoveIt is a state-of-the-art robot motion planning software which incorporate manipulation, control and navigation, kinematics and obstacle avoidance. Since its creation increasing number industrial robots are utilising it (Moveit, 2018). It can be set to work with the default motion planners and Inverse kinematics solver, or it can be set to use new applications for these matters.

Gazebo- Gazebo (Koenig & Hsu, 2013) is a robot simulation software which started under ROS ecosystem but now it can be used as independent software. It can simulate the robot and the physical environment. It has been used on simulations needed for developing the last prototype.

Every other software module used in the process of this thesis had to be either programmed from scratch or heavily modified to meet the needs of this robot.

University of Malaya

CHAPTER 4: DESIGN AND DEVELOPMENT

In this chapter details of design and development process is discussed. In first section a detailed report on the hardware design of the manipulator is presented. The chapter continues with specifications and considerations led to the design of registration, biopsy and endoscope manipulation. Last section focuses on the software and controller of the robot and detailed explanation of the developed software for the Alfa prototype.

4.1 Hardware

This section follows the same steps introduced in methodology chapter, it starts with design problem identification and kinematic analysis which is done based on the results from task space analysis and requirements introduced in introduction chapter. Section continues with report on the process of design and development of the working prototype based on the kinematic analysis. The first section continues with report on developing process of a working prototype.

4.1.1 Design problem identification and analysis

Captured data from task space analysis used as a foundation in the design process of the robot. These data together with environment observations (video recordings and personal observations), have identified size and geometry of the task spaces in forms of positions and orientations of the tools. Based on the objectives of this project and task space analysis, the kinematic requirements of this project can be described as follow:

- The robot should be overall small and easy to relocate. In kinematic terms this means that robot links should be designed as short as possible to avoid a big structure. Manipulator designs with longer links (link lengths and link offsets) demand bigger joints as the torque increases with the size of links.

- The goal of this robot is to perform assistive tasks (which were observed in task space analysis). In kinematic terms this translates into:
 - The robot's workspace has to cover as much of the observed task space as possible.
 - The parts near the operating area should be small enough not to block surgeons' access. This means manipulator's wrist and link connecting other parts of the arm to the wrist had to be designed small. Furthermore, Manipulator being designed to work alongside the surgeons therefore, the robot's disturbance in their access to the operating area had to be minimum (if the wrist was too big it could block their access to the operating area, as usually the operating area is small in neurosurgery).
- The ability to register the patient to medical images means that the manipulator must have access to the landmarks on patient's face. the registration is often done by scanning the patient's face surface as it has enough distinct landmarks. In cases that patient's face is not accessible because of the patient positioning (prone positioning or extreme lateral angle of the head), robot should have access to any fiducial markers attached to head.
- This robot must have obstacle avoidance ability. In neurosurgery cases surgical microscope is used frequently, the ability of the robot to avoid colliding with and disturbing this device had to be addressed. Other bulky devices that may cause colliding risks are C-arms and intraoperative CT scanners. Furthermore, the surgeons should be able to remove the robot from the operating area without the robot disturbing their access to the operating area. therefore, the robot had to be designed with ability to either avoid collision or move out of the way of bulky devices.

Based on these remarks, the kinematic analysis had to be used to answer the designed questions, location of the base, DOF number and topology of the robot. Answering these questions led to kinematic structures design of a manipulator however dynamics requirements had to be answered separately by simulations done on designed kinematic structures.

4.1.2 Kinematic analysis

For a clearer understanding of the observed surgeries, the tasks performed under the observation can be divided into three categories (they are all assistive tasks). 1) Tasks that happen entirely outside operating area. 2) Tasks that have transition between operating area and outside area and 3) tasks that happen entirely inside operating area. First group includes tasks such as pointing a laser pointer to the targets planned before surgery, which the manipulator works outside operating area and does not touch the patient or when the tools touching the scalp only and not inside tissue, such as using an IGS probe to mark the opening incision on the scalp. Second group consist of tasks that take an instrument from outside area to operating area. For example, while handling an endoscope manipulator can take out the endoscope, clean it and position it back in the operating area or when a suction tube is taken outside of the operating area for cleaning. The third group consists of the tasks that help surgeon holds an instrument in place (such as holding a retractor) or provide trajectory guidance for the instruments (such as a cannula which provide guidance for biopsy needles or electrode).

Each of these categories impose different challenges to the robot's design as they have different task spaces. As an objective of this project the aim is to target all these categories and as many assistive tasks as possible, this will also help the future research and development of new functions for the system (as all assistive task fall in one of these categories). Third category task space is small and only covers the operating area, robots

that are designed for these specific tasks are usually small and have small workspace such as Mazor Robotics' Renaissance (Joskowicz et al., 2011). For the first category the task space is wider, robotic systems that target such tasks, exclude the operating area from the workspace such as Modus surgical robotic microscope (Waqas et al., 2017). The largest task space belongs to the tasks in second category, this task space covers the other two spaces as well. Figure 4.1 shows an example for one of the observed surgeries while surgeon used IGS probe to mark a scalp opening incision.

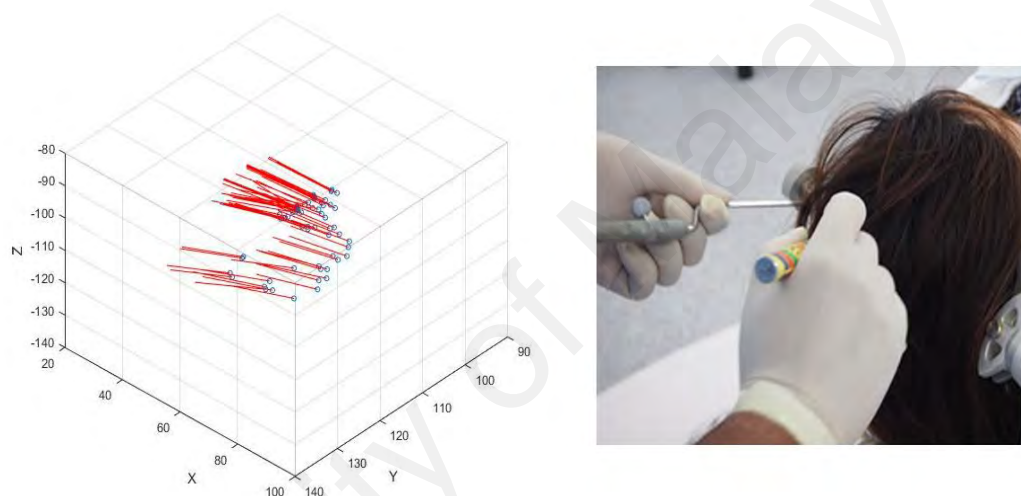


Figure 4.1 In this picture the surgeon is marking the incision on scalp of the patient. The tool's movement is illustrated on the left, the movement is small and does not move deep inside the head which indicates category 1 of assistive tasks.

This figure shows a tiny portion of a surgery, it represents first task category. As it was recorded while surgeon was outlining the operating area, the changes in depth (direction which goes inside patient's head) is small. However, as operations advanced, recordings of the tools' movements along the depth became larger, for example, Figure 4.2 shows an Endoscopic Third Ventriculostomy (ETV) case in which endoscope side movements (ZY movements, X direction is going inside patient's head) are limited and it mainly moves along the depth. Handling an endoscope in ETV operations is considered a third category task, using an accumulative task space of third category tasks a good guess on the size and shape of a typical operating area were calculated.

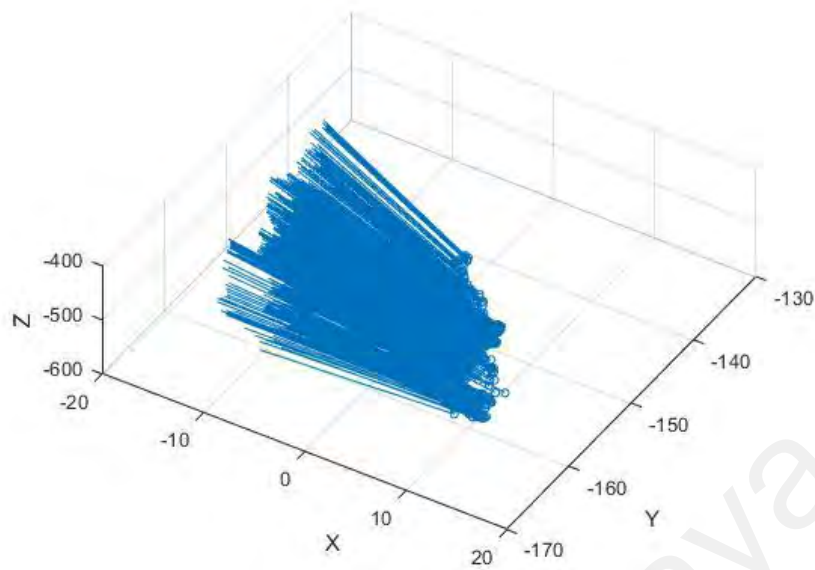


Figure 4.2 The endoscope movements in an ETV operation, the movement along the operating area is significant. This type of tasks helped to determine the size and shape of operating area in these operations.

Identifying the task space for first category was hard to achieve as there was minimum access to instruments that perform such tasks (only IGS probe in scalp marking could be observed). However, a combination of recordings of other tasks and video recordings of full surgeries provided details about the operating area and its surroundings, Figure 4.3 shows an example. By calculating these data which indicate the distances between operating area, surgical staff and instrument table a good presumption on the needed position workspace of the robot could be calculated.

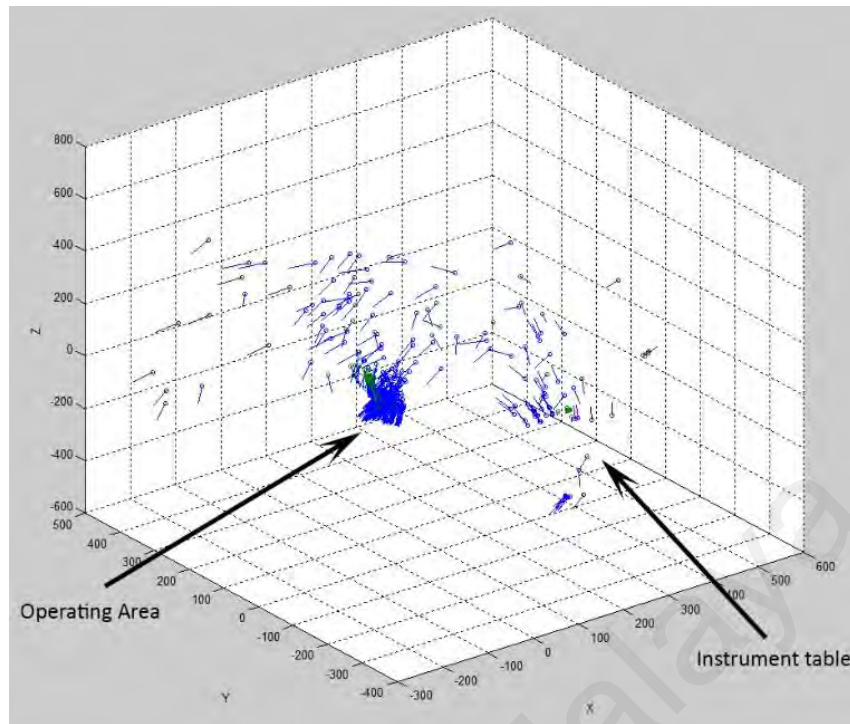


Figure 4.3 A full observation of the surgery as far as the IGS camera range could allow. Matching this data with video recordings of the operation provided data on positions of Operating area and its surroundings.

These data reveal a large travelling area for the instruments, between surgeons and assistant surgeon, or nurse (which can reach to 1.5 m). If task category two were chosen to consist of these travels, the resulting workspace had to be designed as large. This would have made the robot's size illogically big. On the other hand, these travels are not necessarily crucial for the functions of this robot, as it is described later.

The long travels of instruments between the staff is basically to hand over the tool and it is not necessarily a surgical assistive task, Therefore, the tasks that demand long travel between the operating area and staff (for example where surgeon finish with a tool and give it back to the scrub nurse) has been excluded from category two. The tasks that are included are tasks in which the instrument is temporarily taken out of operating area for cleaning and adjustment, they still have a travel from outside operating area and back into it but now, this category includes tasks with shorter travels. An appropriate example for this type of tasks is handling endoscope in transsphenoidal surgeries, in which the

endoscope has to be moved regularly out from operating area, cleaned and moved back in nasal canal again. Figure 4.4 shows recorded data during such operation where cleaning process was being done close to the operating area. Sometimes the endoscope needed to be taken further for adjustments or additional cleaning.

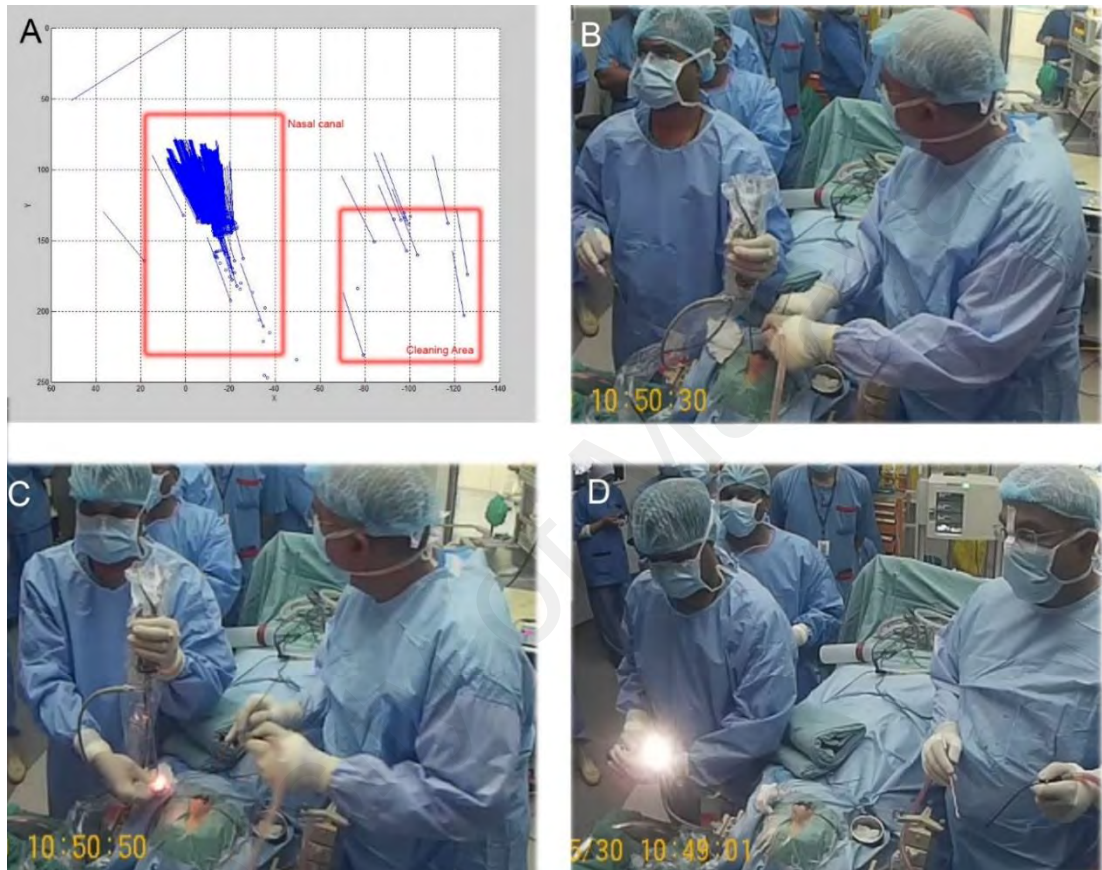


Figure 4.4 The recording of an endoscope movement during transsphenoidal surgery. A) the movements as recorded from IGS system. B) while the endoscope is in nasal canal (operating area). C) The endoscope is out for cleaning. D) the endoscope is out for adjustments.

So, based on the description of tasks in the category two, it was needed to consider a workspace which covers inside the operating area as well as outside space. Outside space should be big enough to make it possible for the staff to clean, adjust or change the instruments attached to the robot. Therefore, the workspace study was filtered to include tasks that carried out in such manner, based on the obtained result an initial guess suggested that a robot's workspace which fills up a hemisphere with the radius of 300 mm with its center at the bottom of patients' head, is a suitable workspace, the hemisphere

only covers the top part of the surgical table and not the bottom. However, further research and observations concluded a more optimized workspace could be achieved.

In neurosurgery, the patient is mainly positioned on the table in prone and supine positions. The position is selected based on the position of the operating area. Surgeons always try to keep the operating area in their direct and ergonomic access, this means that it has been rarely seen the operating area positioned parallel to the surgical table (it is never under surgeon's line of sight) and as the head is flexible, the head can be turned to position the operating area in direct line of sight (lateral positioning of whole patient's body which is called park bench position, is not common³). Even if during the surgery greater lateral angle is needed, the surgery table's angle and height and therefore patient's position can be adjusted. Thus, with this definition the workspace looks more like a spherical cone rather than a full hemisphere. Figure 4.5 shows such a workspace. Further Optimization of the workspace was possible however, it depended on defining the location of the robot's base.

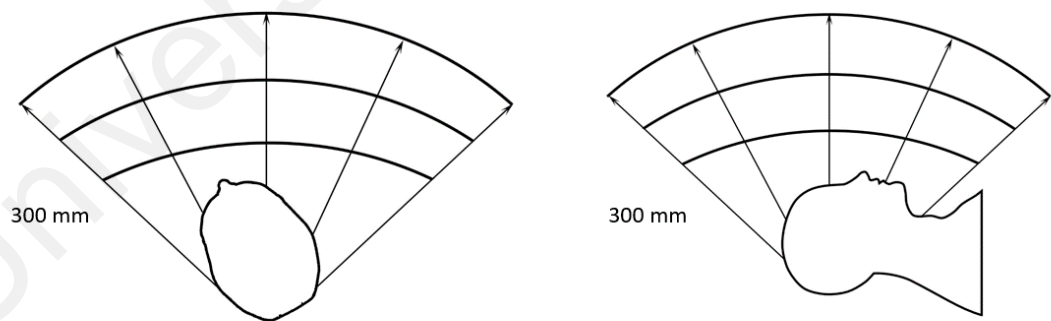


Figure 4.5 the task space needed to be covered by the robot is a spherical cone with patient's head at bottom and center of it.

³ Lateral body position is usually only used in some Cerebellopontine angle (CPA) tumors resections.

Location of the base and mounting is one of the key factors in determining the robot's workspace. In serial manipulators, the base is where the first joint is mounted and where the kinematic chain starts. The position workspace of a robot is like a sphere which base is at its center and its radius is the furthest distance robot's tool can reach (the position workspace is being discussed here; orientation workspace is discussed later in this section). Any position within this sphere that the robot is unable to reach is omitted from the workspace, for example positions that cause a singularity (for example a fully extended arm is at its singular position).

In neurosurgical OR there are three choices for location of the base, ceiling mount base, floor mount base and surgical table mount base. Ceiling mount is beneficial for big robots such as (Briot, Baradat, Guégan, & Arakelian, 2007) that occupy a big foot print, however ceiling mount robots are only limited to only one OR and cannot be moved to other rooms.

Floor mount, which is very popular among surgical robots, usually means the robot is mounted on a cart or trolley that can be moved in and out of OR. Before the surgery the cart is placed near the patient and their position is fixed by lockable wheels. The relative position of robot and patient should always remain constant, in floor mount robot this is achieved by either an attachment to surgical table (sometimes to a frame mounted on patient's head) or by another position sensor, tracking the movement of both patient and robot (usually by optical tracking and reflective markers on both patient's head and robot's tool). Furthermore, these trolleys occupy a big footprint inside neurosurgical OR where lots of equipment are placed on floor and floor space is scarce.

Surgical table mount is considered the appropriate option for this project. A robot with its base mounted on the surgical table is close to the operating area so, it needs shorter links compared to floor mounted robots. Additionally, if the patient's head is fixed to the table (using head clamps), the robot mounted rigidly on the same table is always in constant relation to the patient's head, this lessens the need to use external trackers and attachments. Surgical tables often equipped with rails on both sides which facilitate mounting of different equipment and instruments.

Table mounting effects the task space of the robot as well, mounting the robot on the side of the table gives good access to the patient's head, however, if the desired location is on the opposite side of the table it would be a more challenging task for the robot, because the robot must avoid colliding with the head while working on this side and therefore, it loses some dexterity. This is more apparent when the operating area is located at opposite side of the table and the robot should hold an instrument parallel to the operating area with a distance. It is possible to reach the hard to reach positions with longer links, but to have full dexterity, probably a new joint must be added. As the goal is to keep the design small and less complex, long links and/or extra DOF are not desirable choices, it is possible to avoid longer links and/or an extra DOF.

The essential parts of the task space that the robot has to reach with good dexterity are the operating area and the face surface for registration. The surgical table has rails on both sides, so it is possible to have a robot with shorter links and mount it on the same side that the operating area is located, however, in cases that the face is rotated to the extreme sides, the robot may only be able to access partial of the face not all. Accessing partial parts of the face is still acceptable if enough points for registration can be accessed. Considering this definition, the robot's workspace covers a task space which looks like Figure 4.6.

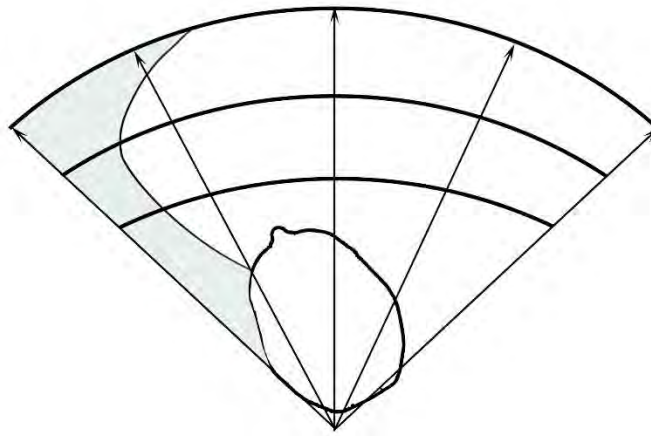


Figure 4.6 The task space when the base is positioned at the side, white area is the task space the robot needs to cover (while positioned on the right side). the grey area is the area the robot cannot cover with full dexterity.

This workspace was not coherent with the spherical cone workspace as it may not provide enough space for cleaning and adjusting instruments. However, the cleaning and instrument adjusting areas that was discussed earlier in this section are not fixed positions, unlike operating area and facial surface these areas can be anywhere around the head if they provide enough access to the tool for the surgical staff. So, with a task space like Figure 4.6, there are still plenty of space for these tasks.

So far, the positioning task space has been covered, the recorded tasks also included the orientation task space (all the orientations that the tools took during observed surgeries). The orientation task space helps in deciding the DOF of the robot. To reach all positions and match all orientations in Cartesian space, a minimum 6 DOF is needed. If the task demands more dexterity more than 6 DOFs should be used, however, in cases that not all orientation axes are utilized less than 6 DOF can be used. The orientation task space in the recorded data suggested that the range of movement around the tool axis is very limited and, in most cases, none. This could be due to two reasons, first, a flaw in recording from IGS systems, the IGS system uses optical tracking while it's camera is pointing to the operating area from only one direction therefore, the IGS system is not capable of fully detecting such movements, it is possible that users are trying to only keep

the tool in that direction and not turn it. Second, the observed tools are not really needed to be turned around their axes or this movement is redundant in their use.

Based on the recorded videos from the observed surgeries the second is closer to the truth. For example, a biopsy canula's revolution around its own axis is redundant and biopsy can be done for any angle of the cannula around its axes. Same is true for endoscope, while turning the endoscope around its axis, changes its image, however, the surgeons always try to keep the endoscope in the same angle throughout the surgery, this is done to keep their frame of reference always in check. What this means is that this axis can be removed from the design.

Removing one axis reduces the needed DOF to five. However, if task space of a robot is constrained, extra DOF may help to avoid the obstacles. An obstacle which is usually present in neurosurgical cases are surgical microscopes, which are bulky and tend to obstruct access to the operating area (the data recorded for line of sight analysis in the methodology chapter showed that while using microscope the operating area is blocked from IGS camera). Moreover, the field of view while using microscope should not be obstructed by other instruments. Figure 4.7 shows the positioning of microscope and its field of view. Theoretically an additional DOF can help the manipulator to avoid colliding with the microscope and its field of view but, it induces more complexity to the design. Therefore, two structures with 5 DOF and 6 DOF designs have been investigated in kinematic optimization.

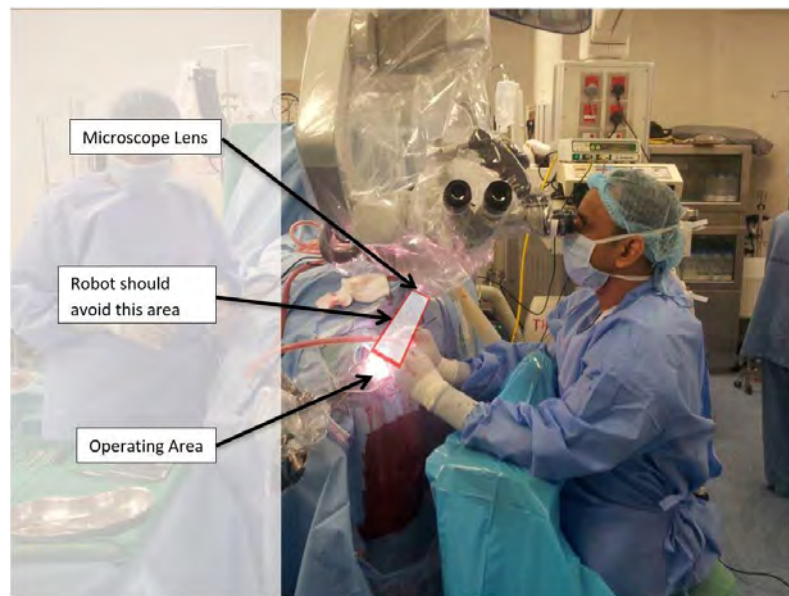


Figure 4.7 Position of the microscope and its field of view.

Topology of a robot refers to the type of kinematic structure it uses, what types of joints, revolute or prismatic. In this project serial robots are in favor as parallel structures despite their high accuracy, are big and may block the access to the operating area, additionally parallel robots have small workspaces compared to their size. There are different types of kinematic structures to pick from, a general serial structure with 6 Revolute joints (general 6R) is usually the choice for general and multipurpose designs e.g. puma 560. General 6R structure consists of a 3R positioning structure, which delivers a 3R wrist to a desired location. As mentioned, the axis in which the surgical tools turn around itself (Roll axis) appeared to be redundant in the observed tasks, this axis would not be actuated, which reduced the 3R wrist to a 2R wrist. One less actuator at the wrist could reduce the wrist size substantially. Figure 4.8 shows a suggested topology for the wrist. This axis is not actuated but, still can be used as a passive joint.

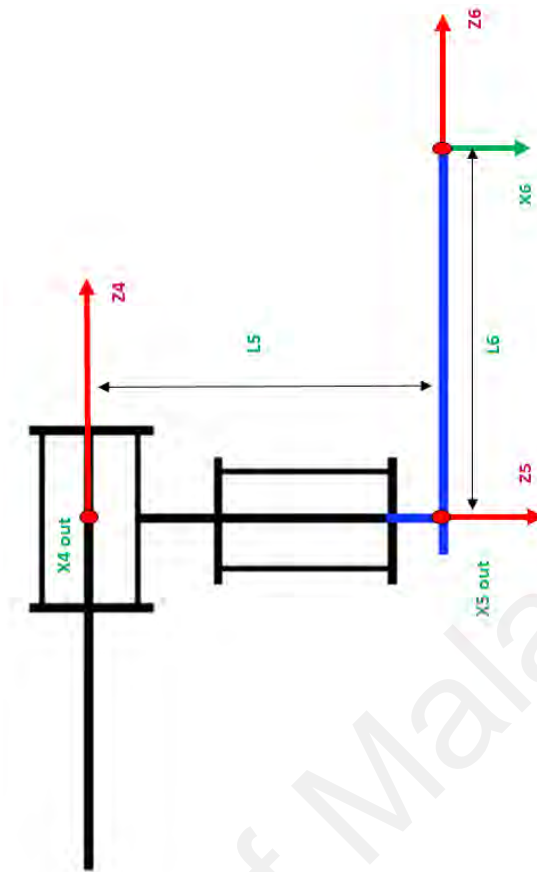


Figure 4.8 The wrist consists of two actuated axes, Z_4 and Z_5 and a passive axis Z_6 . This arrangement is smaller than normal 3 actuated axes.

3R positioning structure has the minimum DOF needed to reach all positions in cartesian space however, if dexterity and obstacle avoidance is desired this structure may shows shortcomings. Some kinematic structures, (Heinig et al., 2011a; Mitsuishi et al., 2013) use an arc shaped link to improve dexterity and positioning, but these manipulators' workspaces only focus on the operating area and tasks inside the operating area. Based on kinematic objectives of this project, the robot's body must avoid colliding and disturbing devices such as microscope and C-arm, to add more dexterity in avoiding these obstacles, one redundant revolute joint is added to the base of a general 3R positioning structure, forming a 4R redundant manipulator that can move the robot body in around one axis without disturbing the tool's position. Figure 4.9 compares the two structures. The intersection of three-axes tends to be bulky but here, the intersection is at the base,

so later using early prototypes it was investigated if this bulky base may cause problems.

These two kinematic structures are then compared in the kinematic optimization section.

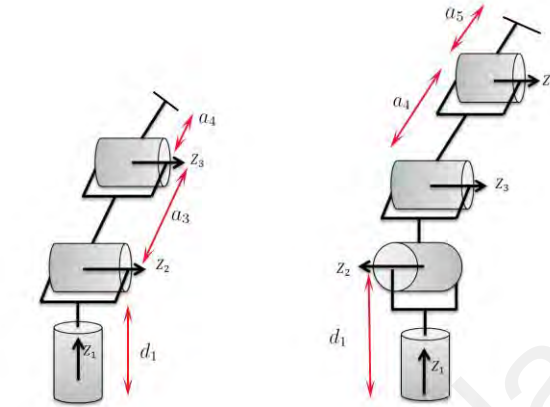


Figure 4.9 The two kinematic topology considered for the manipulator, 3R on the left and 4R on the right.

University of Malaya

4.1.3 Kinematic optimization

Kinematic design optimization has gained major attention in literature. Different approaches to this problem have been made (Carbone, Ottaviano, & Ceccarelli, 2007; Ceccarelli & Lanni, 2004; Paredis, Au, & Khosla, 1994; S. Patel & T. Sobh, 2015; S. H. Patel & T. M. Sobh, 2015; Van Henten, Van't Slot, Hol, & Van Willigenburg, 2009), and algorithms optimization have been researched (Bergamaschi, Saramago, & Coelho, 2008; Shiakolas, Koladiya, & Kebrle, 2002). Despite the rich literature, there is no unified approach to the kinematic design problems. Each design case is different based on the tasks, dynamic requirements, and designer preferences.

In this thesis, the design optimization is solved by developing an evaluation function, based on introduction made in (Van Henten et al., 2009).

$$T = \min_t E \quad (4.1)$$

T is the optimized set of design parameters, t is the set of design parameters, and E is the evaluation function. Based on Denavit-Hartenberg (DH) notation, the kinematic chain can be defined with the joint angle, link twist α , the link length a , and the link offset d (Craig, 1989). By steering the joint variables matrix, minimum value for E and optimized design parameters are calculated. Usually, the numbers of kinematic chain parameters of the kinematic model are chosen as design parameters.

Different methods could be used to solve the optimization function. In this project, numerical methods in Matlab optimization toolbox was used (fmincon which uses interior point algorithm) (Inc, 2013).

Based on the design problem, the evaluation function E was developed. This function evaluates the movement and obstacle avoidance of the proposed structures. Simulation experiments were conducted to put them through different scenarios. Design parameters were optimized based on the results from the simulations.

The joint movement in a kinematic structure should always be optimum. Similar to (Van Henten et al., 2009) the joints movements was used as a performance benchmark (less movement means smaller danger of accidentally hitting the patient or surgeon), it can be calculated by summing up all joint movements during a path-following maneuver. In both kinematic chains all joints are revolute joints, therefore, the movement of the manipulator's structure is defined by the joint angles. So,

$$E_{path} = \sum_{k=2}^N \sqrt{(\theta_k - \theta_{k-1})W(\theta_k - \theta_{k-1})^T} \quad (4.2)$$

where θ_k is the joint angle vector in the K^{th} point of the path. N is the number of the points in the path, and W is the weight matrix that controls the effect of each joint in this function. W is valued as a unity matrix here however if full kinematic chain (positioning and wrist) was considered W gives more value to the positioning structure's joints as their movements map to bigger movements of the links.

It is important that, at the design stage that the ability to avoid blockage to the microscope or other viewing devices be taken into consideration. Therefore, while following a simulated path to the surgery area, the portion of the kinematic structures that intrudes into the surgery area should be measured. $E_{visibility}$ calculates the projection of the links on the eyesight plane, such that

$$E_{visibility} = A * L \quad (4.3)$$

L is the length of the links' intersected portion with the surgery area in 2D eyesight plane. This 2D plane is perpendicular to the viewing direction. A is the weighting scalar, and in this context, is a unity matrix. The evaluation function is the combination of Equations (4.2) and (4.3). So,

$$E = E_{path} + E_{visibility} \quad (4.4)$$

$$E = \sum_{k=2}^N \sqrt{(\theta_k - \theta_{k-1})W(\theta_k - \theta_{k-1})^T} + AL. \quad (4.5)$$

Using Equation (4.5), any structural parameter can be selected as design parameters. In this thesis, the set of link lengths was selected for optimization. Based on DH notation, these lengths are presented by d_1, a_3 and a_4 for general 3R, and d_1, a_4 and a_5 for the new 4R structure, respectively. The links are part of the positioning structure. Therefore, the optimization is based on the ability to deliver the wrist to the desired location. Two simulation tests were conducted to investigate the path-following, base position, and obstacle avoidance. Link offsets were set to zero. The maximum total length of structures was set based on the base distance from the head in the simulations.

First simulation mimics a normal path following around the patient's head and facial landmarks. This is one of the routine maneuvers for patient registration, here the

manipulator should be able to reach these landmarks on a straight face, in case of using fiducial markers for registration, the same distribution can be used. For this simulation, the E_{path} is calculated as an evaluation function. The path planning algorithm was based on inverse kinematics developed in (I.-M. Chen & Gao, 2001). Figure 4.10 demonstrates the planned path. It was calculated for the two base locations in the picture it started with the closest point to the head B1 and continued to B2. B1 is ideal for a smaller manipulator and B2 for obstacle avoidance (to be out of the way in case of C-arm scanning, microscope presence or when surgeon wants the manipulator out of the way).



Figure 4.10 Normal path planned for test 1. The tip point of SAD (UP) should touch the numbered points, not necessarily in that order.

The second simulation was designed to examine the collision of the manipulator body with surgical microscope field of view. The complete evaluation function (4.5) was calculated. Figure 4.11 demonstrates the second conducted simulation. The gray circle indicates the operating area. The intrusion of the links was calculated based on the portion-projected lines of the links on the 2D plane, perpendicular the viewing direction. Figure 4.12 shows how the optimization algorithm changes the eyesight plane to accommodate different viewing trajectories, this trajectory of microscope angles was

calculated based on recorded positions of microscope in real surgeries during task space analysis. In total 3 positions of microscope and therefore 3 eyesight planes were used.



Figure 4.11 The path for collision detection. The simulation calculates how much of the SAD body is in the grey area while it is performing the designated maneuvers.

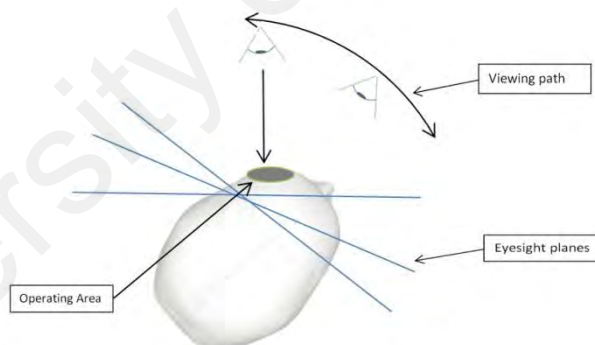


Figure 4.12 The 2D eyesight plane changes with the progression of viewing direction.

The results of the simulations are presented in Tables 4.1 and 4.2. The results generated by test 1 showed the superiority of the general 3R over the proposed 4R, with smaller values of E_{path} . The added revolute joint (joint 2) is redundant to the position of the tip

point in some parts of the workspace. Therefore, the optimization algorithm keeps this angle constant, and prompted other joints to have bigger changes through the path.

Table 4.1 Optimization results for test 1 without considering the obstacle avoidance feature.

	d_1	a_3	a_4	E
General 3R-B1	65mm	310mm	265mm	32
General 3R-B2	140mm	430mm	360mm	33
	d_1	a_4	a_5	
New 4R-B1	60	305mm	275mm	68
New 4R-B2	90mm	401mm	389mm	66

The results of test 2 in general 3R showed that the value of E increased due to the poor ability of this structure to avoid the gray area. The 4R structure on the other hand did not show much of a difference. The orientation of joint 2 enables the controller to avoid the obstacles in less complex movements. With a slight change in the angle of joint 2, the manipulator's links could be tilted to avoid any obstacles in the path. However, the 4R structure does not show much difference in size when the base is closer to the head and the algorithm for the general 3R with base at B1 could not find any solution.

Table 4.2 Results for Test 2.

	d_1	a_3	a_4	E
General 3R-B1	N/A	N/A	N/A	
General 3R-B2	138mm	430mm	371mm	131
	d_1	a_4	a_5	
New 4R-B1	89mm	418mm	390mm	96
New 4R-B2	92mm	423mm	395mm	66

4.1.4 Dynamic simulation

The dynamic simulations were done in Gazebo software (Koenig & Hsu, 2013). Using this software, models of three arm kinematic structures were created, general 3R with base at B1 and B2 and the new 4R. Aluminum was chosen as material of choice for the body of these models, this metal is light and strong and usually the choice for light weight robotic arms. Models were then programmed to make maneuvers similar to their intended use which consists of small movements of the tool and big movements of lower joints. A payload of 1kg was used as tool (heaviest intended tool is an endoscope with around 900g weight). For the period of these maneuvers running, torque in each joint were measured, as illustrated in Figure 4.13 to 4.15. these figures show the output of a virtual force/torque sensor attached to each joint of the robot.

University of Malaya

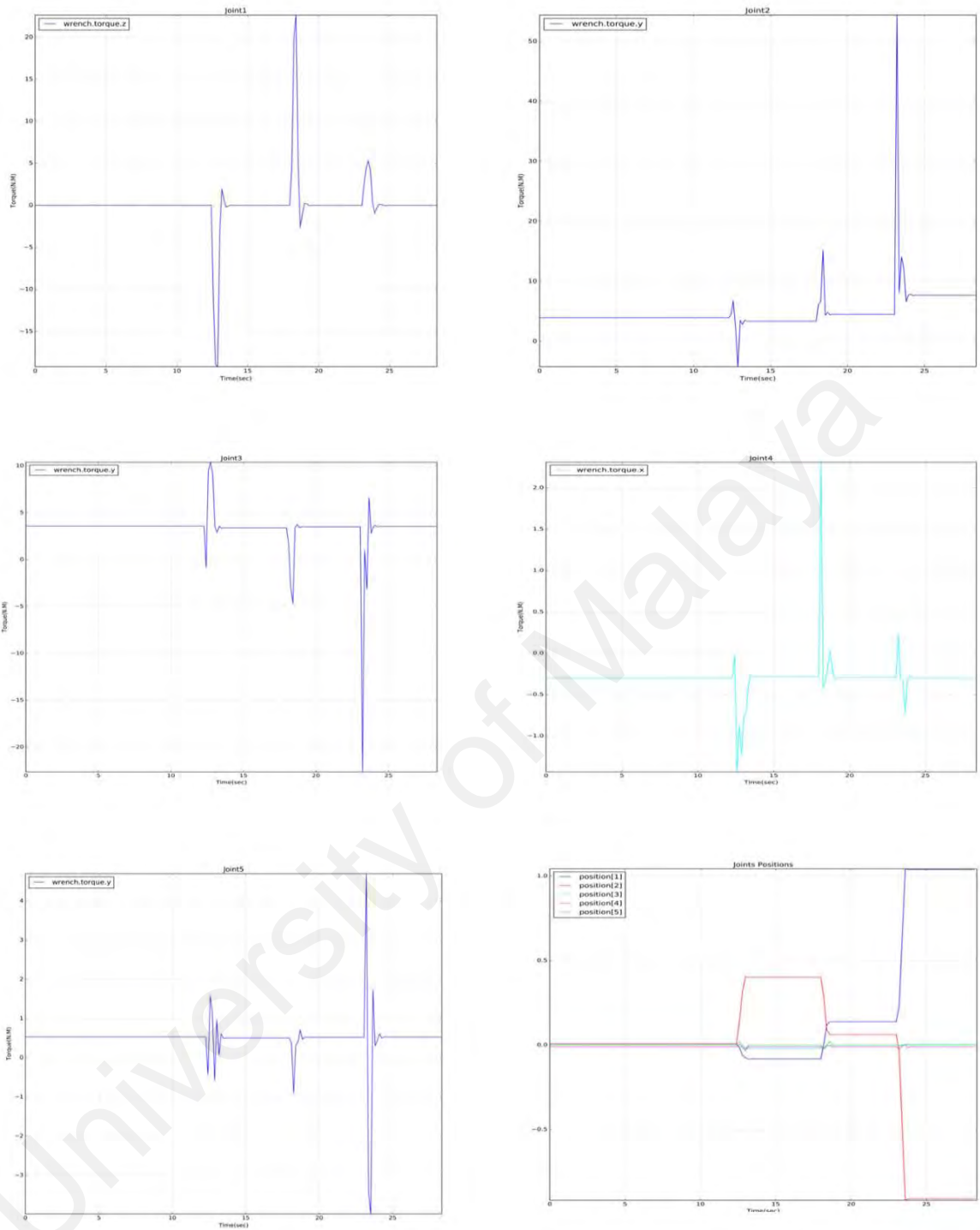


Figure 4.13 The output torque for actuated axes of each joint in 5DOF structure with bases at B1.

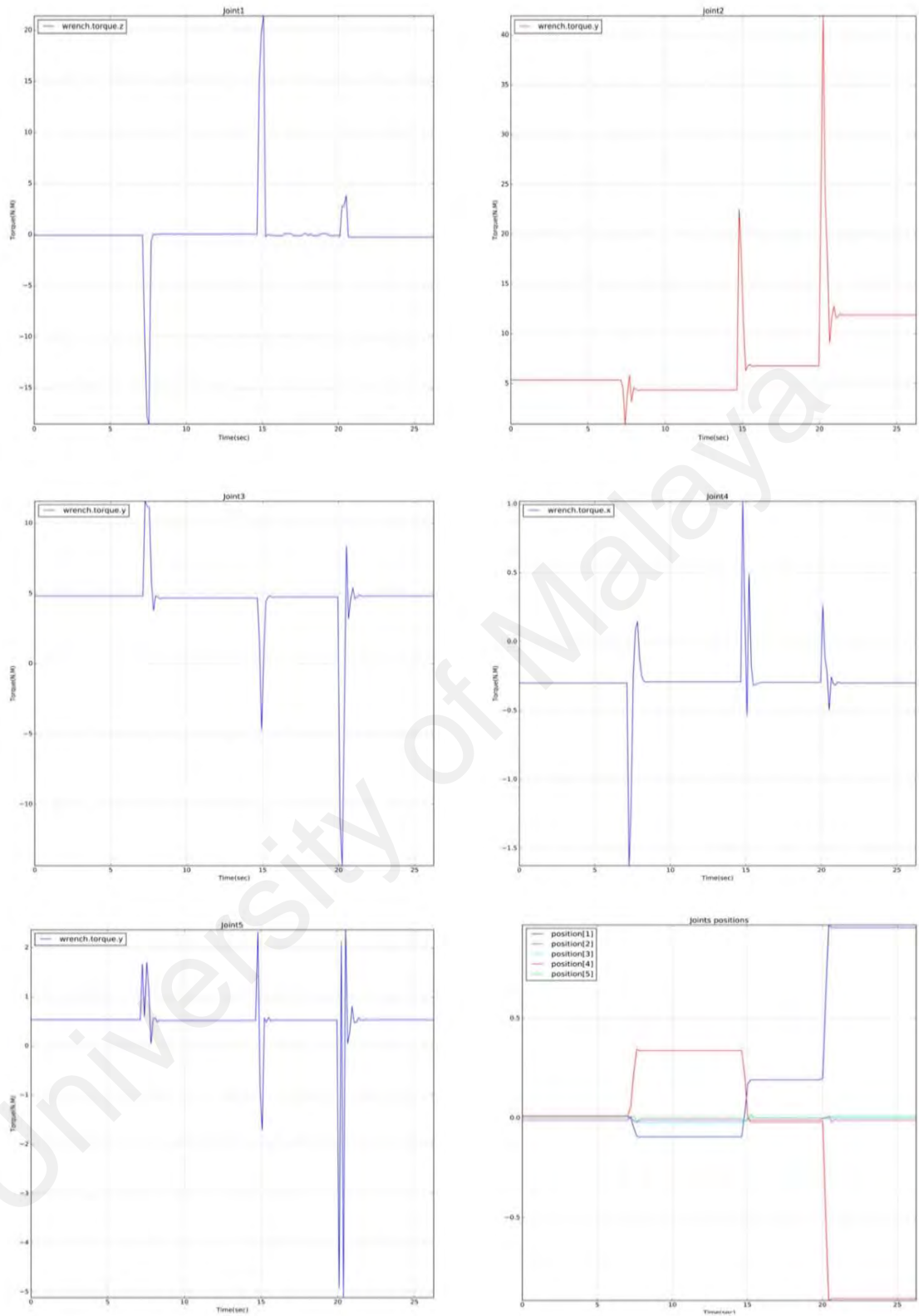


Figure 4.14 The output torque for actuated axes of each joint in 5DOF structure with bases at B2.

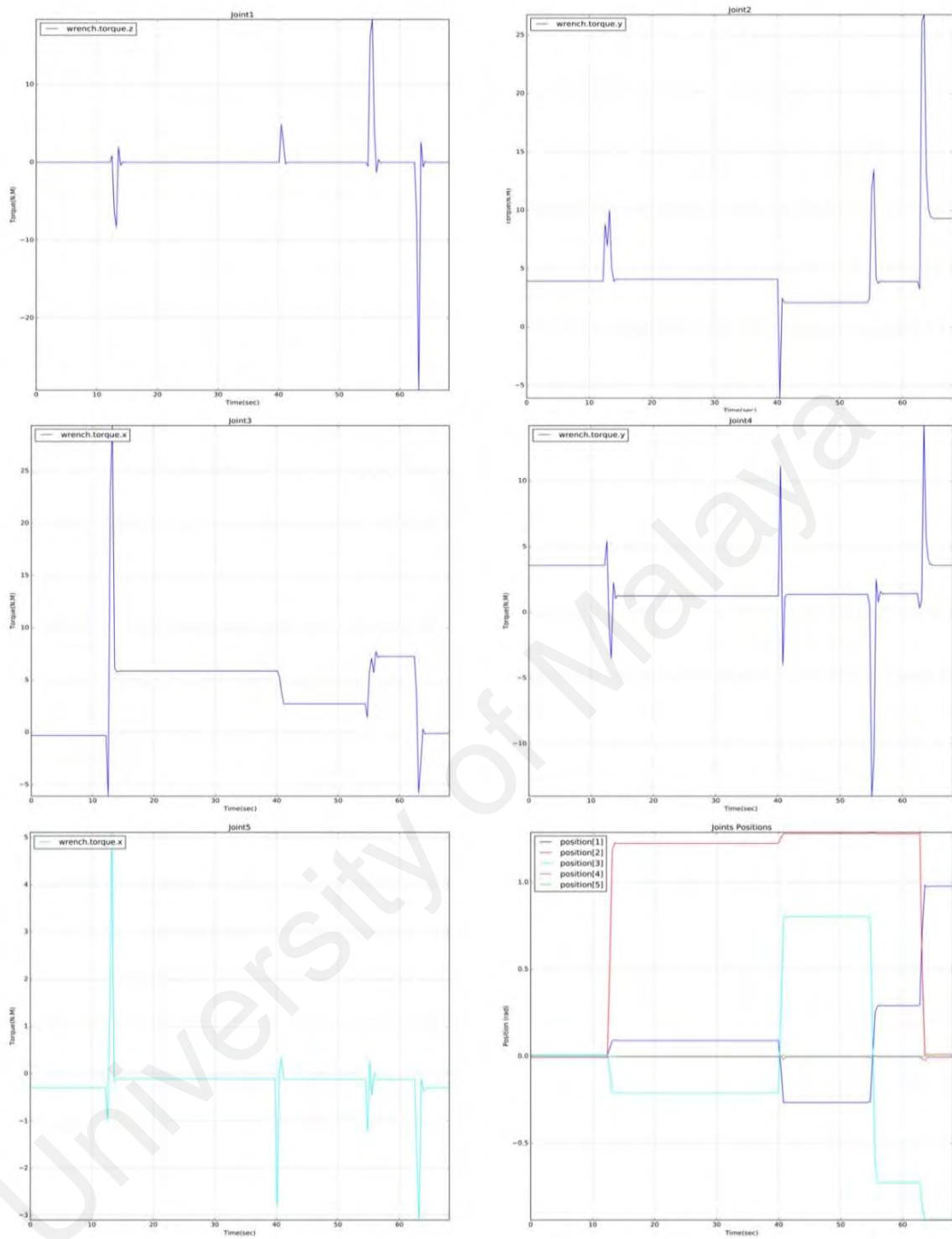


Figure 4.15 The output torque for actuated axes of each joint in 6DOF structure.

In addition to the actuated axis torques, the forces and torques outputs on the first joint of 3R and 4R with base at B2 structure were recorded to measure the effect of the robot

movements on the base of the robot (Figure 4.16), this was done to check the effect of the additional joint in the base of 4R structure.

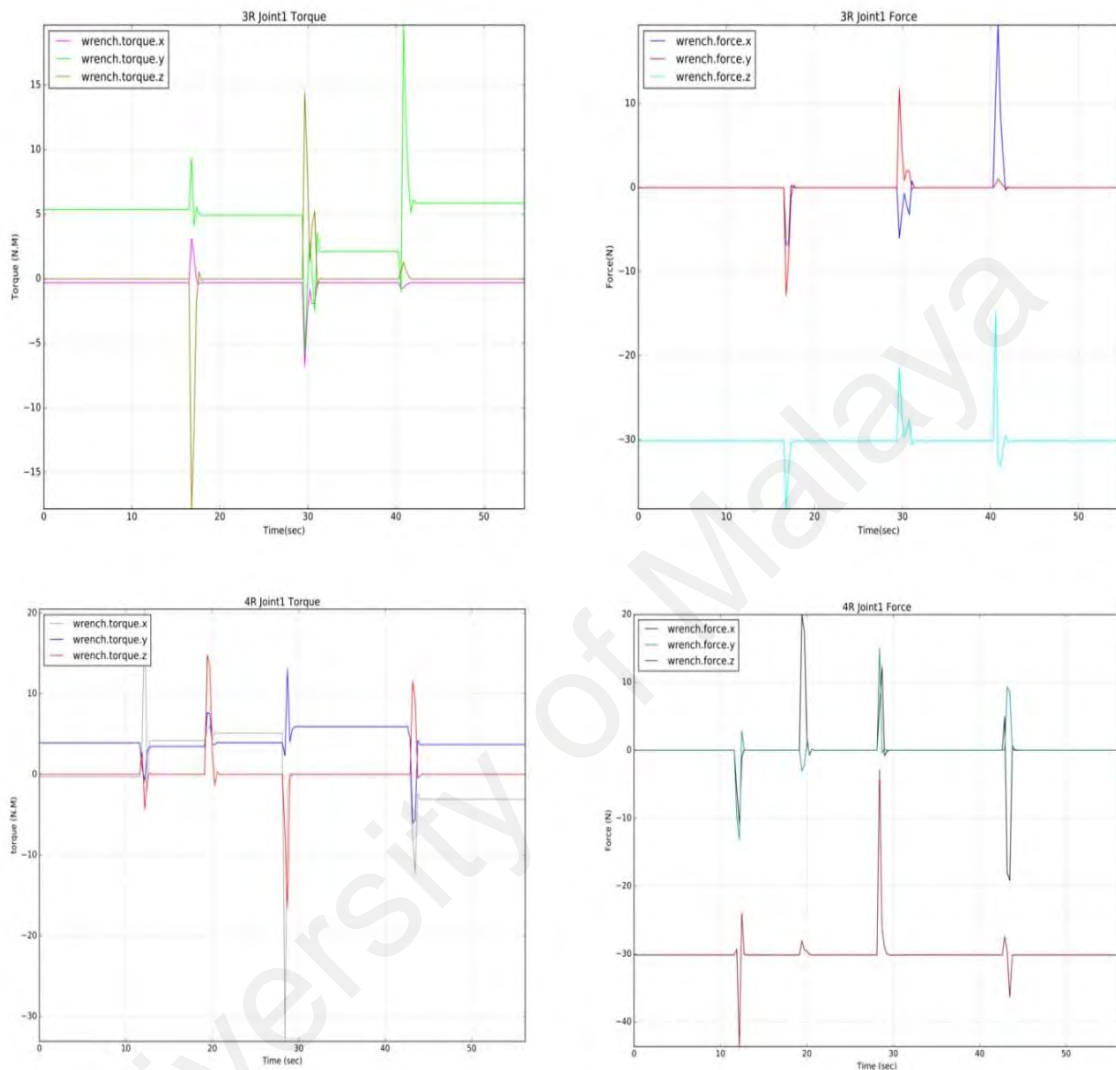


Figure 4.16 Force and torque effects on the joint one of the two main structures, 3R and 4R. this shows stress on this joint as the robot is moving

The following conclusions were derived Based on the results from the dynamic simulations.

- The 3R configuration with base at B1 shows lower required joint torque to move because of shorter links.

- Compared to 3R configuration, in the 4R configuration there are more stress on the first joint which means more support is needed in this area.
- The moving and stall torques needed for these models are in the range of 20 ± 5 N.M.

4.1.5 Pre-Alfa prototypes

Three prototypes were developed based on the results of the kinematic optimization. These prototypes were made to investigate three major aspects of the designs:

Functionality, using these prototypes the idea of using a robotic arm with navigation software and without using external IGS system was investigated. This acted as a proof of concept to show a robotic arm can be used as an IGS tracker.

Workspace and size, the sizes suggested by kinematic optimization was tested using these prototypes. Three prototypes were developed for the two optimized topologies.

Dynamics, mainly the torque for each joint was investigated. The robot should be able to move and hold an instrument in place, the intended speed of the final prototype is low, this is a surgical robot and safety and accuracy is preferred over speed. Therefore, these prototypes were intended in defining minimum torque needed for each joint while the robot is holding an instrument in place rather than needed torque to achieve a certain speed.

Precise servomotors are used in the joints in these prototypes. These servo motors can provide location and torque feedbacks as well as actuating the joints. To test the functionality and workspaces, the prototypes were tested with the tumor bio-model introduced in the methodology chapter.

A Matlab application was developed for testing the navigation features. This application reads the joint value from each servo motor, calculates the location of the tool tip in cartesian space using transfer functions in DH notation for forward kinematics. The CT scan of the patient and a 3D render of the scan (STL file) are imported in the software, the tumor model was registered to the CT scan and the rendered model using multiple landmark points with distinct location in the CT scan and tumor model, points such as eyes' medial commissures and nose sides. Registration is done by comparing and calculating the coordinates of the landmarks in the CT scan and their corresponding location in the robot's cartesian space. This calculation was done based on Singular Value Decomposition (SVD) method introduced in (Besl & McKay, 1992), this method is a very simple and reliable method to find a rigid transformation matrix between three corresponding points in space. A homogenous transform matrix is calculated to transform the tool tip location data into CT scan coordinates. The location of the tool compared to the 3D rendered model was shown by a simple 3D representation of it and compared to the CT images by a crosshair. Figure 4.17 shows examples of both. This software is developed based on the work of (Shen, 2014).

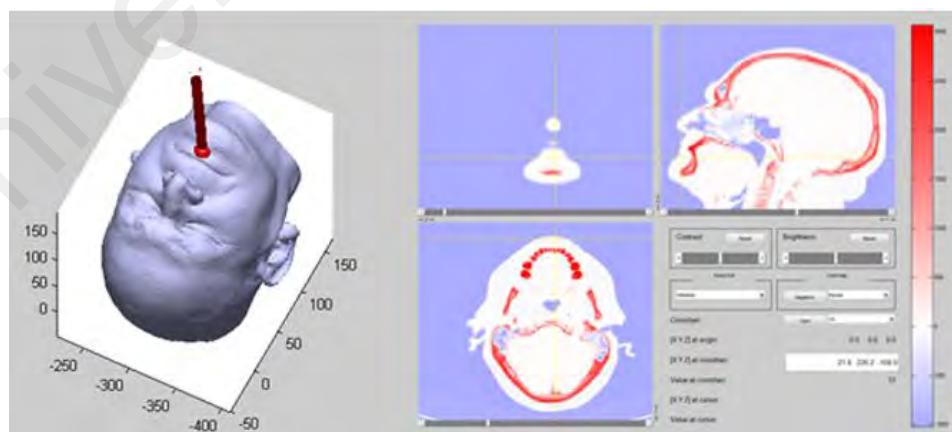


Figure 4.17 The tool's location and orientation are being tracked by the algorithm. The slices shown based on the tool's location.

The first prototype was developed based on the optimized 4R kinematic structure and the 2R wrist, as shown in Figure 4.18. This was used in conjunction with the developed navigation software to test the functionality and workspace size. The servo motors used are small low torque versions (8.4 Nm. stall torque), however with relatively precise position sensors (0.08 deg). This prototype had two problems, large backlash in the servos which changes the position of the tool with any slight force and high torques imposed on joints 2, 3 and 4. The backlash caused inaccuracies in the position reading of each joint. These motors suffer from bad gear backlash which worsens when they are used as arm joints. In the next prototype the joints were coupled to electromagnetic brakes to solve these issues.

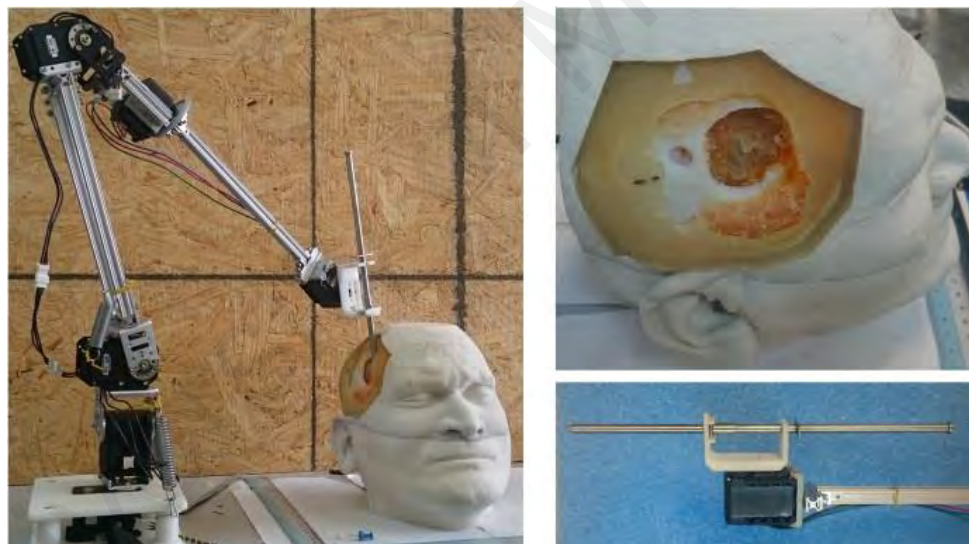


Figure 4.18 a) The designed structure is touching a point on a head model with the tip point (universal probe). b) This 3D model has a slot that can accept replaceable cartridges. These cartridges mimic different pathological characteristics. c) The small wrist of the robot and the attachment of universal probe to the wrist.

The second prototype was based on the optimized 3R structure with the same 2R wrist as shown in Figure 4.19. In this prototype magnetic brakes were used in first 4 joints. These brakes were used to add rigidity in each joint while the robot was holding the tool in place. The brakes were chosen based on their size and torque ratings, two sizes of electromagnetic brakes were used, lighter version with 0.339 Nm static torque and 45mm

diameter for joints 3 and 4 and heavier version with 0.791 Nm static torque and 62mm diameter for the first two joints (as these joints experience greater imposed torque). While brakes were engaged the structure could hold the tool firmly in place, using brakes also improved the negative effect of backlashes in the servo motors (the same servo motors as the first prototype are used in this prototype).



Figure 4.19 The second prototype uses electromagnetic brakes to keep the joints rigidly when it is needed. The joints were load balanced to put less pressure on the servo motors, at joint 2 two synchronized servo motors were used to handle the needed torque.

The second prototype was designed with counter torques on joints 2 (springs) and 3 (the brake and servo for next joint is placed on opposite side of the link), this led to a more balanced structure. This prototype was also used to test the movements of the robot and test the velocity and ability of the servo motors in delivering smooth movements. As this was an early prototype the body of the robot was made using 3D printing and ready-made aluminum protrusions (prototyping profiles). The last joint which provided a connection to the universal probe is using the same design as the first prototype.

Third prototype was developed based on 3R configuration with base at B1, to test functionality of this kinematic configuration, the movements and relative accuracy of new servo motors (Figure 4.20). This prototype was developed after the dynamic simulations and first two prototypes showed the used servo motors are incapable of powering the robot's joints even after load balancing. In this prototype new servo motors with higher torque (>10 Nm) and accuracy ($< 1 \times 10^{-4}$ deg) have been used. The movements were smoother in this prototype due to the higher torque delivery of the servo motors. In the development of this prototype all aluminum attachments have been used to minimize mechanical inaccuracies; the base was fastened to a table using screws to avoid any drift in the robot's base. In addition to the universal probe a laser point was also used as tool on this robot to test the ability of the robot to indicate a point on patient's head without touching the patient.

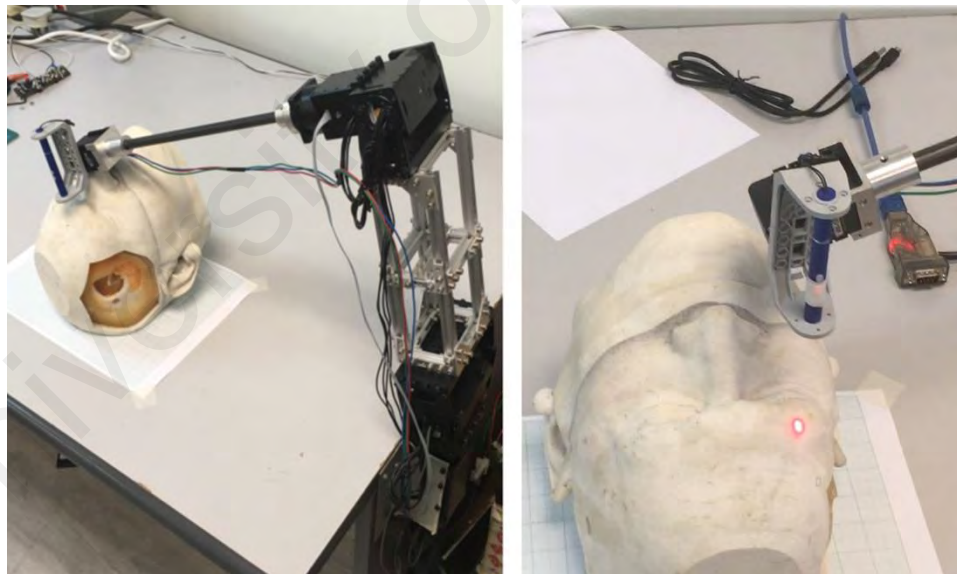


Figure 4.20 The third prototype was developed using more accurate and powerful servo motors, all the attachments were made using metal. the picture on the right shows the point indication feature of this prototype.

This prototype showed better torque and accuracy compared to first two prototypes.

The three prototypes proved the concept and functionality of the design. All successfully could show the location of the tool in relation to the head and CT scan data.

They can reach the desired points on the head model. A good accuracy was not the goal of these prototypes (due to less accurate servos and using plastic and soft metal in the body), but they relatively showed good accuracy (within 1cm of the target for first two prototypes and 0.6 mm for the third). the main goal of developing these prototypes were however, to find the flaws with each design and their functionality.

The flaws of the optimized designs tested using these prototypes are as follow:

- For the first two prototypes the dimensions of the robots demanded high torques on the joints even in the second prototype with the electromagnetic brakes. The possible solution was to optimize the design only for Base locations near the head to avoid long links.
- First prototype was successful in reaching point on the head with the manipulator not blocking the viewing line. However, it required more complicated kinematic calculations, as the value of third joint was redundant to the position of the tool. This could cause in a very complex inverse kinematics as well.
- The third prototype lacks the functionality of obstacle avoidance, but it showed the best accuracy among the three and dynamic performance due to the shorter links and better servo motors.
- The 3 axes intersection at the base is big and bulky, especially if the bigger servo motors are used.

So, based on the dynamic simulation and the results from the prototypes, the challenges to the design where addressed by using the 3R configuration with base at B1 which uses shorter links compared to others, this configuration lacks the ability to avoid collision however slight changes to this configuration could address this issue. For the Alfa prototype the chosen configuration was 3R with a moveable base that could move the whole manipulator in and out of surgical area. This could help when a C-arm scanner

and microscope come in operating area and the manipulator needs to exit. This, however, means that the robot cannot be used while microscope is being used which is a tradeoff between design and functionality.

4.1.6 Alfa prototype

With a moving base the 3R configuration changed into 3R1P (3 revolute and 1 prismatic joints). Besides helping with obstacle avoidance, this configuration could help with functionality as the location of the base is adjustable without changing the frame of reference. This basically means that the location of the base is measurable and known to the controller software at any position so, if during the operation the surgeon wants the robot out of the area it can be done automatically without destroying the patient image registration. The moving base design was implemented by using two linear rails and a slider (Figure 4.21), the slider moves using belt and pulley system by a servo motor which can move the slider to a desired location as well as providing position feedback for the robot controller.

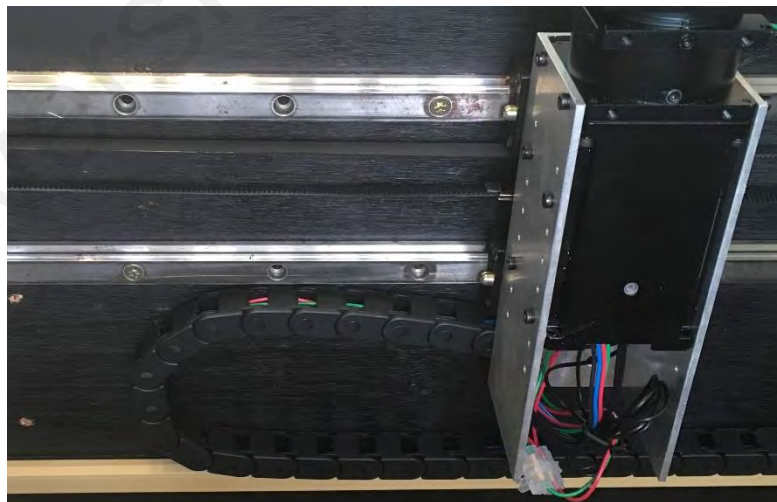


Figure 4.21 The moving base of the Alfa prototype. the base slides on two parallel rails, the movement is controlled by a servo motor which can provide position feedback for the controller.

This is an Alfa prototype which means in the future the design may change slightly so, the effort was to avoid from using proprietary body parts what are hard to change. In

this prototype the two main links of the robot were designed based on market available aluminum protrusions. This helps changing the links sizes easier and less costly. The joint connection parts, however, are designed and developed specifically for this configuration and their design may change for the Beta prototype and clinical trial. This mechanical design ensures that the robot won't reach its singularities (the tool tip cannot reach the base).

The main difference of this prototype with the third pre-Alfa prototype is in the wrist, the new wrist is bigger, mainly due to lack of high rigidity and accuracy in the third prototype' wrist. A support structure added around the fourth joint's motor; this structure supports the power transmitting rod from fourth joint to the fifth. In the third prototype the fifth motor was a smaller servo motor which did not perform good so, a bigger more powerful and more precise servo was added. These changes greatly improved the rigidity in the new prototype. Figure 4.22 shows the Alfa prototype near to one of the head models.

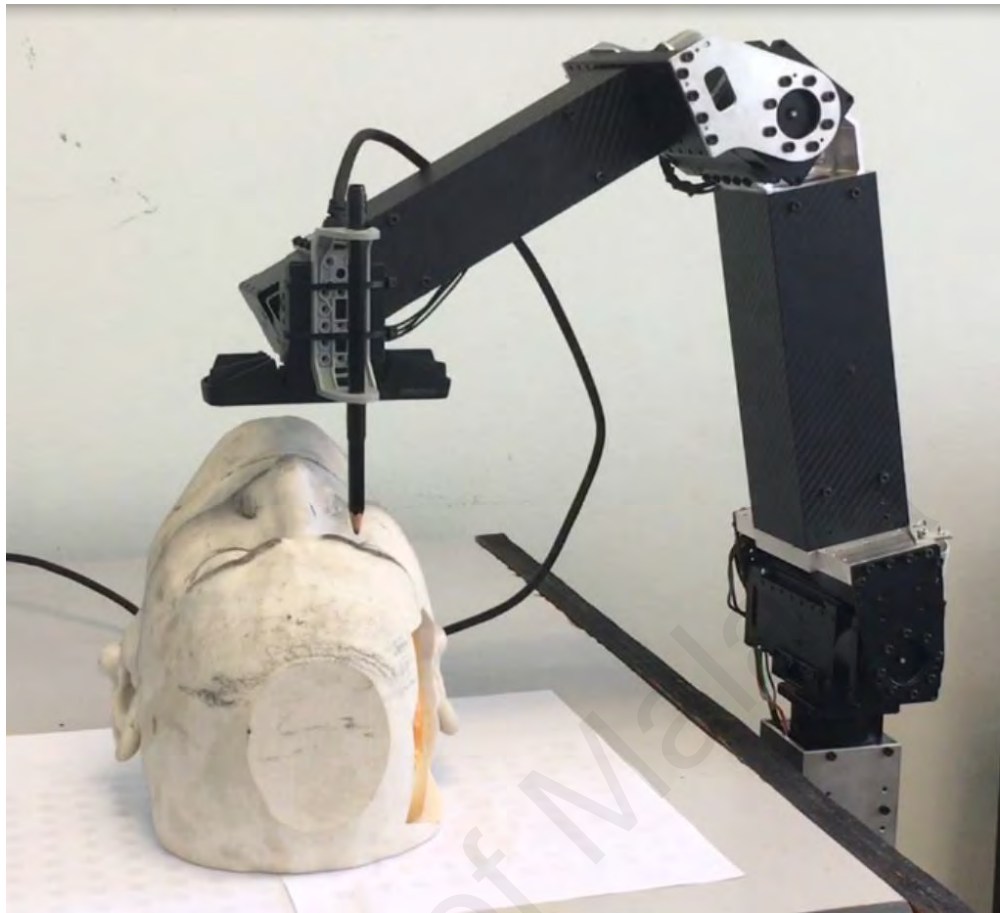


Figure 4.22 The Alfa prototype holding a pencil as a pointer on a selected point from tumor model's medical image.

The tool connection point of this prototype is the servo motor's connection hub (last joint) which can accept different brackets and clamp for different tools if the design of these brackets has matching holes (matching size and pattern) on them. To adopt the presently available surgical tools, brackets should be designed and developed. Referring to the tasks chosen for this thesis two main tools has been used with this prototype, biopsy needle and neurosurgical endoscope. Both these tools are commercially available samples which are presently being used in neurosurgical cases. Figure 4.23 shows the cannula and 3D camera attached to robot's wrist.



Figure 4.23 A bracket for the robot, designed to house a 3D camera and a cannula housing for needle placements.

For registration this prototype uses two methods, first is using landmark (or fiducial) registration using a simple probe (Universal probe), and just touch the desired point with the probe by moving the robot and record the location in the navigation software. Second method was developed as a faster and more accurate way of registration for the robot, for this method the robot uses a 3D camera to scan for point clouds, and it connects to the tool connection point of the wrist same as other tools. Two brackets have been designed to hold the three mentioned tools rigidly to the robot's wrist.

For the brackets and link connections at the joint 3 (link connections between joint3 and other joints), a similar design to the joints in (Robotis, 2017) was used, this is an off-center design in which the links are attached to the joint with an angle to its center. This design was chosen because it gives robot the ability to access more points closer to the base without colliding with its body, using this structure the two links can fold on together to occupy a smaller space compared to normal joints.

The Alfa prototype was used as the main result of this thesis, this robot was used for tests and experiments that delivered the objectives of this project. This prototype was not

ready to run a clinical trial, more works needs to be done to ensure patient's and personnel's safety before continuing to Beta prototype and clinical trial.

4.2 Assistive tasks applications

Before presenting the details of programmed software for this robotic platform, details of the application designed based on the objectives of this thesis is elaborated.

4.2.1 Registration

Stereoscopic cameras are industry's standard for motion tracking and as mentioned have been widely used in IGS systems. Although they are accurate and reliable and using them in conjunction with the robot can potentially guarantee high precision, they are big and as shown they suffer from line of sight problem. Therefore, it was decided to refrain from using external sensors. Serial manipulators not necessarily possess good absolute position accuracy however, they conventionally showed good repeatability. This suggest that if the process of registration made accurately serial manipulators can have accuracy enough for the objectives of this thesis.

As per the review chapter different registration methods were explored to be used in this project as using external position sensors are not favorable, the possibilities narrowed down to two position obtaining methods, using robot's forward kinematics and using a robot attached position sensor. With robot having highly accurate position transducer coupled to each joint and calculating forward kinematic, the position of the tool tip can be easily obtained and used in the registration process. Rigidly attaching a position sensor to the robot's body and using kinematic calculations the sensed position value can be simply transferred to robot's coordinates. in both of these cases the robot's structure remains small without extra structures (such as camera boom).

Two modes of patient-robot registration have been designed for this robot, manual and semi-automatic registration. First is the manual fiducial registration, in this method the user moves the robot's tool point to distinct landmarks (at least three) on the patient's head and record the tool's tip position inside the UI. These distinct landmarks are also visible inside the medical images obtained for the patient. The software calculates the transfer function between the two sets of points. Landmarks can be of any type, anatomical landmarks, or any type of fiducials used in current IGS systems. This method is reliable and accurate but is slow, moving the robot manually for every fiducial is time consuming.

A suitable choice for a body mounted position sensors is to use a 3D camera attached to the robot's wrist during its operation (Carfagni et al., 2017). An attached 3D camera could be easily calibrated to the kinematic model of the robot and provide accurate positioning data in form of 2D images with addition of registered depth data. This camera was utilized in patient image registration as it can provide point clouds with accurate 3D data with addition of colour data (Red Green Blue, RGB). This camera (Intel Realsense SR300 was chosen for this purpose (Intel, 2019)) has been designed to function in near proximity of a target (mainly for facial detection, tracking and recognition features) and is different from 3D cameras used in robot's autonomous driving and space scanners.

The semi-automatic registration is using surface scan method as a base for robot-patient registration. The camera provides a real-time point cloud of the area in front it. Every point cloud carries color and 3D position information for every pixel. As the camera is mounted on the robot it's position to robot's coordinates is known so the generated point cloud can be used to obtain patient's facial surface as it is seen in robot's point of reference for registration.

Before using a scanned point cloud in registration process, it should be ensured that it includes facial features of patient and not the area around the head (head clamp or the surgical table) or any attachments connected to patient's face (oral tubes for example). Manually positioning the attached camera in front of the patient is not possible as the viewing angle of the camera in the recommended distance is wide and includes area bigger than a typical size of human head. However, selecting the desirable area in the point cloud can be done in the software level. To do that a point cloud selection algorithm that uses facial landmarks detection was developed to help identify the areas of interest.

Using facial landmarks detection adds another valuable advantage to the registration subroutine, the benefit of using ICP (Iterative Closest Point) (X. Chen et al., 2014) for the surface registration. ICP is a very powerful and reliable method to perform registration between two sets of points without the necessity of having a twin sets of points (each point is corresponding to one point in the other set) however, ICP can easily get trapped in local minima which suggest the two sets of data should be close to each other before the ICP process. Facial landmarks detected in the point cloud extraction algorithm can help to bring these two sets of points close to each other as it is relatively easy to point the facial landmarks inside medical images (which are obtained for IGS procedures and can be rendered into 3D models). So, before ICP involvement these sets of data are going through SVD (singular-value decomposition) registration algorithm. Detailed description of the facial landmark detection implementation is delivered in the software section.

4.2.2 Biopsy

Biopsy application is a straightforward application. After registration an entry point on the scalp of the patient and a target inside patient's skull is chosen (basically assign a biopsy trajectory) and the robot has to place a cannula in the trajectory of biopsy so that a biopsy needle passing through this cannula hit the entry point and target point on

patient's head accurately. Figure 4.24 shows the cannula designed for this purpose; the needle is a standard commercially used biopsy needle.

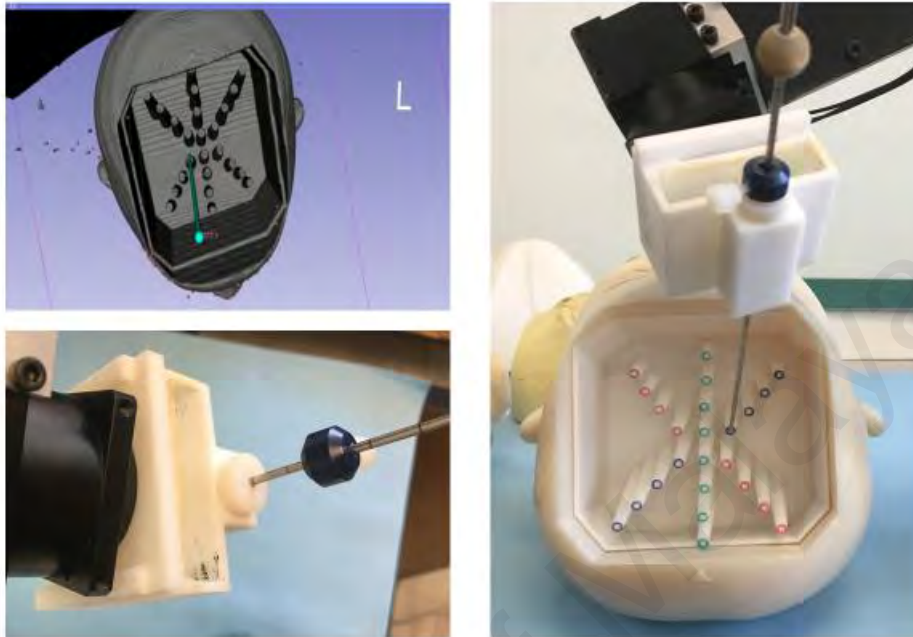


Figure 4.24 The biopsy trajectory in software and robot's spaces.

The process of biopsy using the robot on surgical head models act as accuracy assessment of the robot. To accurately reach the target inside the head models both accurate positioning and registration is needed so, calculated error in this application represents mechanical and registration error.

4.2.3 Endoscope manipulation in transsphenoidal surgeries

The manipulation of endoscope in transsphenoidal surgeries differ from other types of endoscopic surgeries from dimensions viewpoint and from structural viewpoint. In transsphenoidal surgeries the operating area is smaller compared to laparoscopic surgery which has an advantage due to the big space in the abdominal cavity. And compared to intraventricular operations, for transsphenoidal approach many more tools and surgical space is needed. The nasal canal is small, and its limited space is used for endoscope and surgical tools during the operation, therefore thinner and single lenses endoscopes are

avored in this type of surgeries. Furthermore, in laparoscopic surgery the entry incision for the endoscope (and other incisions for other instruments) acts as a pivot point as well. This suggests that the entry incision for endoscope acts as a four-axis passive joint for the instruments (3 rotational and 1 prismatic). However, in transsphenoidal endoscopy the endoscope and instruments pass through one small canal and it is not possible to rest the endoscope or instruments on any point of this canal, in other word there is no physical pivot point for the endoscope. This worsens the limited space problem in transsphenoidal surgery.

The robot also should be able to have autonomous functions such as moving the endoscope out for cleaning and changing the nasal canal entrance. Another characteristic of transsphenoidal endoscopy is that the endoscope is frequently moved out of the nasal canal to be cleaned, compared to other types of endoscopy which the endoscope is moved out of the body less often. Sometimes the trans nasal approach must be done through both nasal entrance and it is very possible that during the surgery the endoscope is moved to between the two entrance.

Handling of endoscope during this type of surgery is a very important task and surgeons use different approaches to this task. Some part of the surgery may be done with two hands approach which the surgeon handles the endoscope and another tool during the surgery. Third hand approach is also very common in which the surgeon is doing the surgery with both hands handling surgical tools and an assistant is handling the endoscope. The assistant responsible for it has to keep the endoscope steady without unnecessary movements and also keep following the main surgeons' movements and his/her verbal cues. A typical transsphenoidal surgery may take hours to complete which can cause hand fatigue and therefore tremors on the endoscope image, so having a robot

as third hand can be beneficial. The requirements for this robotic application, are as follow.

- **The application should be able to accept simple commands such as right, left, up, down, zoom in and zoom out from the surgeon while inside the nasal canal.** This is the same way surgeon instruct the assistant to manipulate the endoscope.
- **The application should be able to autonomously bring the endoscope out with simple commands.**

Researchers have worked on this issue and the peculiarity of Robotic endoscope manipulation in trans nasal surgeries. Authors in (K. Eichhorn & Bootz, 2011; K. W. Eichhorn et al., 2015; K. W. Eichhorn et al., 2017) analyze clinical requirements for such a task and define a workspace needed for this task, these papers introduce a prototype and its comparison with manual surgery. (Trévillot et al., 2013; Villaret et al., 2017) introduce new robotic approaches to this problem while (Chan et al., 2016; ve Pozisyonlandırıcı & Sistem, 2015) focus on controlling a robot in this application. This thesis's approach to this problem is different from mentioned papers (maybe due to different surgical techniques nevertheless, this approach is based on observed data from real life surgeries).

As mentioned in the methods of this thesis, movements of endoscope have been observed and recorded during multiple transsphenoidal skull base surgeries. These observations have been performed to gain a good image of the workspace (positions and orientations of the endoscope during these types of operations) of this task safety areas and the possibility of having a virtual pivot point in the workspace. The workspace analysis has been performed previously by (K. W. Eichhorn et al., 2015; Trévillot et al., 2013) however, these studies have shown the existence of a virtual pivot point on the entrance of nasal canal for trans nasal sinus surgeries (which are done similarly to skull

base) and no pivot point for skull base surgeries (the authors in (Trévillot et al., 2013) have concluded that the pivot point is constantly moving without a position to assign as a virtual point). However, recorded data showed that despite the free movements of endoscope, its movements are constrained to the nasal bone area (Figure 4.25). This bony area limits the translational movement of the endoscope, to have a view of the bigger areas towards the inside of the nasal canal and base of skull the surgeons have to pivot the endoscope to have a view of obstructed areas. These constraints create a funnel shaped workspace for the endoscope. At the narrowest part of the funnel is a plane which is limited by the nasal bone. Every pivot action happens at a point within this plane. The data suggest this plane can be used as a pivot plane.

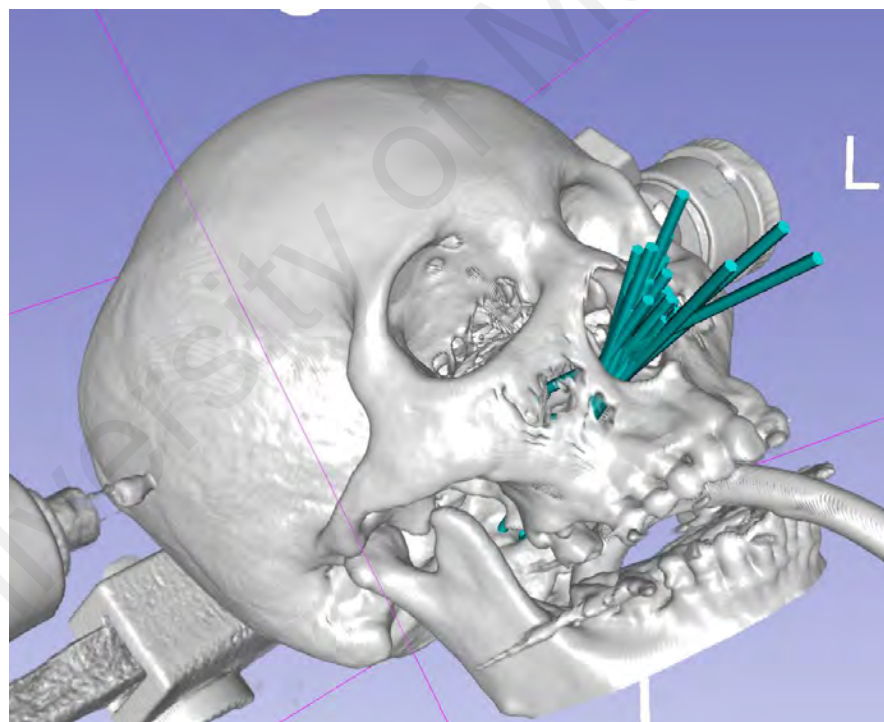


Figure 4.25 The summation of recorded endoscope positions in a transsphenoidal surgery

The analysis (accumulation of all endoscope position during surgeries) suggest that this plane and its boundaries can be determined by three points at the extremities of the nasal bone as illustrated by Figure 4.26, two of these points are located at lower part of nasal canal (on maxilla) and third one is located at upper area of the nasal bone.

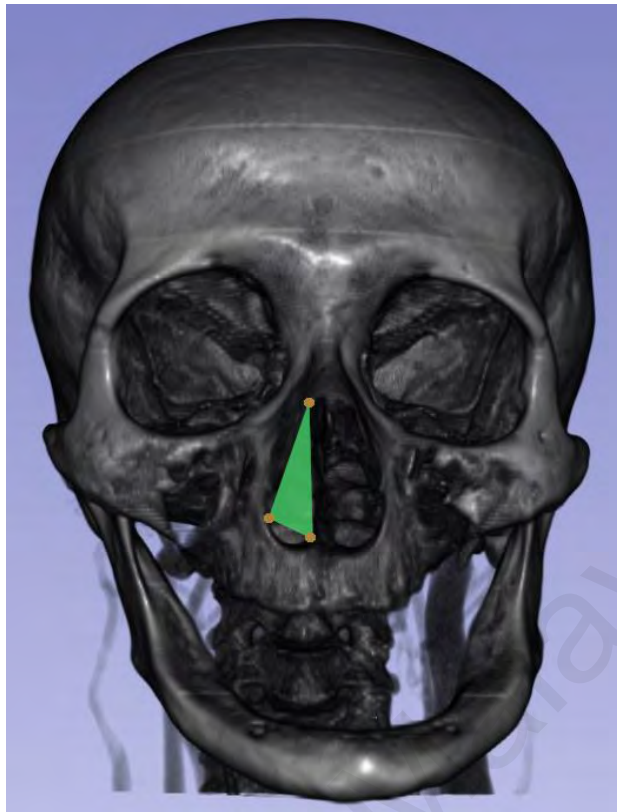


Figure 4.26 A pivot plane for transsphenoidal surgery based on boundaries defined by nasal bone.

Having a pivot plain rather than a pivot point is more complex however, it still simplifies the control by constraining the pivot point within a safe area. The pivot point is the intersection of the endoscope with this plane, the pivot point has a translational movement compared to this plane, so the endoscope viewing angles are calculated compared to this plane.

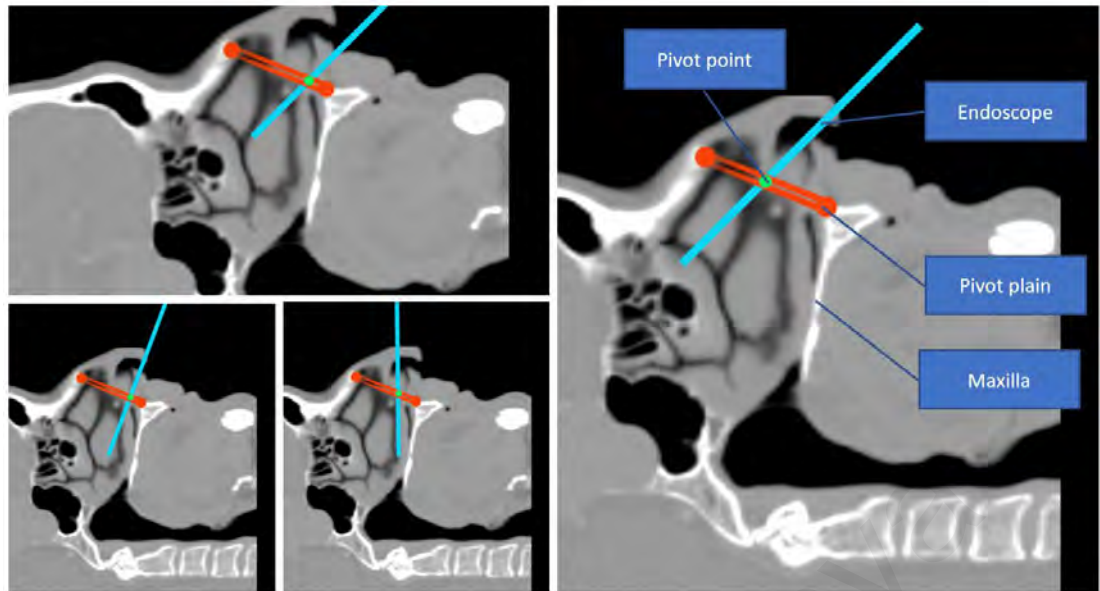


Figure 4.27 cross section of nasal cavity and the suggested position of endoscope compares to pivot plane.

Figure 4.27 illustrates few scenarios based on the suggested approach. Movements of this point are determined by the angle of the endoscope needed for a view and the preferences of surgeons. This means the control algorithm keeps the point in its current position while the endoscope's movements are limited and moves it when the demanded endoscope viewing angle is not achievable by pivot's point current position. Additionally, this approach favors to not move the pivot point until it is necessary, so an initial place should be decided for endoscope during the operation. Often the tendency is to keep the endoscope at one corner of this triangle to create enough space for the other tools inside the nasal canal. However, in the beginning of the operation as the endoscope is still very close to the nasal canal entrance the pivot point might change more translationally than orientationally. So, the controller controls the pivot point location based on the value determined by zoom. Zoom equals to zero means the endoscope tip point is at the pivot point, while negative value shows the endoscope is moved towards outside of the nasal canal. The controller was programmed to move the pivot point (and the endoscope) translationally with the directional command if the zoom value is between -2cm and 2cm (2cm range is used only based on guess works and no evidence could be found to measure

this value). Smaller than -2cm means the endoscope is out of operating area for cleaning and zoom values bigger than 2cm indicates the controller priorities the orientation and if it detects the endoscope would collide with the safety area is translationally move the endoscope.

This algorithm needs initial inputs from the surgeons for the three boundary points and the initial pivot point (Figure 4.28). As the three boundary points are visible in CT scan or MRI the initial point selection can be done pre operatively during the planning stage, however, it is not necessary to use an image guided approach for this algorithm, the point selection can be done manually by surgeon (the surgeon can place tip point of the endoscope at the boundary points desired positions while it is attached to the robot). The same is true for initial selection of the pivot point however, the manual selection is preferred as it usually lays on soft tissue.

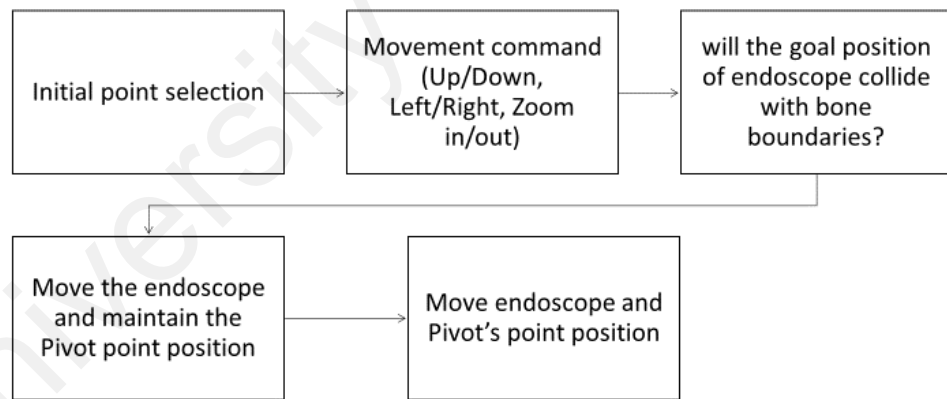


Figure 4.28 Steps of the designed endoscope manipulation application.

The safety of the endoscope movements is ensured based on the safety area determined by the position of the maxilla bone. Maxilla bone is basically the no-touch zone during these operations however, soft tissue in and around the nasal canal can be moved around and pushed over. The decision of manipulating the soft tissue while moving the endoscope is based on surgeon's choice but, the bone boundary should not be crossed at

any circumstances. To predict the position of the maxilla bone as the surgeon chooses the initial points the software creates a virtual plane perpendicular to the pivot plan, the two plans have their intersection line between the two lower points of pivot plan. The robot has semi-autonomous functions (for cleaning) during these maneuvers surgeon cannot decide if he/she is willing to put any pressure on the soft tissue so, the robot controller was designed to have two safety modes, one while it is being controlled by the surgeon the boundary is limited to the bone area and second the soft tissue is also added to the safety boundary. So, when the robot is asked to perform an autonomous function it brings the endoscope to a safe area (in the middle of nasal canal) before moving it out or in the nasal canal (basically it goes back to the initial position of the endoscope which was determined by surgeon either using IGS or manually). To move back in the soft tissue area the robot would wait for the surgeon to give the proper directional commands.

A virtual pivot point with 6 DOF was created to mimic an entry incision similar to laparoscopic procedures. The position of this point is determined by three prismatic axes X, Y and Z the position of the pivot point is inside the bone triangle for each nasal canal. The orientation of this pivot point is determined by rotations around X and Y axes. Last axis is the zoom axis which is a prismatic joint determining the endoscope distance from the pivot point. The robot is tasked to keep the endoscope in the same position and orientation of this pivot point.

The task space data was analyzed for the autonomous functions as well. Typically, in trans nasal surgeries two autonomous maneuvers were in mind, taking out the endoscope for cleaning and repositioning the endoscope between left and right nasal canals. Table 4.3 shows the frequency of these maneuvers done manually by surgeons. The number of times the robot needs to change the nasal canal is small and negligible compared to the cleaning and adjusting maneuvers. The nasal canal change can be avoided with correct

planning from the beginning of the operation. The path planning for autonomous functions in this thesis is focused on the cleaning and adjusting and not the nasal changing maneuver.

Table 4.3 Frequency of endoscope removed from nasal cavity for cleaning and changing of nasal canal.

Operation	Taking out the endoscope for cleaning or adjusting	Changing the nasal canal
1	72	5
2	54	2
3	57	1
4	12	0
5	46	0

The endoscope manipulation happens in two phases, first the position selection which determines the position and orientation of starting pose for pivot point and second the handling the control to user which can only change the two rotation and zoom axes. The other axes are controlled by the software to avoid complicated user control and also ensure safety of the patient.

The control of the pivot point is done by a joystick in this project. The joystick has the options to convert proper and simple directional commands from the user to the robot controller. Furthermore, the mode of command can be changed in the future with voice command or foot pedal.

4.3 Software

The software of this project has been coded in two main environments, Robot Operating System (ROS) and 3D Slicer. Every piece of program that is related to control of the robot such as planning, position feedback and hardware communications has been programmed in C++ with a ROS wrapper, ROS facilitates the communication between these subroutines. 3D slicer has been used to accommodate all programs related to

medical images and models rendered using these images, Slicer IGT plugin in 3D slicer facilitates the communications and surgical navigation fundamentals. The user interfaces (UI) coded for the robot's control have been also coded as plugins to 3D slicer. Figure 4.29 shows overall diagram of the software design. The communication between the two environment is managed by a program developed based on (Frank, Krieger, Leonard, Patel, & Tokuda, 2017). In this section each of the subroutines illustrated in Figure 4.29, are described in detail. Every program under ROS has been coded using C++ and Python language has been used for 3D slicer plugins.

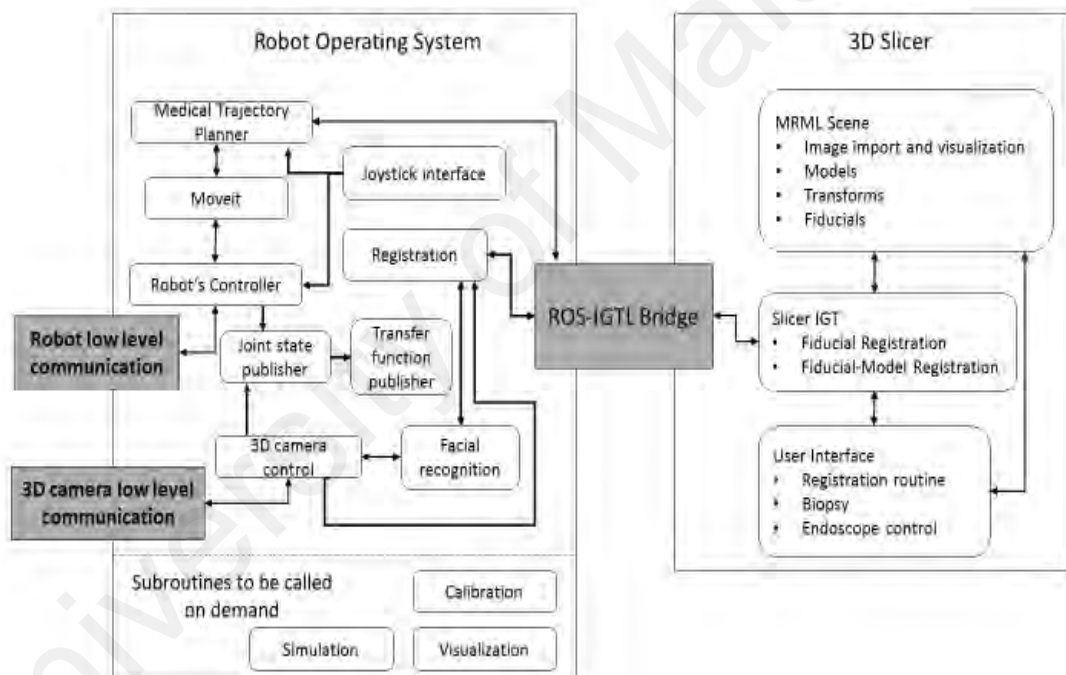


Figure 4.29 Software diagram of the Alfa prototype.

It should be mentioned that both ROS messages and IGTLLink are network capable protocols therefore, these software packages can be distributed between different machines if necessary. In this thesis the whole software system was divided between two computers, one small portable unit (Intel NUC with i7 processor) for all robot and camera related processes and one a Dell workstation with Intel Xeon processor for 3D slicer,

medical image handling and user interface programs⁴. All the codes have been coded and worked in Linux operating system (ROS kinetic kame and 3D slicer 4.8 on Ubuntu Xenial). Every third-party code used in this thesis are open source material that allow their use in academic and commercial applications.

There are lots of benefit in coding the controller software in ROS environment, codes are open source and most of them can be reused without commercial liability. The ROS system is constantly being updated and debugged which helps keeping the robot's software up to date, and its codes are not hardware dependent which means if in future the hardware such as the servo motors are changed most of the codes can be reused and only the codes communicating with the hardware have to be changed.

In the process of developing the software introduced in this thesis, any use of proprietary software was avoided. For portions of it, where no open source equivalent could be found, they were programmed and coded from scratch, or when the open sourced lines of code could not be used due to software bugs (which was unfortunately often the case) or use of unsupported legacy libraries, the codes were heavily modified to enable reliable performance for the robot. As far as the literature review showed, no similar attempts were made for a complete surgical robot fully reliable on Open source programs.

⁴ 3D slicer and the UI programmed inside it can be loaded on any PC or laptop with Windows, Linux or Mac operating systems.

4.3.1 Robot low-level communication

The servo motor used in the Alfa prototype are controllable via serial communication. The motors are daisy chained together using RS-485 data lines. The RS-485 data line is connected to the controlling computer using USB to RS-485 converter. Communication with each motor is done via an ID which is unique to each motor. Each motor has list of registers that their value can be read or write by the robot controller to control the motor (Robotis, 2018). The most important registers are

- ID, this register holds a changeable unique ID of the motor in the daisy chain.
- Torque limit, using this register the maximum torque on the motor can be adjusted, if the torque reaches this level the motor will shut down. This helps the robot to avoid serious damages in case of any collisions.
- Torque enable, changing the value of this register activate and deactivate the motor. While the torque is enabled the joints cannot be moved by hand (motor's electrical break). But if the user needs to move the robot by hand (for example during the manual registration), the torque has to be disabled.
- Goal position, each motor has an absolute encoder which makes it easier to control the goal servo position and in result angle of each joint. The value for this register is calculated by the Robot controller subroutine.
- Present position is a read only register that holds the value of the absolute position encoder.
- Velocity limit can be used to assign the maximum allowed velocity for each motor. Which are valued very low for surgical tasks.
- External ports, these motors are equipped with an external expansion ports which can be programmed into analogue or digital inputs or outputs.

- Shut down, this read only register returns an error number matching to any error which caused a shutdown of the motor.

The data line for the base servo motor use different protocol (TTL level communication) so it uses a separate data connection to the controller with its own USB to TTL convertor. The controlling registers for the base servo are also use different configuration than other parts of the robot, but the names and used are similar to them. So, at the low-level communication the controller has to differentiate between the commands going to the base or other parts and act accordingly (the power level is also different 24 Vdc for manipulator motors and 12 Vdc for the base motor). So, a simple power circuit was used to take 24 Vdc from the power supply and provide the base joint with 12 Vdc output.

4.3.2 ROS-Robot controller

This is a piece of code which acts as the main robot controller, the program that translate ROS topics to the servo motors commands. Robot controller communicate with other programs through ROS subscribed messages, set mode, Joint pose and Goal, and output Joint state. Set mode dictates which mode the robot should be in by the UI to the controller, there are three main modes, first mode is called enable, which puts the robot in normal working mode which is used by endoscope manipulation and biopsy applications, second mode is disabled which totally disables the controller from receiving or sending data to/ from the robot but keeps the robot in place with static torque which makes it hard for the joints to move (this mode is used while biopsy or needle insertion, to keep the robot from moving accidentally by hand or by the controller), and third mode is torque-off which disengage the servo motors and make it possible to move the robot freely but is still able to receive position data from the robot (this mode provides the freedom to the surgeon to move the robot by hand for manual registration and endoscope

application). Every positioning command sent to the controller will be ignored if the mode is not set to enable.

Joint pose message act as direct control of the robot joints, by sending command to this topic the controller try to put the joints in the values provided by this topic. This topic is only used in debug and troubleshooting modes in which the user provides the joint values manually (by a publishing a message to this topic using ROS topic command) to make sure everything working correctly on the robot and controller side.

Goal topic is provided to the controller by the Moveit module, it carries the desired goal position of each joint. The controller takes the data, calculates a finer trajectory by calculating extra points between point provided by Moveit and velocity and acceleration provided by the programmer. Using the new set of points, the controller produces a trajectory matrix with 6 columns for each joint and number of rows as needed for the trajectory, each row representing a point in the trajectory. This matrix is then sent to the low-level controller through serial communication.

This program continuously reads the position value of each joint from the low-level controllers. These values are then converted to suitable values for ROS messages (radian for revolute joints and meters for the prismatic joint) these values are then published by joint state publisher and used by Moveit to calculate the current state of the robot.

4.3.3 ROS-Moveit

Moveit is the main motion planning software framework for the ROS. This framework consists of powerful and open source solutions for motion planning, 3D perception, kinematics, obstacle avoidance and navigation. The Moveit has been configured to work with the alfa prototype, the configuration includes, kinematic model (which is based on joint axis configuration), different kinematic chains to control (with moving base and with

locked base), self-collision matrix (joint configurations in which parts of the robot collide with its other part), joint limits (position, velocity and acceleration limits), planning algorithm (OMPL from (University, 2018)) and Inverse kinematics solver (KDL kinematics from Orocos (Project, 2018) project which is a numerical solver). It is possible to change the inverse kinematic if a more suitable algorithm is developed.

OMPL or Open Motion Planning Library is an open source software designed based on Sampling-based Motion Planning. In sampling-based motion planning the algorithm cycles through different state of the robot and search for a path to connect these robot states without colliding with any obstacle in the workspace.

Moveit receives the goal position and orientation of the tool and safety boundaries from the medical trajectory planner, as well as current state of the robot from joint state publisher. Moveit then calculates the trajectory based on these information as well as primary configurations and sends the data to the robot controller. There are also functions that can be used to define an area of safety in the moveit configuration which can be followed despite any command by medical trajectory planner.

4.3.4 ROS-medical trajectory planner

This module acts as a mediator between Moveit and UI, after the registration is done this module receives commands such as location of a target, point of entry and endoscope manipulation from the 3D slicer environment and calculate the necessary conversions based on the available transfer functions (register transfer function between image and patient). The conversions in this program are geometrical conversions in which the coordinates of the target and other points are converted from the medical image coordinate system to the physical patient coordinates. These data are then sent to Moveit as goal points for planning a trajectory.

Any no entry zones and safety areas are calculated and assigned by this program. In case of endoscope manipulation after UI sending the initial points, the medical trajectory planner calculates and assigns the safety areas in Moveit. When joystick interface send movement data medical trajectory planner calculates the suitable movement of endoscope (if the pivot point needs to move or not) and sends the planning commands to Moveit.

4.3.5 ROS-Joystick interface

This module starts and listen to inputs from a Joystick. One button on the joystick corresponds to torque off (disable) mode on Robot controller and allows the surgeons to move the robot by hand. Other directional buttons correspond to endoscope manipulation if the controller is in enable mode.

To manipulate the endoscope simple arrow commands (up, down, left, right, in and out) to control the position of the endoscope and command for endoscope cleaning maneuver. Endoscope cleaning maneuver brings the endoscope out of the operating area and waits for it to be cleaned by surgical personnel and move it back inside the canal exactly in the same position as before. These commands are transferred to medical trajectory planner for necessary coordinate conversions.

4.3.6 ROS-Registration Module

This module facilitates the ROS side of the process of registering the patient (model) to the corresponding medical image, this module deals with the manual and semi-automatic registration algorithms. This module receives point clouds from camera controller and facial recognition module, simplify them by removing unnecessary points from the cloud and send the resulting cloud to the 3D slicer. A typical point cloud provided by the 3D camera has more than thousands of individual points, 3D slicer cannot

handle this number of points, sending all these to 3D slicer can end up in the software crash. So, using the facial landmarks' location the point clouds are simplified, and only necessary point have been sent to 3D slicer. Mainly the point cloud from upper face and nose is selected. In the case of manual registration this module just sends the location of tool tip point to 3D slicer as one individual point.

Based on the calculation done in the 3D slicer environment this module receives the transfer matrix for conversion between physical patient and medical image, convert the data into ROS transfer functions format and send them to transfer function publisher for continuous publishing. The registration module in 3D slicer performs two types of registration, SVD and ICP. SVD is used for manual registration and also the first step of ICP registration. In ROS registration module the transfer matrix from SVD publishes as head_registered_1 transfer function and from ICP corresponds to head_registered_2 transfer function. In the case of head_registered_2 not available the medical trajectory planner uses head_registered_1 as primary registration transfer function.

4.3.7 ROS-Joint state publisher

this is a ROS native program which collects the joint position data from robot controller and publish it continuously for every other module that need this data. Every joints position is updated constantly by this program, this is to be used mainly by Moveit in motion planning and kinematics calculation.

4.3.8 ROS-Transfer function publisher

This also is a ROS native program which collects receives coordinate data from relevant programs such as Moveit and registration module. The following transfer functions are published by this program:

- Every axis in the robot's kinematic chain (joints, tool and camera). Each of this axis is defined in an URDF (Universal Robot Description Format) file, this is the type of file which define robot's physical model in the ROS environment.
- Patient's head. The facial detection module provides the position and orientation of the patient head as transfer functions. This is the data used by registration module.
- Registration transfer functions head_registered_1 and 2. This transfer functions which are provided by the registration module is basically the conversion needed to bring the geometrical data from medical image coordinates to robot's coordinates.

4.3.9 ROS-facial detection

to implement the semi-automatic patient registration, the robot system should be able to accurately find the patient in 3D space and provide the registration algorithm with enough surface data. To perform this the robot must take the following steps:

1. Using the 3D camera, the robot should find the patient's head position.

We roughly know the patient's head is located at the top part of the surgery table, to pinpoint is more accurately the facial detection module is used. By scanning the top area of the surgery table, the module will be able to provide data on the position of face and as conclusion the position of the patient's head.

2. The robot should be able to estimate the patient's head position, so it positions the 3D camera in an optimal viewpoint of the patient's face. This is possible by using facial landmark detection and using the landmarks location to estimate the head position. This is possible both

using normal camera and 3D camera, 3D camera provides better estimation due to providing depth data besides RGB data.

3. The robot must be able to provide the registration software with an initial guess on the location of registration point cloud. The registration software uses this to perform pointset registration using SVD algorithm performing ICP method in surface matching registration. This initial guess is provided by matching facial landmarks on both render of the medical image and the patient's face.
4. The robot should generate a registration point cloud based on available surface area on patient's face. Usually while patient is getting ready for surgery the mouth or nose is blocked by tubes (placed by an anesthetist) tapes and/or wires. These attachments block some areas of the face from using for registration (usually lower nose face area), additionally sometimes the full head is not scanned in the medical images (again the lower face and head area is the left-out area) as not necessary for medical purpose.

In surface registration the navigation software needs enough distinct points from patient's head surface to calculate the registration transfer function, facial surface is the most suitable surface to provide these points. To design a proper facial recognition, in addition to the mentioned requirements, the algorithm had to follow the following requirements, first the algorithm had to be fast, as the robot have to find the face and locate the head in a sweeping motion. Second the algorithm must be able to detect the tilted faces as well as straight faces, as the patient is not always positioned supine. Third the algorithm should be able to estimate the head's position as the robot have to move the camera in an optimized position, it is not necessary to scan the face exactly from front as side of the face also provides good amount of data however, positioning the camera

directly in front of the patients face, provides the chance to scan bigger number of facial landmark points in the registration point cloud. Fourth the algorithm must detect the facial landmarks, as the system need the landmarks for the initial guess process, the landmarks coordinates are also needed in simplifying process of the registration point cloud. There are different available methods for face and facial landmarks detection but the most popular methods are using two main object detectors for facial detection, HAAR Cascade detector (Wilson & Fernandez, 2006) and HOG (Histogram of Gradient) Cascade detector (Zhu, Yeh, Cheng, & Avidan, 2006). For the purpose of this thesis two main face detector libraries have been investigated, OpenCV (Opencv, 2019) which uses HAAR and Dlib (davis, 2019) which uses HOG. Facial recognition algorithms developed for both libraries where they use data streams from the 3D camera controller and detects the patient's face and its landmarks such as nose and eyes. Based on the four mentioned requirements of the facial detection module the Dlib library with HOG cascade detector performed batter and was chosen as the facial detection method in this thesis, mainly due to ability of this library in detecting tilted faces, Table 4.4 summarizes the comparison derived for the two algorithms.

Table 4.4 A comparison between two facial landmark detection methods used.

	Speed of face detection	Detection of tilted faces	Heads position estimation	Facial landmarks detection
Dlib	Slightly slower than OpenCV	Very good as long as the head is not completely turned	Good	Good (68 points detection)
OpenCV	Fast	The angle of face tilted is less than Dlib	Good	Good (68 points detection)

This module is coded based on heavily modified version of the head pose estimation method used in (Lemaignan, Garcia, Jacq, & Dillenbourg, 2016). The facial landmark detection in this work used Dlib landmark detection which itself has been derived from

(Kazemi & Sullivan, 2014). However, the data set used in this algorithm is based on 68 points facial landmarks which includes mouth and areas around the face. A new model had to be used to include only areas available (upper nose area).

A dataset with 1000 human faces was derived from the I-Bug 300 Faces In-the-Wild Challenge (300-W) dataset (Sagonas, Antonakos, Tzimiropoulos, Zafeiriou, & Pantic, 2016) to decrease the training speed of the HOG descriptor and linear Support Vector Machine (SVM) object detection model. The 300-W dataset was reduced from its large number of human faces images to 1000 images. Since, this project required the camera to detect and mark the landmark of the faces excluding the lower nose face area (to avoid confusion of the algorithm while patient is intubated). The original 68 mark-up points were reduced to 31 mark-up points as shown in Figure 4.30.

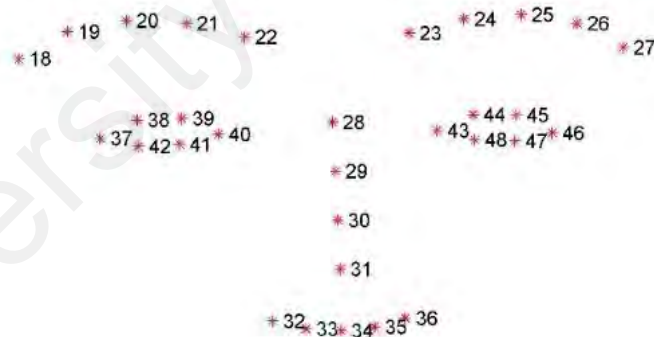


Figure 4.30 Modified 31 mark-up points for facial landmarks excluding the unused points

Hence, a dataset named half_face_ibug_300W_1000pcs_aspect_ratio_1.xml was created. After the creation of the dataset, the models for the facial recognition system were trained. There were two models to be trained. One of them was an object detection model which is face detector in this case by using HOG and SVM model and the other one was the

shape detector which is facial landmark detector in this case which located the annotation by using Ensemble of Regression Trees (ERT). The training parameters were the same one which was used by the full face 68-points landmark predictor model provided by the Dlib.

The program was written to link camera which acquired image data and by using the camera data the program would track and annotate the desired landmarks for any faces. The facial detection subroutine was then tested to ensure smooth landmark detection, as shown in Figure 4.31.

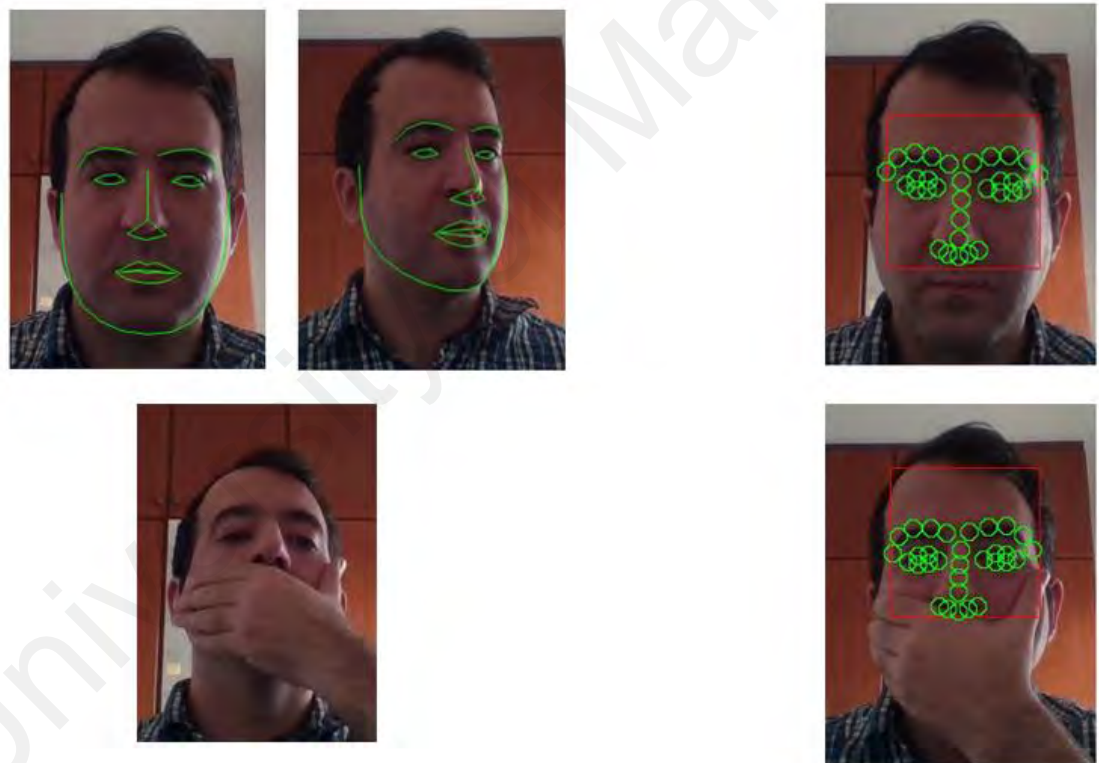


Figure 4.31: Detection of the trained model on the right vs normal face model on the left, normal face model fails to detect landmarks while the mouth is covered or blocked.

The moment the facial recognition module finds the face, it sends info to transfer function publisher to publish head's physical location and orientation, the center of the transfer function is located at the center of face somewhere between the eyes (Figure

4.32). The robot then places the camera directly in front of the face (if it is within the workspace of the robot) and in continue the facial detection module publishes the facial landmark points and facial point cloud.

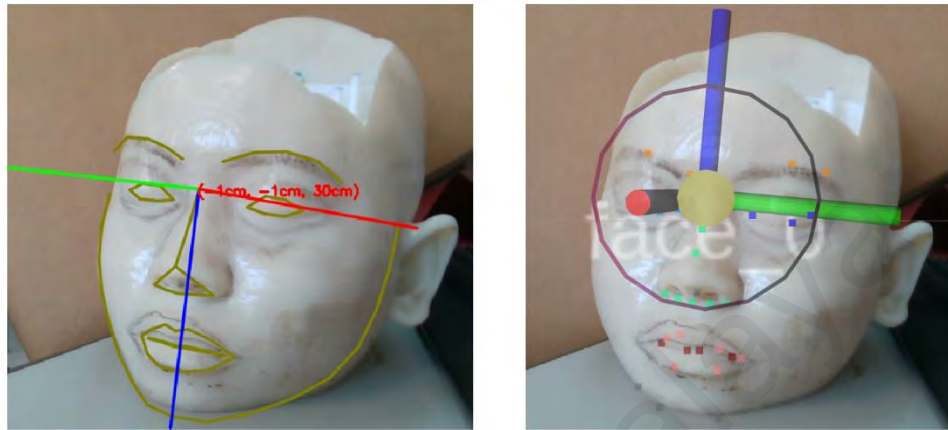


Figure 4.32 The algorithm used in this module to detect the faces and facial landmark uses the trained facial landmark detection algorithm. On the left the image shows a typical output of the Dlib facial landmark detection and on the right the output of a ROS wrapper written for this algorithm is shown, this image shows the facial landmark points in different colors (for example green for the nose area).

This algorithm detects the face using RGB stream of the camera and initiates the landmark detection using this stream and then uses the registered depth data stream to provide 3D coordinates of 31 points in a point cloud, this point cloud is then sent to registration module to be used as first step (initial guess) of registration.

4.3.10 ROS-3D camera controller

The camera controller is basically a ROS driver which communicates with the 3D camera through USB port and publishes the related topic to ROS environment. The controller publishes all the necessary topic which includes streams of RGB video, infrared video, depth data and point clouds. The camera hardware provides raw data such as RGB and infrared video streams to the driver, in return the driver process the data and based on the camera intrinsic data provides the processed data in form of point clouds and registered video stream. Registered data is basically the mapped data from both RGB and

infrared data streams. This driver has been developed by Intel; however, ROS also has a native 3D camera package that can be used for other types of cameras.

4.3.11 ROS-simulation

It is possible to run the Gazebo software with the model of the Alfa prototype as simulation. This simulation communicates with other parts of the software and act same as the physical robot. Moveit also provides a demo mode which can be used to check the motion planning and Moveit configuration without the need for Gazebo or physical robot.

4.3.12 ROS-visualization

Information such as the motion planning, point clouds, and transfer functions can be visualized using ROS native software Rviz. It is possible to run the ROS portion of the software with no visualization however, in the development phase and troubleshooting the visualization helps to speed up the process.

4.3.13 ROS-Calibration

in this application the camera acts as a position sensor, during the registration the depth data from the camera measures the position of patient's head in relation to robot's base. Therefore, camera's attachment to the robot should be defined accurately to lessen any error in the measurement. This is done by the calibration routine which can be called anytime the user needs to calibrate the camera again. This calibration method is based on work in (industrial).

In this routine a circle pattern (checked pattern can be used however in orientation detection circle patterns are more reliable) with known dimensions is used to calculate the position and orientation of the camera. This is done while multiple images of this pattern are recorded with different robot's positions. The output of the calibration routine is the best guess on the position of the camera in relation to wrist of the robot. This guess

is calculated using CERES (Sameer, Keir, & Others). CERES solver is an open source project by google which is very powerful in solving optimizations with loop closure problem. Figure 4.33 shows three of positions the Alfa prototype was positioned at for calibration process.

The process of calibration which is to change robots position and collect image data for minimum 20 different robot poses is done automatically, after the CRES solver finishes with calculation, the user has to change check the results and if suitable change the URDF file manually (the automatic URDF change is rather not necessary as the user has to confirm the correctness of the calibration). Intrinsic parameters calibration was not necessary for this camera as it has been calibrated by factory however, for other types of cameras it is possible to perform intrinsic calibration.

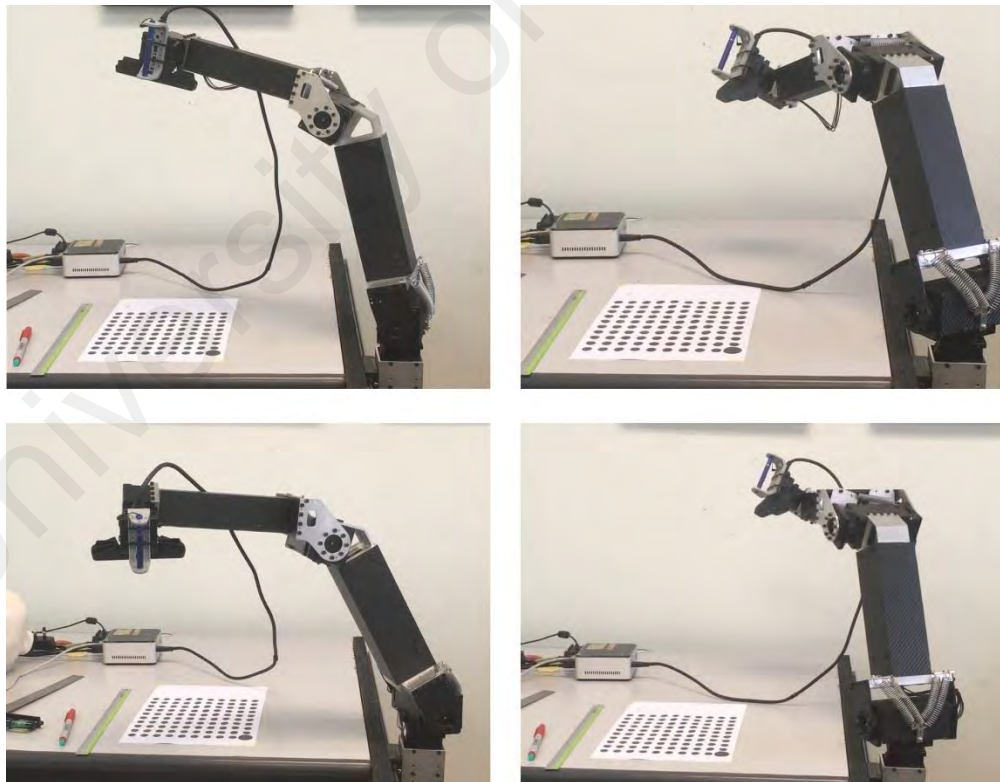


Figure 4.33 During the calibration procedure the robot points the camera to a circle pattern from different directions and with different poses.

4.3.14 3D slicer-main modules

3D slicer provides an open source platform to work and manipulate medical images. 3D slicer is equipped with multiple core modules which they provide fundamental functions needed in working with medical images. This software project provides different ways for developers to write their own plugins and extensions. Extensions are software modules that can be added to this software for more functionality and plugins are a fast way of scripting new features inside the software. The plugins and extensions use the core modules to access and modify the medical images in slicer, the following core modules are some of the core modules:

1. DICOM, this module handles the importing storing the DICOM data from files.
2. Editor, this module allows the user to perform segmentation on an imported image.
3. Volume rendering, this module facilitates the 3D rendering of the image data, using which the user can render an 3D model of the patient's head (or any other organs).
4. Markups, this module handles the creating, storing, visualizing and manipulating of markups in a scene. Markups are basically fiducial points.
5. Subject Hierarchy, this module acts as a graphical interface organize the available data in a scene. This module provide feature such as cloning, transforming and show/hide.
6. Transforms, this module handles the creation and manipulation of transform matrices. Using transform matrices all the geometrical entities in the scene, such as markups, scene view and models can be transformed. This can be done by moving a desired data under a transform using subject hierarchy module.

7. Models and model creator, using these modules whole or segments of an image can be converted into 3D models. These models can also handle geometrical and imported models inside a scene.
8. OpenIGTLinkIF, this module connects the 3D slicer software to other software such as PLUS and IGSTK (Lasso et al., 2014) and hardware such as robots and trackers (optical, Electromagnetic, . . .). This module follows the IGTLink protocol and over TCP/IP (Tokuda et al., 2009). This module also provides an interface into 3D slicer data management using which the outgoing data such as transforms, images and markups can be selected, the incoming data can be stored using 3D slicer data management as well.

4.3.15 3D slicer-Slicer IGT

This is an extension module for image guided surgery that can be installed in 3D slicer (Ungi, Lasso, & Fichtinger, 2016). This module facilitates the necessary connection features to work with trackers and necessary algorithms for registration and visualizations demanded for a basic image guided surgery software.

4.3.16 3D slicer-User Interface

The user interface has been developed by Python and under 3D slicer plugin capabilities; Using this method new plugins can be imported in 3D slicer without the need of rebuilding the whole software code. The user interface has been developed to handle user's inputs and choices for two main functions of the robot, Registration, Biopsy (or needle placement).

By starting the applications in ROS, the ROS-IGTL-Bridge will be initialized and start searching for IGTL server (based on IP and port configurations inside a config file), the server is configured in 3D slicer by the registration UI. After connecting the 3D slicer software to the ROS environment using OpenIGTLinkIF through ROS_IGTL_Bridge the

registration UI is initialized and prompt for three markups on the facial area of a model (rendered from an imported image) to be used in fiducial registration. There is a list of 31 points to be chosen (but minimum 3 is necessary to be chosen from 31 points), 31 points are the points that indicate nose, eyes and eyebrows areas. If manual registration is chosen in addition to facial landmarks the user can also select other types of distinct points such as fiducial markers. UI then sends request to registration module in ROS for the equivalent number of points on the physical patient (printed models), after receiving the points from ROS the UI performs the SVD registration algorithm from the slicerIGT module and produces a transform matrix. At this point an image patient registration have been performed (at this point manual registration is complete and head_registered_1 is already being published as registration transfer function) however, for surface scan method this registration can be more accurate, So, this transform matrix can be used as an initial guess for the ICP algorithm in surface matching technique.

The UI sends the initial calculated transform matrix to registration module in ROS, the registration module in return sends a simplified point cloud of patient's face to the UI. The coordinates of each point in this point cloud is transformed by the initial transform matrix provided by the UI. The incoming point cloud from the 3D camera is dense and full of unnecessary points, the simplified point cloud has maximum number of 100 points which provides coordinates from area of interest. The area of interest is by default the area on top of the patient's nose line, as this area is usually not blocked by surgical attachments, the area of interest itself contains lots of points in which the registration module on ROS side brings down the resolution of point cloud to a manageable number. After receiving the point cloud, the UI then calculates a more accurate transform matrix using the point cloud and ICP algorithm. The second transform matrix (head_registered_2) is then sent to ROS for transform function calculations hereafter.

Biopsy and needle placement are a simple UI module which prompts the user for two points, entry and target. The entry point is usually selected on the surface of skull and indicates the location to make incision and drill the cranium, target point is usually selected inside the brain to take a sample from a pathology or a specific brain tissue to place an electrode. The user selects the entry and target point and sends the data to robot (ROS-medical trajectory planner) to place the biopsy cannula on top of the entry point and in orientation with the target point, so when a needle is placed through the cannula it hits the entry point on scalp and after incision and drilling, by moving the needle further it will hit the target (and in case of biopsy sample tissue is taken). The distance of the cannula from the entry point is fixed to 30mm (no technical reason but the surgeon was comfortable with this distance), the length of the biopsy needle should be adjusted based on the distance from target to the cannula's position (as its being done for current methods of biopsy). The biopsy needle used for this project is a commercially available produced which is equipped with attachments to adjust the insertion length of the needle.

CHAPTER 5: RESULTS

In this chapter the results from the validation step of this robot are presented and discussed. Based on objectives of this thesis this robot had to be small, had to be able to register to head models using their CT/MRI scan, perform two assistive tasks and had to perform them in reasonable accuracy. The results are presented in slightly different order. The size and workspace of the robot is evaluated in the first section (Section 5.1 Size and workspace) the chapter continues with section 5.2 which delivers the results for line of sight experiment, it showed the magnitude of line of sight issue. Registration, biopsy and accuracy performances are correlated to each other so, their respected results are presented in one section (section 5.3). Endoscope application performance results are presented in 5.4. Discussion is the last section of this chapter.

5.1 Size and workspace

This robot is designed to reach needed locations on patient's head with smallest possible link lengths. The dimensions and geometrical characteristics of the robot is delivered in Figure 5.1. The main controller of the robot is an Intel Nuc with a mini pc size factor. The robot, controller and power source can be placed inside a normal cabin sized luggage bag.

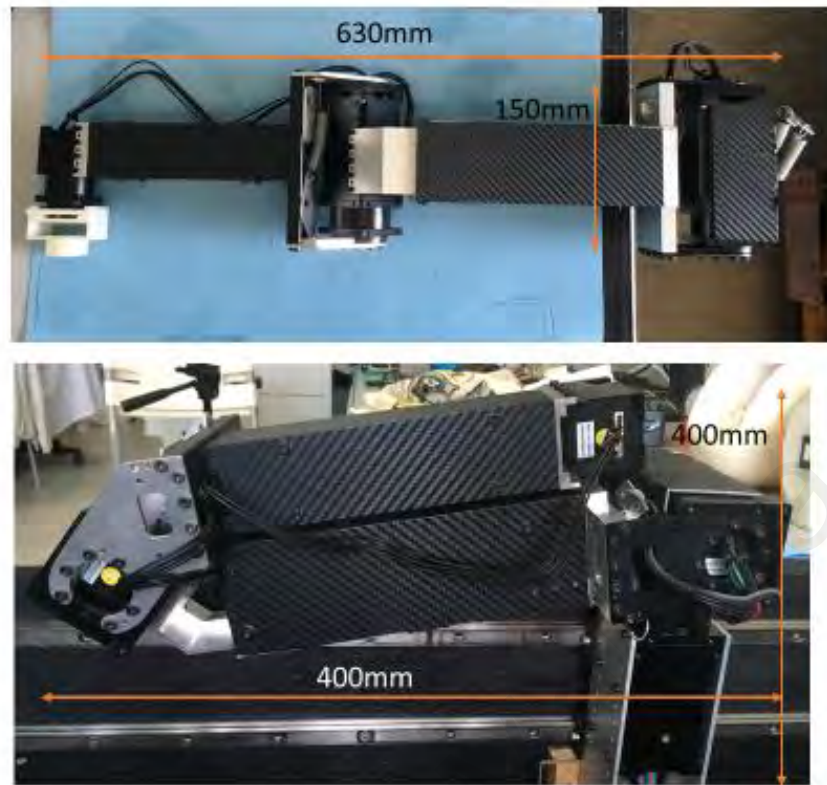


Figure 5.1 Overall dimensions of the robot

The reachability of the robot was tested with several head models (all introduced in methodology). The robot's tool point can reach all the points on the head models however, as suspected, robot loses dexterity for the points on opposite side of the robot (operating area). As it was intended if the patient's head is tilted away from the robot the robot still can see (from wrist camera point of view) the facial features. However, if the head angled more than a certain point the loss of sight on facial features would be too significant to have a suitable registration. This angle (which beyond it the registration is not acceptable) varied for each head model. As observed the suitable registrations achieved when the camera could see both sides of the face (right and left side of patient's nose) or at least one side completely in addition to a small portion of the other side of the face. As a rule of thumb, the head shouldn't be turned more than 90 degrees towards the sides.

The robot can comfortably handle endoscopes weight a full load tolerance test was not needed however, 1kg of load on the wrist introduced no major challenge for the robot to handle. On the torque enabled mode where the motor electrical breaks are engaged the robot stays sturdy with a maximum flexing (free play) of 3mm at the tool point (it was measured using a laser pointer inside the cannula and a camera looking directly at laser pointer's reflection as shown in Figure 5.6).

5.2 Results observed from line of sight analysis

Performing the line of sight experiments was to investigate the magnitude of this problem and to provide an insight into the decision of eliminating the use of external optical trackers. The methods of this investigation were done simultaneously with the workspace study, full details are delivered in methodology chapter, here a detailed view on the results of this investigation is delivered.

The 15 observed surgeries in this study were including transsphenoidal pituitary surgery, acoustic neuroma resection, meningioma resection and endoscopic third ventriculostomy. The line of sight error occurred in almost all the 15 surgeries, some with a higher frequency than others. Table 5.1 shows the frequency of line of sight error occurrence in these surgeries. It also shows happened subset frequency of line of sight errors during the intraoperative phase. The errors during intraoperative phase were highlighted as an error during this phase can cause more problems, as the patient is covered, and patient-image registration is done, and the reference star cannot be moved. So, an error during this phase may cause a longer delay than pre-op phases.

Table 5.1 The frequency and period of line of sight error for the observed operations.

Operation Number	Type of operation performed	Frequency of line of sight error	Error during the intraoperative phase
1	transsphenoidal	9	9
2	Craniotomy	1	1
3	Craniotomy	9	9
4	Craniotomy	0	0
5	transsphenoidal	3	3
6	Craniotomy	3	3
7	Craniotomy	7	7
8	Craniotomy	9	9
9	transsphenoidal	11	11
10	Craniotomy	13	13
11	Craniotomy	1	0
12	Craniotomy	2	1
13	Craniotomy	4	4
14	transsphenoidal	3	3
15	Craniotomy	8	8
	Total	83	81

To better understand the magnitude of this issue during the surgical procedure, an analysis of the total time of line of sight error was compared against the total time of use of image guidance, as measured by the image guidance software (Table 5.2).

Table 5.2 the total lasted time of error during each operation compare to the total use of image guidance.

Operation	Total error time (seconds)	Total image guidance time (seconds)	usage total duration of the operation (minutes)	Error percentage compare to total IGS use
1	53.45	95.25	87	56.1
2	39.86	541.42	89	7.3
3	96.817	1520	180	6.3
4	0	450.74	50	0
5	61.96	241.53	59	25.6
6	45.85	251.9	202	18.2
7	42.417	1000	181	4.2
8	69.85	239.96	112	29.1
9	76.6	175.195	149	43.7
10	130.32	441.20	136	29.5
11	30.43	162.66	191	18.7
12	43.75	151.45	246	28.8
13	465.2	1203	193	38.6
14	30	614.29	152	4.8
15	57.15	594.91	139	9.6

The arrangement of operating theatre, devices and personnel are very important factors to avoid line of sight obstructions. However, as seen in this study, line of sight error happens despite the precautions taken prior to the surgery.

The reasons that the error happen can be divided into 4 main causes. First, the surgeons' hand or body blocking either the reference star or the instrument. Second, the nurse or other personnel is blocking either the star or instrument. Third, one of the surgical instruments or devices in the field blocking the view. Fourth, the reflective markers are dirty (e.g. blood spills on them) and camera cannot detect them. Table 5.3 shows the rate of occurrence of each causative error.

Table 5.3 Summarised reasons of line of sight errors.

Reason	Number of occurrences in 15 operations
Surgeon	44
Other Personnel	13
Tools and devices	23
Dirty reflective markers	3

In this study, the image guidance system was only utilised for relatively short durations during the surgery (Table 5.2). Yet, the line of sight issues occupied a significant portion of the time, in one case up to 56% of the time image guidance was used. The IGS utilization time is small yet, it is crucial to be available and working well when the surgeon needs to identify important or difficult anatomy. This issue can be more severe while acting as robot's external tracker since the robot needs tracking without interruption all the time it is being utilized.

As table 5.3 suggests, most of the line of sight error occurred during the intra operative phase. The error in this phase cause more problems as it may disturb the smooth flow of surgery. For example, in operation number 9 from Tables 5.1 and 5.2, each time the surgeon was trying to use the IGS pointer, he had to move backwards to make way for the IGS camera to see the reference star. In operation number 7 from Tables 5.1 and 5.2, the scrub nurse was standing on a raised platform to be able to reach the operative area. Every time the image guidance was needed, she had to step down and step away from the patient so as not to obstruct the camera (Figure 5.2). These situations can cause delay and add to unnecessary movement of staff and equipment.



Figure 5.2 The bottom picture shows a scenario where the nurse was blocking the IGS camera. The scrub nurse had to move away from the patient so that the image guidance camera can see the instrument in the top picture.

Table 5.3 reveals the primary reason of obstruction of navigated instruments are related to the surgeons themselves. This includes the surgeon not pointing the instrument in the optimal direction or inadvertently blocking the tracking array with their hands. An ergonomic positioning of the camera and tracking array in direct visualisation of the surgeon pre-operatively would prevent these errors.

The next most common reason was obstruction of the reference array by other surgical instruments like suction tubes, diathermy and ultrasonic aspirator wires, the operating microscope and even the bulky drapes themselves. Positioning of each of this equipment must be considered pre-operatively to avoid a clash with the line of sight of the IGS. The array may have to be elevated higher than normal in patients who may be obese and thus obstruct the array once the drapes have been placed.

The scrub nurse or surgical assistant can similarly cause a line of sight error. Optimal positioning of the viewing camera, considering the intraoperative positioning of the nurse and assistant is necessary to avoid this error. The optimal position of a camera at the time of registration may not be the optimal position during the surgery itself.

5.3 Registration, biopsy and accuracy

The error recorded in mock biopsies on the accuracy models, shows the overall accuracy of the robot. This means total error of the whole process, which is the summation of Robot's positioning error, registration error and the models' manufacturing errors. The models have been analyzed extensively using clinical equipment; different aspects of positioning errors present in the models have been investigated. On the other hand, robot's positioning error depends on movement accuracy and repeatability of the robot. The movement accuracy is the accuracy of the robot in moving the end effector from one point

to another. The repeatability of the robot is arguably the more important value as it depends on many mechanical factors such as temperature fluctuation and mechanical imperfections.

In this thesis overall accuracy refers to accuracy of the robot in biopsy task which is determined by accumulative errors from all aspects of robot's functionality, Positioning error and registration error. The overall accuracy had to be measured after the process of registration however, repeatability and movement accuracy could be measured independent of the head models.

5.3.1 Models' accuracy

Table 5.4 shows the calculated error between the IGS based coordinates and original imaging coordinates utilizing the 3 different methods of registration. Figures 5.4 and 5.5 show the deviation of the data in the form of a box plot for each of the three methods.

Table 5.4 the calculated error between the IGS based coordinates and original imaging coordinates utilizing the 3 different methods of registration.

	Registration with original image	Registration with model CT scan	Automated Registration
Total Mean Error for 24 marker points (model 1)	1.11mm	1.07mm	0.67mm
Standard Deviation	±0.48	±0.47	±0.18
Total Mean Error for second model 12 points (model 2)	1.28mm	1.082mm	0.74mm
Standard Deviation	±0.3	±0.4	±0.17

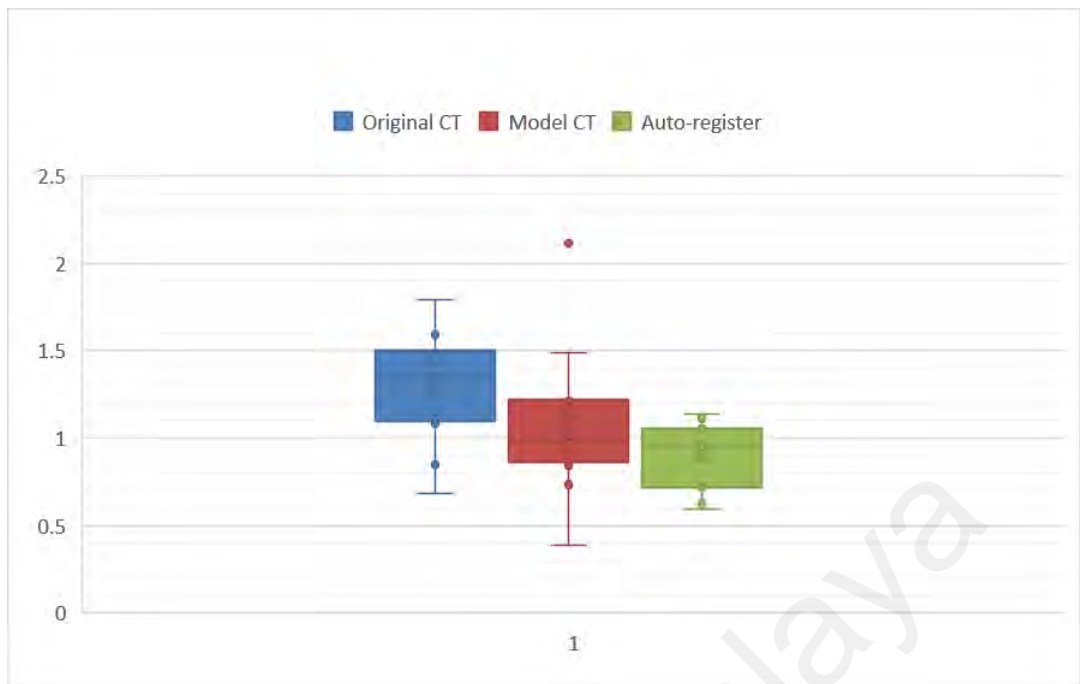


Figure 5.3 Box plot for error deviation among the three registration methods for first model.

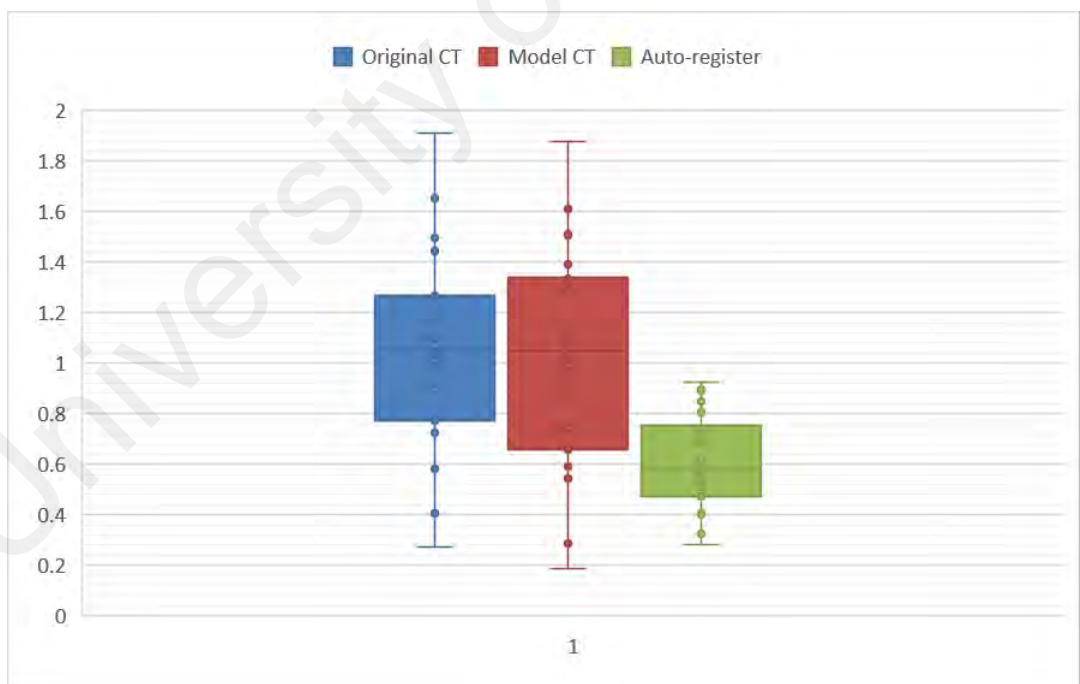


Figure 5.4 Box plot for error deviation among the three registration methods for second model.

The results show better accuracy for the first model compared to the second model. There was a bigger difference between the two models in the registration with the original CT scan compared to the other two methods. Results show a significant difference between the different methods of registration, with original CT images registration being the least accurate and Auto registration being the most accurate experiment.

Previous attempts in accuracy assessment of 3D printed head models have been limited to the landmark detection technique in which a landmark inside the printed model were compared with its original location using surgical navigation. These landmarks were usually chosen from distinct bony structures such as internal auditory meatus and jugular foramen (Waran et al., 2012). Issues with this methodology is that first, the targets sizes are variable and second it depends highly on the surgeon's experience to detect if the navigation probe is on target or not. There is no detailed spatial accuracy assessment in the literature, however there is sufficient literature on the printer's accuracy and its effect on the model's accuracy (Rybicki & Grant, 2017). Printer's accuracy is not the only factor in determining the precision in printed models, in total three areas of possible errors have been identified (from the tests done on both models):

1. Preparation error, which comes from all the work that was done on the DICOM file of the patient to make it ready for fabrication, and mainly includes segmentation works and STL conversion.
2. Fabrication error, this error basically was added to the models during the fabrication process which includes the 3D printing and manual work. If the manual work is none to minimum the fabrication error is the 3D printer error; it is the difference between the printed models and the STL files uploaded to the printer.

3. Errors due to the navigation registration process. Registering the models to their respective CT image induce an error to the process. This error's magnitude depends on the mode of registration; manual or automated.

By comparing the error obtained in the first two experiments the effect of the first source of error was removed when the model was directly rescanned, and the new image set was utilised in the registration process. In comparing experiment two and three the human error involved in registration was removed by comparing human registration with automatic registration.

The three registration methods individually showed different outcomes. This is due to different approaches taken in each one. The first set of tests compared the acquired data from IGS with the original patients' CT images, so every imposed error by fabrication and preparation on the original CT images were present in these tests. However, in the second set of tests the acquired data was compared with the CT images of the already fabricated model, so the fabrication and preparation errors were least likely to be present in this test. In these two sets of tests the same method of manual surface registration was used to register the model to images. This means that the registration error present in the first two sets of tests were expected to be similar to one another.

In the third set of tests, CT images of the fabricated models were used in automatic registration. Automatic registration as reported repeatedly (Sipos & Heisey, 2015; Stelter et al., 2012; Uhl et al., 2009) is more accurate than manual surface registration. So, in the third set of experiments, which is similar to the second set with using the models' CT images, the fabrication and preparation errors have been eliminated. Furthermore, using automatic registration reduced the registration error significantly. Via this concept, each error present in using these 3D printed models can be estimated.

Results show a distinct inaccuracy in the second model compared to the first in the first set of tests (0.17 mm compared to 0.01 mm in second set of tests). This is expected due to the fabrication error. In the first model, given the base to vertex orientation of the head, the poles did not require support material as part of the printing process, however in the second model given that the general model orientation was rotated to the left, the poles required a significant amount of support material as part of the printing process. Because this is part of the post-printing processing stage, this material had to be removed and it was likely that the actual pole orientation may have been distorted. As a result, marker points have moved compared to their original positions in the original CT image.

In the first registration method, the models were registered using manual surface registration with the original patient's CT scan. The error obtained from the first set of experiments shows the summation of all error mentioned, which was an average of 1.11 mm \pm 0.48 for the first model and 1.28mm \pm 0.3 for the second. In the second registration method, the printing and fabrication error is eliminated. The average of error in the second set of experiments shows 1.07 mm \pm 0.47 for the first model and 1.08mm \pm 0.4 for the second. Comparing the first and second registration methods allows for the estimation of the preparation and fabrication error which is 0.04mm for first model and 0.2 mm for the second. As discussed, the fabrication error in the second model is the combination of 3D printer's error and manual work done on the model but, no manual work has been done on the second model. So, 0.04 mm is the 3D printer's error plus preparation error. Looking at the data deviation for second model in this experiment, 0.04 mm is concluded as not statistically significant as the fabrication and preparation error. However, the maximum accuracy of the utilized 3D printer is 0.02mm. This suggests that the preparation and printing processes had been carried out well enough in the second model for these errors to be negligible.

In the first two experiments, the registration method used was the manual surface matching registration, which is an accurate, clinically approved method. However, it still generates degrees of inaccuracy. The third set of experiments allowed for registration to be performed using automated registration. The registration error in the automated method is not zero but, it is significantly better than the surface matching technique (Sipos & Heisey, 2015; Stelter et al., 2012; Uhl et al., 2009). Hence, the obtained average errors in the third experiment (0.67 for first model and 0.74 mm for second model) show the total of a residual error, which is probably the summation of small registration errors, IGS error and CT scanner error. If the third error is deducted from the second error, it shows the surface registration errors, which is 0.4 for first model and 0.34 mm for second model. This suggests that the surface registration error (which is widely being used as the standard registration method) is significantly bigger than the 3D printer's error. This is because as the 3D printed models provide better surface registration (they are rigid and do not suffer from soft tissue shifts which make the surface registration even less accurate in real patients).

Summarisation of the discussion is as follows:

- Minimum total error as seen in the first test is 1.11 mm \pm 0.48 (without considering manual works on first model).
- Minimum preparation and fabrication errors are negligible compared to other errors.
- Minimum surface registration error is around 0.34 mm.
- Minimum residual Error is around 0.67 mm.

It should be mentioned that these numbers are estimations of the mentioned errors. They show the distribution of the errors more than the exact embodiment of them. For example, surface registration accuracy (which depends on surgeon's skills and facial

features of patient) is a bigger factor than 3D printer's accuracy. These results suggest that the spatial accuracy of a 3D printed head model depends a lot on first, the fabrication process and then accuracy of the printer. Furthermore, if the fabrication is done properly, using an accurate 3D printer, the method of registration can affect the accuracy of the training simulation.

However, The precision studies of image guided surgeries (Labadie, Davis, & Fitzpatrick, 2005; Vercruyssen et al., 2014) shows that in real clinical operations an error of $2.0 \pm$ mm is expected in image guided procedures (in some cases the error can reach 5mm). This inaccuracy is mainly from soft tissue shifts (such as skin and brain). So, in conclusion two accuracy models were created and tested. The testing results showed that these models are comparable with human models and they can imitate surgical procedures for surgical trainees. Their precision was tested with IGS systems and IGS probe.

These experiments provided a benchmark for the robot's functions, as the robot's physical accuracy is within sub millimetre range the biopsy tests will show the registration accuracy process and as it was established a maximum registration error in a clinical IGS on the head models is below 2mm.

5.3.2 Repeatability

Repeatability error in a robot is the error measured between tool point positions while the robot is commanded to take the same position repeatedly. The repeatability measurement in this thesis is a simplified version of ISO 9283:1998 standard which introduced a protocol to measure repeatability in industrial robots. Here is a simplified protocol, which was used for this thesis:

1. The robot was turned on and commanded to reach few random positions as warm up (so the motors and gearboxes reach temperature stability).
2. Send identical commands to bring the robot to 3 different positions for 7 times. Between each of the 7 attempts robot takes few other random poses.
3. Measure the reached position using a dial indicator with 0.01mm resolution as shown in Figure 5.5.
4. Repeat the process 3 more times with 2 hours in between the attempts.

Here is the calculation method to be used to obtain the repeatability from the data:

For N measurements, with commanded position reached position (X_i, Y_i, Z_i) :

$$\bar{X} = \frac{1}{N} \sum_{i=1}^N X_i \quad \bar{Y} = \frac{1}{N} \sum_{i=1}^N Y_i \quad \bar{Z} = \frac{1}{N} \sum_{i=1}^N Z_i \quad (5.1)$$

These equations calculate the mean of positions for X, Y and Z.

$$l_i = \sqrt{(X_i - \bar{X})^2 + (Y_i - \bar{Y})^2 + (Z_i - \bar{Z})^2} \quad (5.2)$$

l_i is the direct line between each of the reached positions and the mean position.

$$\bar{l} = \frac{1}{N} \sum_{i=1}^N l_i \quad (5.3)$$

$$S_l = \sqrt{\frac{\sum_{i=1}^N (l_i - \bar{l})^2}{N - 1}} \quad (5.4)$$

S_l is the standard deviation for the error between each reached position and the mean position.

$$R_l = \bar{l} + 3 \times S_l \quad (5.5)$$



Figure 5.5 using a dial indicator with 0.01mm resolution to calculate repeatability in X,Y and Z at one point of the robot's workspace.

R_l is the desired repeatability of the robot which suggests that the position of the robot almost always falls within this repeatability value. Table 5.5 shows the l_i value for 7 returns to the same position and 4 different attempts within time period of two hours (in millimeters).

Table 5.5 distance of the tool point from a desired position attempted 7 times after taking few random pose and the whole process was repeated every 2 hours for 4 times.

Pose	Attempt1	Attempt2	Attempt3	Attempt4
1	0.046035856	0.053247535	0.0484076	0.07212004
2	0.020911719	0.067626178	0.0779955	0.06604014
3	0.045368491	0.037300134	0.0464898	0.03551479
4	0.064103822	0.049348759	0.0192691	0.04526919
5	0.059559214	0.025481366	0.0484283	0.04655427
6	0.055329016	0.043165959	0.022963	0.06096966
7	0.051578096	0.077571258	0.0521277	0.07319358
\bar{l}	0.050427507			
S_l	0.016058223			
R_l	0.098602176			

Repeatability test suggests that the robot can reach an identical point in space with 0.098mm accuracy, which is good value for a serial manipulator (a typical industrial robot's repeatability is between 0.01mm to 0.1mm).

This suggests that in a surgical task after the registration and during the process of surgery, the robot will not lose accuracy more than 0.098mm and no re-registration will be needed. For example, if the robot needs to precisely hold an instrument in a place for periods of time throughout the surgery, it can do it without a significant drift in its position.

5.3.3 Movement accuracy

The movement accuracy experiment was performed to ensure the robot's accuracy in fine movements and the viability of the inverse kinematic algorithm. The robot was positioned in a pose that can be touched by the dial indicator. Next the robot was commanded to change position in cartesian space within the direction and range (1 cm) of the dial indicator. This was done for 10 points and 3 attempts for X, Y and Z. Figure

5.6 shows the experiment's setup. The results showed a mean error of 0.09 mm between the indicator and robot's inverse kinematics. Sometimes due to a big load or mechanical defects the robots are unable to show suitable accuracies in fine movements, however, this robot can perform this type of movements with desirable precision.



Figure 5.6 movement accuracy is tested using the dial indicator which has 1cm range. The robot was commanded to change the tool position along the indicator's plunger. The differences between the calculated forward kinematics and the indicator showed the error value. The camera and laser pointer are to measure the flex in the tip point.

It should be noted that this test was done to ensure robot can perform reasonably fine movements. The error calculated here is not correlated to position and repeatability errors. It mainly represents the ability of the controller embedded in each of the servo motors to execute fine adjustments. As stated, the encoders used in servo motors of this robot are high precision encoders so they can sense any accidental drift in each joint's position and help the controller to perform a fine adjustment.

5.3.4 Registration and Biopsy

The biopsy experiments were conducted with two methods of registration. For manual registration 3 of the incorporated points (pole structures) were used as registration fiducials. This is in line with real surgeries as fiducials can be hard attached to anatomy of the patient (titanium screws). The process of biopsy and error measuring conducted after registration with the user selecting all the targets and entry point one by one and commanding the robot to place the cannula in line with the biopsy trajectory. The error was measured based on three situations that could happen, first situation the biopsy needle precisely hit the divot inside the pole structures so, error of zero mm was recorded, second the needle hit the coloured area around the divot, so an error of 1.5 mm was recorded (the two scenarios is illustrated in Figure 5.7) and last, the needle was out of the coloured circle so, a calliper was used to measure the distance.

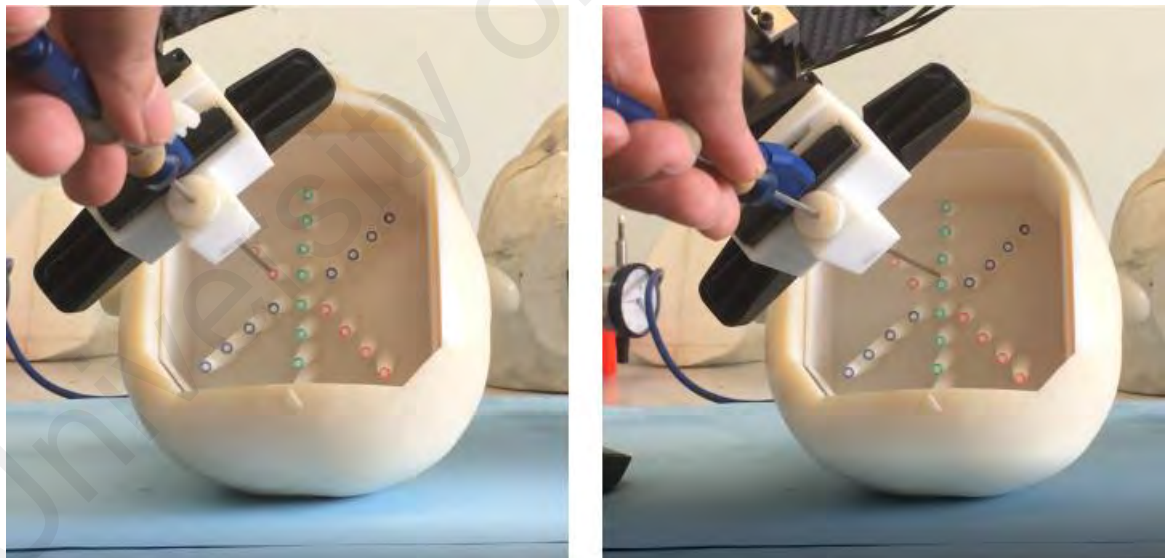


Figure 5.7 Left the needle hits the colored circle which means the error was recorded as 1.5 mm and on the right a caliper had to be used to measure the error.

Figure 5.8 shows the box diagram for the two accuracy models with manual registration. Which shows an error of 3.36mm for paediatric model and 3.38mm for tumour model. Which are below 5mm and for assistive tasks considered suitable.

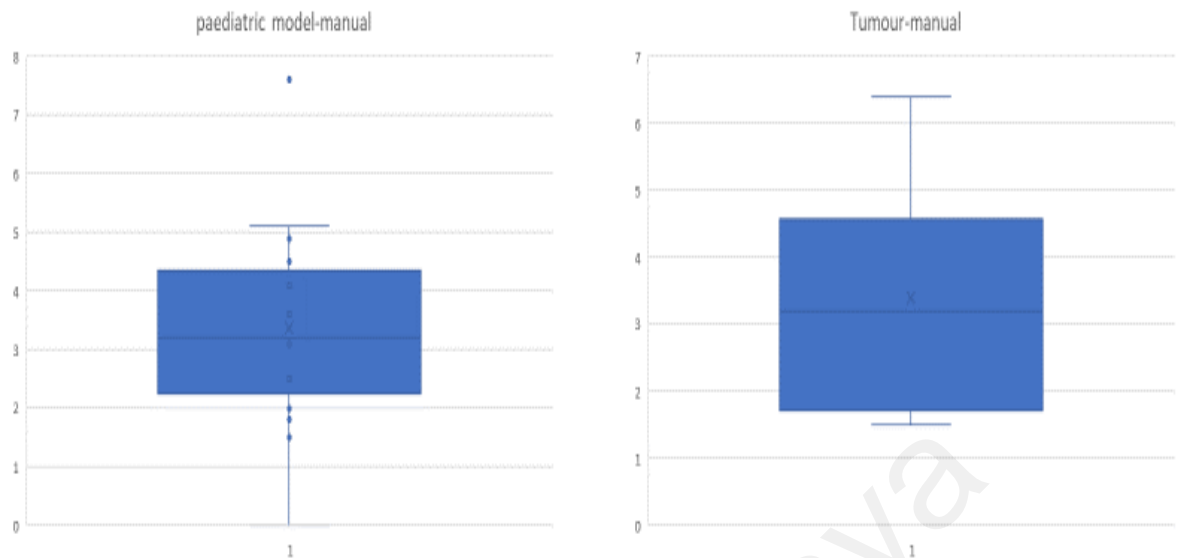


Figure 5.8 biopsy error recorded for manual registration on the two accuracy models. Paediatric models mean error is 3.36mm and 3.38mm for tumour model.

For automatic registration, first the facial landmark detection had to be evaluated. The areas of detected landmarks were big and not as accurate as original trained model. Additionally, while the head was significantly tilted the algorithm failed to align the landmarks correctly as Figure 5.9 shows (this is mainly due to less data zone to detect in the trained model and also using head models without proper colour contrasts of real human face) however, the direction of the head could be detected correctly and consistently so the face-follow feature coded to place the camera directly in front of the face greatly facilitated recording of consistently homogenous point clouds.

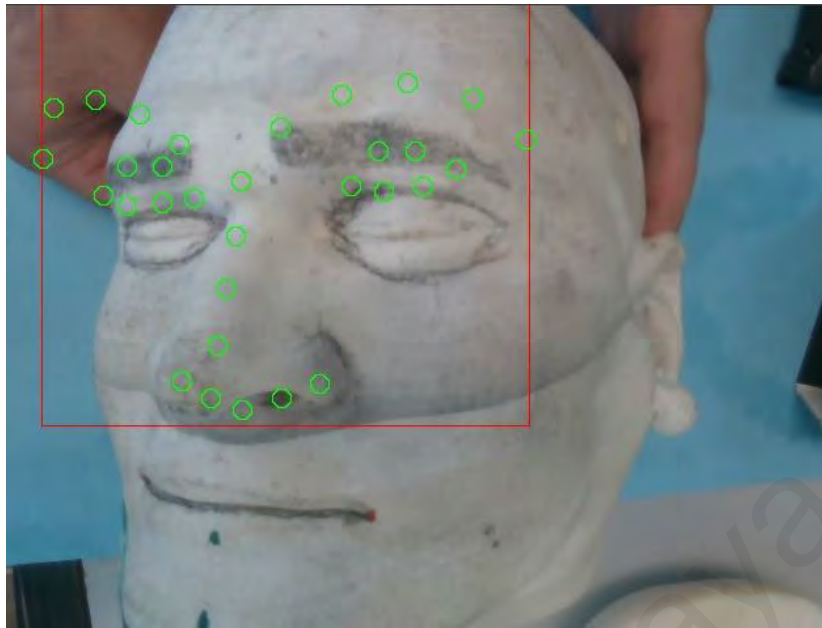


Figure 5.9 while the head was tilted the facial landmark algorithm hardly could align the facial landmark to the model's face however, the direction of the head estimated correctly.

Therefore, the process of semi-auto registration starts with the robot sliding base moving towards the top of the table, if it can detect a face it aligns the wrist camera directly in front of the face, if no face is found it does a lateral sweep movement to cover all the possible angles of the head. If the head is tilted so much that the face cannot be detected even after the lateral sweep, the semi-auto registration cannot be used. The point cloud registration is illustrated in Figure 5.10.

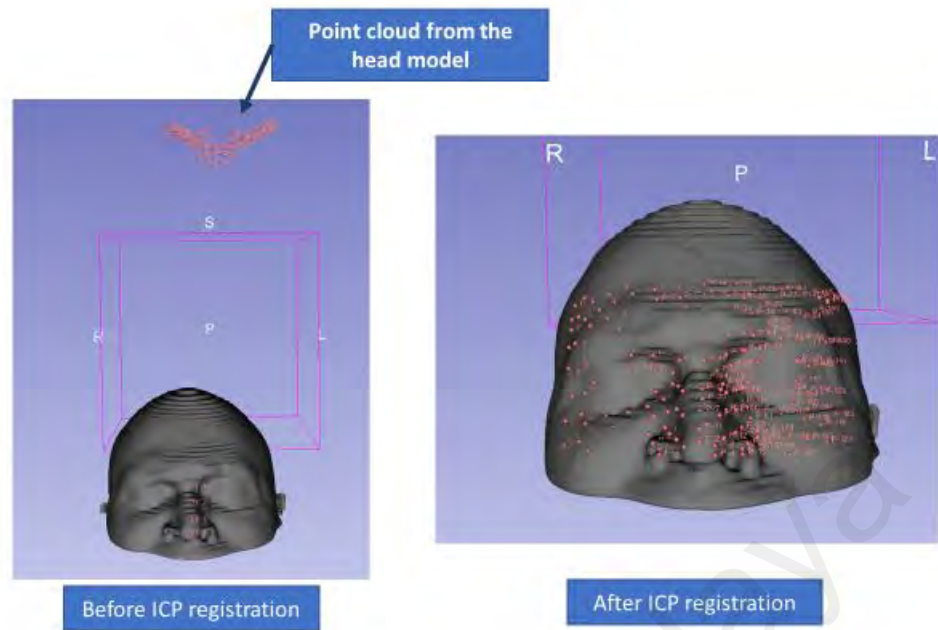


Figure 5.10 the recorded point cloud vs registered point cloud.

The mock biopsy performed in the same fashion as the manual registration. Figure 5.10 shows the results obtained from mock biopsies using semi-auto registration.

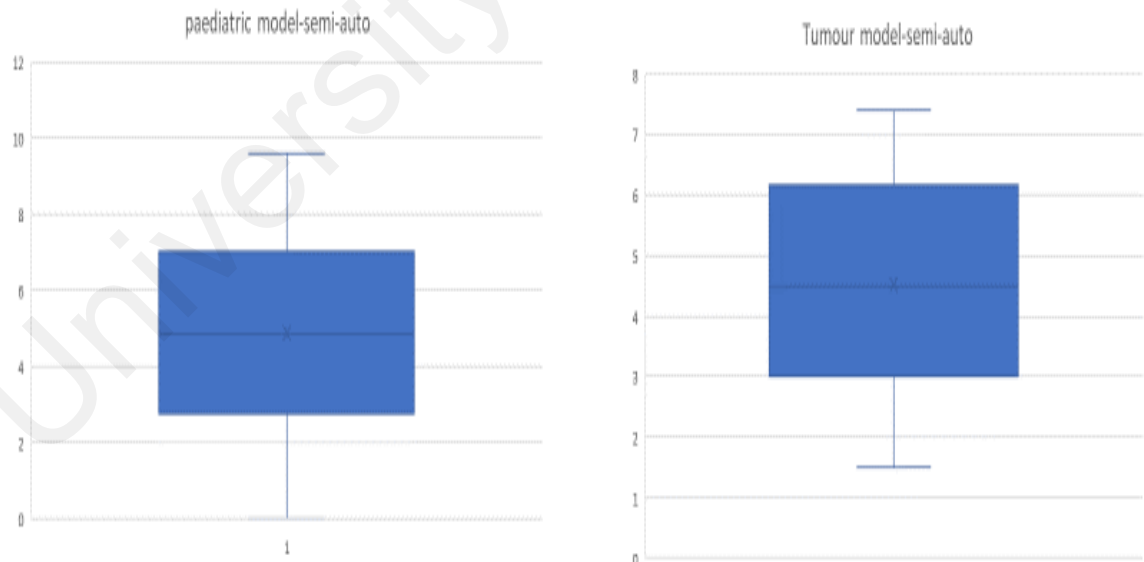


Figure 5.11 represented error in biopsy operation using semi-auto registration. Mean error for paediatric model was 4.85mm and for tumour model it was 4.51mm.

First and foremost, results from manual and semi-auto registration show good accuracy to successfully perform assistive tasks, tasks such as skin marking, holding instruments or manipulating exoscope. However, to perform precise stereotactic specific operation the robot needs accuracy below 2 mm (as an accepted accuracy by several medical devices standards). This robot in this state cannot be used in clinical biopsies of targets smaller than 7mm “yet”.

5.4 Endoscope manipulation

Endoscope application was performed as a mock pituitary adenoma surgery. An experienced Neurosurgeon performed this surgery and evaluated the application in three different criteria.

1. The performance of the application in the opening phase.
2. The performance of the application in the longer tumour resection phase.
3. The performance of the application in taking the endoscope in and out (for cleaning).

The initial point selection was performed by holding the endoscope on the desired points as planned. The surgery was conducted while the robot controlled the endoscope’s movements by joystick commands from a third user synched with surgeon’s verbal cue.

Figure 5.12 shows the setup for this experiment.

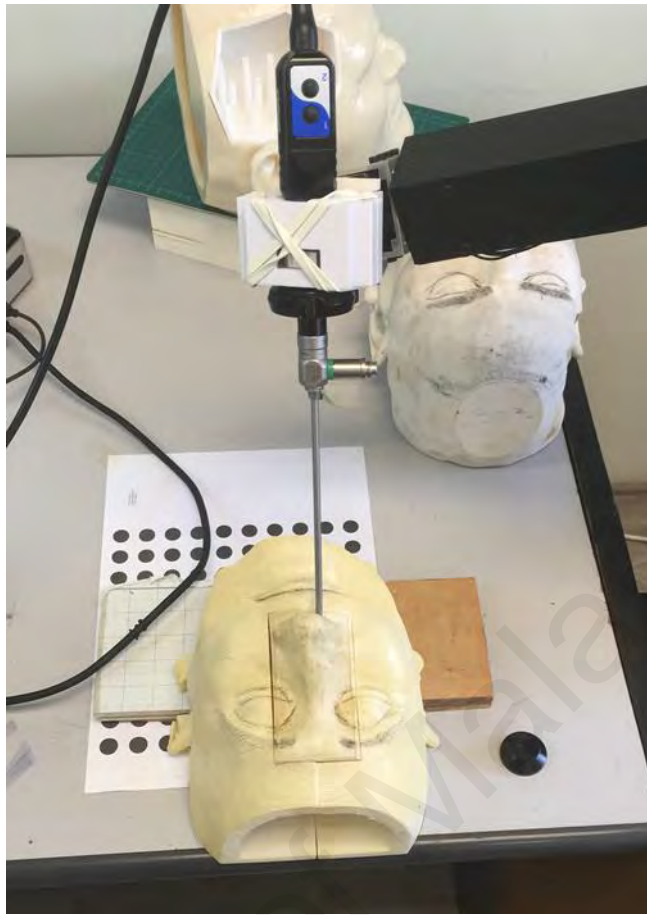


Figure 5.12 Setup for endoscope manipulating application.

In overall the surgery went well, and the endoscope application handled the endoscope as planned. However, few observations have been made.

- The opening phase includes lots of movements which are rapid and fast compared to what the robot can handle. During this phase the endoscope is still near the entrance of nasal canal and despite the persuasions made in the development of the application it makes it hard for the surgeon to control the endoscope using only joystick commands. This situation exacerbates as sometimes the surgeon uses the endoscope to push some of the soft tissue away or to the side.
- During the tumour resection the demanded movement of the endoscope was limited compared to the opening phase and it made it easier to manipulate the

endoscope using the robot. During this phase the surgeon could use both his hands and there was no need for an assistant just to hold the endoscope.

- Using the safety area (maxilla bone plane) protected and also limited the endoscope movements however, the orientation of this plane depends solely on the selection of the initial points and if the upper point is selected carelessly the plane can be placed behind the nasal bone or too in front that it limits the endoscope more than necessary. So, a good percussion is to add a fourth point in which the surgeon can activate when reached near the pituitary. The point should be selected far posterior to the brain opening. Selecting this point can reconfigure the safety plane in a more desired angle.
- The cleaning maneuver was successful in taking the endoscope in and out of the operating area. however, it should be mentioned that the re-entry of the endoscope in some instances was very close to the soft part of the nose and it could potentially damage the patient. So, the re-entry should be very slow and with surgeon's supervision.
- The surgeons tend to keep their frame of reference steady and keep the endoscope's camera angle straight. As there is no tool axis actuation in the robot when the robot changes the orientation of the endoscope it cannot reposition the camera angle properly so, the camera angle turns clockwise or anticlockwise. This can be solved by manually turn the endoscope while mounted on the robot. However, it did not cause major issue for the surgeon in the operation.

Based on these considerations the developed endoscope application is helpful in the longer process of tumour resection while the endoscope movements are short and slow. In the beginning phase of the operation this application failed to add value to the manual handling of the endoscope.

CHAPTER 6: DISCUSSION

Based on the objectives of this thesis the results reported on five main points,

- The size of the robot and its mechanical characteristics. Which related results are delivered in section 5.1 and 5.2.
- The performance of the developed 3D printed head models. Which related results are delivered in section 5.3.1.
- Robot's performance for registration and accuracy based on the mock biopsy operations. Which related results are delivered in section 5.3.2, 5.3.3 and 5.3.4.
- Robot's performance in handling an endoscope. Which related results are delivered in section 5.4.

The size of the robot and its mechanical characteristics. The goal for this robot was to be small so it can be carried between medical centres and be used in more surgeries so it can be cost effective this is one of the contributions of this thesis as the literature shows one of the problems with current neurosurgical robots is the lack of portability (Smith, Jivraj, Wong, & Yang, 2016). The workspace analysis helped to design a serial link robotic arm structure based on data acquired from real surgeries. This structure is a 5 DOF robotic arm which can be mounted on side of a surgery table. One of the major decisions in the process of design and development was whether to use an external optical tracker or not however, after considering the big footprint of optical trackers and the problem they have with line-of-sight it was decided not to use them. Line-of-sight problem was investigated in parallel with the process of workspace analysis.

The main reason Line of sight was investigated was that there is no research in the literature that delivers quantified results for this issue. Additionally, the causes of this

problem have also identified in order to have a better understanding of the problem. While optical based navigation has become an essential tool, line of sight issue continues to be a problem that disrupts and delays the smooth flow of an operation. But as the IGS is utilised for small amount of time, line-of-sight problem may not show as a very significant issue. However, if continuous tracking of an instrument is demanded, such as in robotic applications line-of-sight can cause serious problems and interruptions during the surgery. Therefore, based on line-of-sight analysis and the fact that it adds to the system's footprint it was decided not to use IGS optical trackers as external trackers for the robot.

Not using external optical trackers may prove to be a controversial decision. Using a non-mechanical precise tracker can definitely improves the accuracy of the robot but at the same time it adds to the cost of system, it increases the setup time and makes the whole system bigger than what is intended for in this research. Additionally, the precision this robotic system is aiming for is good enough for general assistive tasks. As it can be observed from literature review, there are many other successful stereotactic and microsurgery robot available in the market which can be used for extreme precise tasks if needed.

Robot was tested for its load handling, reachability and amount of free play (flex) in its tool point. The tests were considered successful in handling the expected load which was a typical endoscope setup (endoscope and camera attached to the tool point, from Storz, Germany). However, if the head is tilted to the extreme side (more than 90 degrees) the robot had hard time observing the face with the wrist mounted camera. So, in these cases a point-based registration should be used.

Amount of flex in the tool point was about 3mm. This is while a clinically approved pneumatic holder suffers from minimum 15 mm of flexing (MITAKA arm USA (Nakamura, 1997)). MITAKA arm was tested in-house during a surgery which it was

used to hold an endoscope during a long operation. To test the flexing, a relatively high force had to be imposed, the act of inserting a biopsy needle did not cause any flex or relocation of the tool point which means normal biopsy operation or a simple accidental push by hand will not cause any considerable flex in the position of the tip point. Additionally, the high precision encoders in each servo enabled the controller to sense any small deviation from desired position. Such a deviation results on controller commanding the joints to move back to the desired position. This feature can also be done more accurately by robots with parallel structure such as (BrainLab, 2018) and (Nimsky, Rachinger, Iro, & Fahlbusch, 2004; Zimmermann, Krishnan, Raabe, & Seifert, 2004). However, as mentioned before parallel structure is too big and bulky for transsphenoidal surgeries.

When the torque off mode is activated, or electricity is cut off the arm tends to slide downward because of its own weight. Therefore, few springs on the second and third joints were used to balance the robot weight while motor brakes are off. Using springs eliminated the drifting in torque off mode and made it possible to keep the relative position of the tip point as stable as possible. However, the torque off mode was implemented for a manual control over the robot. It was easy to move the robot by hand in torque off mode, a heavy load on the tool point will make the robot drift towards the gravity so, using torque off should be limited to the situations where users hand is holding the robot beforehand, the best solution would be to position the torque off button on the wrist of the robot or other parts of the body to make sure when user's hand is not in place this mode is not activated.

The performance of the developed 3D printed head models. As mentioned in Methodology chapter, two head models were developed for testing the accuracy of the robot in form of mock biopsy surgeries. Before using these models with the robot, they

had to be investigated to first, calculate the error present in them from various development processes which is not only from the 3D printer (Rybicki & Grant, 2017) and second, have a clear benchmark for the robot's accuracy test. These models were investigated using commercial clinical equipment which provided good information on the accuracy of the models and the magnitude of error expected while working with current clinical equipment.

Using head models versus using cadavers may also prove to be controversial. However, using cadavers imposes many challenges that makes 3D printed head models a better choice. Acquiring cadavers is costly, their MRI/CT scan had to be available which made this choice even costlier (in some cases it is not even possible to scan the cadavers if a non-clinical scanner is not available due to cross contamination issues), this is while compare to cadavers, head models are less costly and made from medical images so, in the worst case scenario their original patient's MRI/CT is available where based on the observed results the error present is still less than 2mm. In a best-case scenario these head models can be scanned by a clinical CT scanner without causing any contamination issue. Experimenting on cadavers must be in a controlled wet lab environment while experiments on head models could be done anywhere. And last, the facial landmark detection registration developed in this research would not work on cadavers as the facial area on cadavers is almost always deformed.

Robot's performance for registration and accuracy based on the mock biopsy operations. In order to test robot's performance in biopsy which itself is a good indication of robot's accuracy in neurosurgery, its repeatability and movement accuracy was tested using a dial indicator, these numbers are good indication of robot's mechanical accuracy. The results showed accuracy of almost 0.09mm which is enough for the purpose of this robot.

With having a good understanding of robot's mechanical accuracy and model's accuracy error while used with clinical IGS system next step was to perform the mock biopsy and measure the robot's overall accuracy. The average error present in models while using their scan (and not patient's original scan) is less than 1.1mm which sets a benchmark for current IGS systems. So, robot's overall accuracy which is the accumulation of all the errors from mechanical to registration error, is compared with 1.1 mm.

The repeatability (ISO 9283:1998), movement accuracies of the robot itself and the accuracy analysis of the head models suggest that the biopsy error mainly comes from the registration procedure which is worse in semi-automatic registration. The error present in the registration is largely due to inaccuracies from the generated point cloud itself. The 3D camera technology is not yet near to sub millimetres accuracy. Additionally, the camera used in this experiment is a coded-light 3D camera which depends highly on the internal laser projector of the camera to project a pattern in front of the camera lens, and the distortion in the pattern helps the camera processor to calculate the depth associated with every pixel in the image. This method depends highly on the environment lighting, in order to produce an optimal point cloud, the lighting condition should be optimal (for example in a very bright environment the camera fails to produce a suitable point cloud). This is a shortcoming which is addressed in the next generation of RGBD cameras, the upcoming generation use stereo cameras and parallax effect to calculate the depth and hopefully will help in more accurate image-patient-robot-registrations. So, while the accuracy is not enough for highly accurate tasks it is still enough for general purpose tasks. More research on the use of RGBD cameras is needed to improve the registration accuracy.

Robot's performance in handling an endoscope. The last phase of robot's validation was to use it as an endoscope holder in transsphenoidal surgeries. As mentioned, while plausible for later parts of the surgery this application failed to be useful for beginning phase of this surgery due to rapid movements of the surgeon during this phase.

One point that should be mentioned in this discussion is the use of FT (force and torque) sensor. In the endoscope manipulation application, it was clear that a hybrid manual-automatic control method would greatly improve the operation in similar applications. For such a hybrid control, using a 6-axis FT sensor is the appropriate choice. These sensors can be mounted on the wrist of robots and sense the induced forces and torques on the tool point of the robot, with the feedback from this sensor the robot can be commanded to execute certain manoeuvres. Manoeuvres such as following the hand movements of a surgeon in endoscope manipulation application. Additionally, this sensor can sense the force on the endoscope itself which while it is inside the patient's nose canal translates to the pressure that robot is putting on the patient's internal tissues. Such information is important in safety percussions of this robot's applications.

However, price of a reliable FT sensor is equivalent to 80% of the robot's cost in the Alfa prototype stage so using such a sensor would have increased the total cost tremendously. There are alternatives to this sensor for example the Alfa prototype was programmed to have torque ON/OFF mode which makes it possible for the surgeon to totally disengage the motors and move the robot manually, this was useful in setting up the robot and in applications where high range fast movements are not intended. However, for this type of applications (such as the endoscope application) according to surgeons, torque ON/OFF method was not enough and proved to be cumbersome. Another alternative to FT sensor is to implement current control in which the torque on each motor calculated based on the drawing current (the servo motors are usually

equipped with hall effect sensor). Drawing current can be translated into the load torque on the motor and can be used to hold or move position of each joint. This method was also research and tested in endoscope application however, the controller response was too slow to follow a human hand commands and concluded in unreliable and unsafe motions by the robot, so, it was scrapped from the design board.

The solution to hybrid control which is cost effective and reliable will continue as future works in this project.

University of Malaya

CHAPTER 7: CONCLUSION AND RECOMMENDATIONS

The goal for this project was to design and develop a robotic platform for general neurosurgical tasks. The term platform refers to the fact that the goal was not only to develop a manipulator but, a complete ecosystem to research on neurosurgical robotics. So, beside the manipulator, a method to investigate real surgeries and a method to validate the robot were needed. The first method helped to investigate the workspace of assistive tasks in real surgeries without interfering with the OR fellow. This data helped in developing a table mount 5 DOF serial manipulator. Additionally, the validation method helped to benchmark the robot against clinical IGS systems. To track robot's tool point there are three choices, electromagnetic trackers, mechanical position feedback and Optical trackers. Electromagnetic tracking was scratched off in the beginning due to the fact that metal parts presence (robot is almost entirely made of metals) in the field can cause interferences. Mechanical position feedback relies on kinematic calculations and position sensor on each joint which was necessary to implement for manipulator position calculations. Using optical tracking as an external position feedback had to be examined.

In addition to workspace analysis and to investigate the use of optical tracker in the design of this robot. The workspace analysis data was used together with video recordings to analyze the line-of-sight issue in optical IGS systems, since this has never been quantified before. This experiment showed that if a continuous tracking of an instrument is desired, line-of-sight issue can be a serious problem. Continuous tracking is a requirement in this surgical robot and line-of-sight issue can be troublesome in its functionality. This is in addition to the fact that using optical trackers increases the cost and footprint of the robot. Therefore, Optical trackers were not used in the design process.

Size of the robot was a point of interest, since it was designed to be small and portable between medical centres and ORs. The robot, controller and power supply can all fit

inside a small cabin sized bag and used in different locations if needed. Being portable will help for higher utilization. Beside the size, load handling was also investigated, the robot can comfortably handle a neurosurgical endoscope assembly which is the heaviest intended tool.

In order to validate the robot's function, two 3D printed head models were developed. The use of cadavers and animals were avoided due to cost, ethical and logistics issues. However, 3D printed head models are not a widely accepted validation method so, these models had to be validated primarily. These models were tested thoroughly using clinical equipment (IGS and Intra-op CT scanner) utilizing different modes of registration to make sure they can replace older validation methods. The results showed these models are reliable and precise alternatives to cadaveric and animal tests.

The two assistive tasks developed for this platform were biopsy and endoscope manipulation applications. Biopsy worked as a benchmark for the robot's overall accuracy. The robot can be registered to a patient using medical images by traditional manual methods as well as a semi-automatic registration. The semi-auto registration technique uses facial landmarks detection to find the patient's head and to generate a refined point cloud for surface matching registration. This method worked successfully with reasonable precision for assistive tasks. It was shown that when assistive tasks are required, the registration accuracy is adequate. However, if higher precision is demanded it will be achievable with the same semi-auto registration technique but with more precise 3D cameras.

Endoscope-handling application was successful in parts of transsphenoidal surgery. Parts in which rapid and regular movements are uncommon. The robot can hold the endoscope and refine its position for hours without fatigue and tremor. However, the initial parts of the surgery which involves rapid movements of the endoscope needs a

robot with faster adaptivity and a control system that can follow surgeons' movements rapidly, precisely and safely. A desired addition to the alfa prototype to achieve this, would be a 6-axes force/torque sensor between tool and wrist.

The principals of the biopsy procedure can be used in any physical feedback application type in neurosurgery (where the robot is pointing to a predefined point in/on patient's head). For example, few modifications need to be done to use the robot to mark the scalp skin flap before surgery, or a laser pointer can be attached to the same cannula so the robot can show a point of interest inside patients' anatomy. This is significant because, neurosurgeons must know their relative position inside patients' brain, especially for less experienced surgeons who having access to only visual feedback of IGS systems is not enough.

The alfa prototype was not meant for clinical trials but built as a pretest for clinical trials. However, after the tests, results showed that there are few structural changes needed before starting a clinical trial. Changes such as adding a force/torque sensor and extra safety considerations for example, all sharp edges on the robot have to be covered with soft plastic. The alfa prototype could avoid assigned safety areas however, there has to be an extra safety subroutine to monitor any applied pressure on internal tissues. Adding an F/T sensor would not be only for manual control, but also to detect any force the robot is exerting on any internal tissue.

Further research and development on this project should include making this system ready for a series of clinical trials. As mentioned, the Alfa prototype needs to have small structural changes. Clinical trials can start with simple skin markings on healthy subjects and continue with few biopsies in real surgeries. The robot can then be registered to a clinical IGS system as a verification step for the trajectory positioned by the robot. Additionally, further research on the developed semi-auto registration will be helpful not

only for robots but also stand-alone IGS systems. This method can facilitate a faster patient-image registration in these systems. Further research can start with creating a database of patient images for training an artificial intelligence (AI) algorithm to detect the facial landmarks more accurately. This AI can be trained to detect other objects connected to patients' head (such as head clamp) or be used to avoid them during the registration.

University of Malaya

REFERENCES

- Adler Jr, J. R., Chang, S. D., Murphy, M. J., Doty, J., Geis, P., & Hancock, S. L. (1997). The Cyberknife: a frameless robotic system for radiosurgery. *Stereotactic and Functional Neurosurgery*, 69(1-4), 124-128.
- Albu-Schäffer, A., Ott, C., & Hirzinger, G. (2007). A unified passivity-based control framework for position, torque and impedance control of flexible joint robots. *The International Journal of Robotics Research*, 26(1), 23-39.
- Asai, D., Katopo, S., Arata, J., Warisawa, S. i., Mitsuishi, M., Morita, A., Mochizuki, R. (2004). *Micro-neurosurgical system in the deep surgical field*. Paper presented at the International Conference on Medical Image Computing and Computer-Assisted Intervention.
- Auer, L. M., Starkie, S., Auer, D. P., & Davies, B. (2002). *Simulating minimally invasive neurosurgical interventions using an active manipulator*. Paper presented at the International Congress Series.
- Barzilay, Y., Liebergall, M., Fridlander, A., & Knoller, N. (2006). Miniature robotic guidance for spine surgery—introduction of a novel system and analysis of challenges encountered during the clinical development phase at two spine centres. *The International Journal of Medical Robotics and Computer Assisted Surgery*, 2(2), 146-153.
- Beasley, R. A. (2012). Medical robots: current systems and research directions. *Journal of Robotics*, 2012.
- Benabid, A., Cinquin, P., Lavalley, S., Le Bas, J., Demongeot, J., & De Rougemont, J. (1987). Computer-driven robot for stereotactic surgery connected to CT scan and magnetic resonance imaging. *Stereotactic and Functional Neurosurgery*, 50(1-6), 153-154.
- Bergamaschi, P. R., Saramago, S. d. F. P., & Coelho, L. d. S. (2008). Comparative study of SQP and metaheuristics for robotic manipulator design. *Applied Numerical Mathematics*, 58(9), 1396-1412.
- Bergman, W. C., Schulz, R. A., & Davis, D. S. (2009). Factors influencing the genesis of neurosurgical technology. *Neurosurgical focus*, 27(3), E3.
- Bertelsen, A., Melo, J., Sánchez, E., & Borro, D. (2013). A review of surgical robots for spinal interventions. *The International Journal of Medical Robotics and Computer Assisted Surgery*, 9(4), 407-422.
- Besl, P. J., & McKay, N. D. (1992). *Method for registration of 3-D shapes*. Paper presented at the Sensor Fusion IV: Control Paradigms and Data Structures.
- BrainLab. (2018). CIRQ JUMP-STARTING ROBOTIC ASSISTANCE. Retrieved from <https://www.brainlab.com/surgery-products/overview-spinal-trauma-products/cirq-robotics/>

- Briot, S., Baradat, C., Guégan, S., & Arakelian, V. (2007). *Contribution to the mechanical behavior improvement of the robotic navigation device Surgiscope®*. Paper presented at the ASME 2007 International Design Engineering Technical Conferences and Computers and Information in Engineering Conference.
- Butner, S. E., & Ghodoussi, M. (2003). Transforming a surgical robot for human telesurgery. *IEEE Transactions on Robotics and Automation*, 19(5), 818-824.
- Carbone, G., Ottaviano, E., & Ceccarelli, M. (2007). An optimum design procedure for both serial and parallel manipulators. *Proceedings of the Institution of Mechanical Engineers, Part C: Journal of Mechanical Engineering Science*, 221(7), 829-843.
- Cardinale, F., Cossu, M., Castana, L., Casaceli, G., Schiariti, M. P., Miserocchi, A., Arnulfo, G. (2013). Stereoelectroencephalography: surgical methodology, safety, and stereotactic application accuracy in 500 procedures. *Neurosurgery*, 72(3), 353-366.
- Cardinale, F., Miserocchi, A., Moscato, A., Cossu, M., Castana, L., Schiariti, M. P., Citterio, A. (2012). Talairach methodology in the multimodal imaging and robotics era. *Stereotaxy and epilepsy surgery*, 245-272.
- Carfagni, M., Furferi, R., Governi, L., Servi, M., Uccheddu, F., & Volpe, Y. (2017). On the performance of the Intel SR300 depth camera: metrological and critical characterization. *IEEE Sensors Journal*, 17(14), 4508-4519.
- Ceccarelli, M., & Lanni, C. (2004). A multi-objective optimum design of general 3R manipulators for prescribed workspace limits. *Mechanism and Machine Theory*, 39(2), 119-132.
- Chan, J. Y., Leung, I., Navarro - Alarcon, D., Lin, W., Li, P., Lee, D. L., Tong, M. C. (2016). Foot - controlled robotic - enabled endoscope holder for endoscopic sinus surgery: A cadaveric feasibility study. *The Laryngoscope*, 126(3), 566-569.
- Chen, I.-M., & Gao, Y. (2001). *Closed-form inverse kinematics solver for reconfigurable robots*. Paper presented at the Robotics and Automation, 2001. Proceedings 2001 ICRA. IEEE International Conference on.
- Chen, J. C., Rahimian, J., Girvigian, M. R., & Miller, M. J. (2007). Contemporary methods of radiosurgery treatment with the Novalis linear accelerator system.
- Chen, X., Song, Z., & Wang, M. (2014). Automated Global Optimization Surface-Matching Registration Method for Image-to-Patient Spatial Registration in an Image-Guided Neurosurgery System. *Journal of Medical Imaging and Health Informatics*, 4(6), 942-947. doi:10.1166/jmihi.2014.1346
- Cleary, K., Melzer, A., Watson, V., Kronreif, G., & Stoianovici, D. (2006). Interventional robotic systems: Applications and technology state - of - the - art. *Minimally Invasive Therapy & Allied Technologies*, 15(2), 101-113.
- Cleary, K., & Peters, T. M. (2010). Image-guided interventions: technology review and clinical applications. *Annual review of biomedical engineering*, 12, 119-142.

- Comparetti, M. D., De Momi, E., Vaccarella, A., Riechmann, M., & Ferrigno, G. (2011). *Optically tracked multi-robot system for keyhole neurosurgery*. Paper presented at the Robotics and Automation (ICRA), 2011 IEEE International Conference on.
- Comparetti, M. D., Vaccarella, A., De Lorenzo, D., Ferrigno, G., & De Momi, E. (2011). *Multi-robotic approach for keyhole neurosurgery: the ROBOCAST project*. Paper presented at the Joint Workshop on New Technologies for Computer/Robot Assisted Surgery.
- Comparetti, M. D., Vaccarella, A., Dyagilev, I., Shoham, M., Ferrigno, G., & De Momi, E. (2012). Accurate multi-robot targeting for keyhole neurosurgery based on external sensor monitoring. *Proceedings of the Institution of Mechanical Engineers, Part H: Journal of Engineering in Medicine*, 226(5), 347-359.
- Corke, P. (2017). *Robotics, Vision and Control: Fundamental Algorithms In MATLAB® Second, Completely Revised* (Vol. 118): Springer.
- Craig, J. J. (1989). *Introduction to robotics: mechanics and control* (Vol. 74): Addison-Wesley New York,;
- Davies, B., Starkie, S., Harris, S. J., Agterhuis, E., Paul, V., & Auer, L. M. (2000). *Neurobot: a special-purpose robot for neurosurgery*. Paper presented at the Robotics and Automation, 2000. Proceedings. ICRA'00. IEEE International Conference on.
- davis, K. (2019). Dlib C++ library. Retrieved from www.dlib.net
- De Lorenzo, D., De Momi, E., Dyagilev, I., Manganelli, R., Formaglio, A., Prattichizzo, D., . . . Ferrigno, G. (2011). Force feedback in a piezoelectric linear actuator for neurosurgery. *The International Journal of Medical Robotics and Computer Assisted Surgery*, 7(3), 268-275.
- De Momi, E., Caborni, C., Cardinale, F., Casaceli, G., Castana, L., Cossu, M., Tassi, L. (2014). Multi-trajectories automatic planner for StereoElectroEncephaloGraphy (SEEG). *International journal of computer assisted radiology and surgery*, 9(6), 1087-1097.
- De Momi, E., Cerveri, P., & Ferrigno, G. (2009). *ROBOt and sensors integration for computer assisted surgery and therapy (ICT-2007-215190-ROBOCAST)*. Paper presented at the Advanced Robotics, 2009. ICAR 2009. International Conference on.
- De Momi, E., & Ferrigno, G. (2010). Robotic and artificial intelligence for keyhole neurosurgery: the ROBOCAST project, a multi-modal autonomous path planner. *Proceedings of the Institution of Mechanical Engineers, Part H: Journal of Engineering in Medicine*, 224(5), 715-727.
- Deacon, G., Harwood, A., Holdback, J., Maiwand, D., Pearce, M., Reid, I., Taylor, J. (2010). The Pathfinder image-guided surgical robot. *Proceedings of the Institution of Mechanical Engineers, Part H: Journal of Engineering in Medicine*, 224(5), 691-713.

- Devito, D. P., Kaplan, L., Dietl, R., Pfeiffer, M., Horne, D., Silberstein, B., Bruskin, A. (2010). Clinical acceptance and accuracy assessment of spinal implants guided with SpineAssist surgical robot: retrospective study. *Spine*, 35(24), 2109-2115.
- Dlaka, D., Švaco, M., Chudy, D., Jerbić, B., Šekoranja, B., Šuligoj, F., Romić, D. (2018). Brain biopsy performed with the RONNA G3 system: a case study on using a novel robotic navigation device for stereotactic neurosurgery. *The International Journal of Medical Robotics and Computer Assisted Surgery*, 14(1).
- Drake, J. M., Joy, M., Goldenberg, A., & Kreindler, D. (1991). Computer-and robot-assisted resection of thalamic astrocytomas in children. *Neurosurgery*, 29(1), 27-33.
- Eggers, G., Mühling, J., & Marmulla, R. (2006). Image-to-patient registration techniques in head surgery. *International journal of oral and maxillofacial surgery*, 35(12), 1081-1095.
- Eichhorn, K., & Bootz, F. (2011). Clinical requirements and possible applications of robot assisted endoscopy in skull base and sinus surgery *Intraoperative Imaging* (pp. 237-240): Springer.
- Eichhorn, K. W., Westphal, R., Last, C., Rilk, M., Bootz, F., Wahl, F. M., & Jakob, M. (2015). Workspace and pivot point for robot - assisted endoscope guidance in functional endonasal sinus surgery (FESS). *The International Journal of Medical Robotics and Computer Assisted Surgery*, 11(1), 30-37.
- Eichhorn, K. W., Westphal, R., Rilk, M., Last, C., Bootz, F., Wahl, F., Send, T. (2017). Robot-assisted endoscope guidance versus manual endoscope guidance in functional endonasal sinus surgery (FESS). *Acta oto-laryngologica*, 137(10), 1090-1095.
- Eljamel, M. (2007). Validation of the PathFinder™ neurosurgical robot using a phantom. *The International Journal of Medical Robotics and Computer Assisted Surgery*, 3(4), 372-377.
- Eljamel, M. S. (2008). Robotic applications in neurosurgery *Medical Robotics: InTech*.
- Fankhauser, H., Glauser, D., Flury, P., Piguet, Y., Epitoux, M., Favre, J., & Meuli, R. (1994). Robot for CT-guided stereotactic neurosurgery. *Stereotactic and Functional Neurosurgery*, 63(1-4), 93-98.
- Faria, C., Erlhagen, W., Rito, M., De Momi, E., Ferrigno, G., & Bicho, E. (2015). Review of robotic technology for stereotactic neurosurgery. *IEEE reviews in biomedical engineering*, 8, 125-137.
- Fontana, J., Korff, A., Follmann, A., Radermacher, K., & Schmieder, K. (2014). Smart Trepanation System: Preclinical Analysis of Safety, Efficiency, and User Satisfaction. *Journal of Neurological Surgery Part A: Central European Neurosurgery*, 75(05), 398-402.
- Frank, T., Krieger, A., Leonard, S., Patel, N. A., & Tokuda, J. (2017). ROS-IGTL-Bridge: an open network interface for image-guided therapy using the ROS environment.

International journal of computer assisted radiology and surgery, 12(8), 1451-1460.

Glozman, D., Shoham, M., & Fischer, A. (2001). A surface-matching technique for robot-assisted registration. *Computer Aided Surgery*, 6(5), 259-269.

Gonzalez-Martinez, J., Vadera, S., Mullin, J., Enatsu, R., Alexopoulos, A. V., Patwardhan, R., Najm, I. (2014). Robot-assisted stereotactic laser ablation in medically intractable epilepsy: operative technique. *Operative Neurosurgery*, 10(2), 167-173.

Grau, C., Ginhoux, R., Riera, A., Nguyen, T. L., Chauvat, H., Berg, M., Ruffini, G. (2015). Conscious Brain-to-Brain Communication in Humans Using Non-Invasive Technologies. *Brain Stimulation: Basic, Translational, and Clinical Research in Neuromodulation*, 8(2), 323.

Hagn, U., Nickl, M., Jörg, S., Passig, G., Bahls, T., Nothhelfer, A., Konietzschke, R. (2008). The DLR MIRO: a versatile lightweight robot for surgical applications. *Industrial Robot: An International Journal*, 35(4), 324-336.

Hannaford, B., Rosen, J., Friedman, D. W., King, H., Roan, P., Cheng, L., White, L. (2013). Raven-II: an open platform for surgical robotics research. *IEEE Transactions on Biomedical Engineering*, 60(4), 954-959.

Heinig, M., Goveia, M. F., Gasca, F., Dold, C., Hofmann, U. G., Tronnier, V., Schweikard, A. (2011a). *Mars—motor assisted robotic stereotaxy system*. Paper presented at the Neural Engineering (NER), 2011 5th International IEEE/EMBS Conference on.

Heinig, M., Goveia, M. F., Gasca, F., Dold, C., Hofmann, U. G., Tronnier, V., Schweikard, A. (2011b). *MARS - Motor assisted robotic stereotaxy system*. <http://ieeexplore.ieee.org/lpdocs/epic03/wrapper.htm?arnumber=5910555>

Ho, M., Kim, Y., Cheng, S. S., Gullapalli, R., & Desai, J. P. (2015). Design, development, and evaluation of an MRI-guided SMA spring-actuated neurosurgical robot. *The International Journal of Robotics Research*, 34(8), 1147-1163.

Hongo, K., Kobayashi, S., Kakizawa, Y., Koyama, J.-i., Goto, T., Okudera, H., Takakura, K. (2002). NeuRobot: telecontrolled micromanipulator system for minimally invasive microneurosurgery—preliminary results. *Neurosurgery*, 51(4), 985-988.

Hu, X., Ohnmeiss, D. D., & Lieberman, I. H. (2013). Robotic-assisted pedicle screw placement: lessons learned from the first 102 patients. *European Spine Journal*, 22(3), 661-666.

Inc, M. (2013). *Optimization Toolbox User's guide*

industrial, R. Extrinsic calibration of the David SLS-2 mounted on a robot. Retrieved from http://wiki.ros.org/industrial_extrinsic_cal/Tutorials

Intel. (2019). Intel Realsense Library. Retrieved from <https://github.com/IntelRealSense/librealsense>

- Iwata, H., Sato, K., Tatewaki, K., Yokota, N., Inoue, M., Baba, Y., & Shibamoto, Y. (2011). Hypofractionated stereotactic radiotherapy with CyberKnife for nonfunctioning pituitary adenoma: high local control with low toxicity. *Neuro-oncology*, *13*(8), 916-922.
- Jain, A. (2010). *Robot and multibody dynamics: analysis and algorithms*: Springer Science & Business Media.
- Jerbic, B., Nikolic, G., Chudy, D., Svaco, M., & Sekoranja, B. (2015). Robotic application in neurosurgery using intelligent visual and haptic interaction. *International journal of simulation modelling*, *14*(1), 71-84.
- Joskowicz, L., Shamir, R., Freiman, M., Shoham, M., Zehavi, E., Umansky, F., & Shoshan, Y. (2006). Image-guided system with miniature robot for precise positioning and targeting in keyhole neurosurgery. *Computer Aided Surgery*, *11*(4), 181-193.
- Joskowicz, L., Shamir, R., Israel, Z., Shoshan, Y., & Shoham, M. (2011). *Renaissance robotic system for keyhole cranial neurosurgery: in-vitro accuracy study*. Paper presented at the Proceedings of the Simposio Mexicano en Cirugia Asistida por Computadora y Procesamiento de Imgenes Mdicas (MexCAS'11).
- Joskowicz, L., Shoham, M., Shamir, R., Freiman, M., Zehavi, E., & Shoshan, Y. (2005). *Miniature robot-based precise targeting system for keyhole neurosurgery: concept and preliminary results*. Paper presented at the International Congress Series.
- Kazemi, V., & Sullivan, J. (2014). *One millisecond face alignment with an ensemble of regression trees*. Paper presented at the Proceedings of the IEEE conference on computer vision and pattern recognition.
- Keereweer, S., Kerrebijn, J. D., Van Driel, P. B., Xie, B., Kaijzel, E. L., Snoeks, T. J., Mieog, J. S. D. (2011). Optical image-guided surgery—where do we stand? *Molecular Imaging and Biology*, *13*(2), 199-207.
- Koenig, N., & Hsu, J. (2013). *The many faces of simulation: Use cases for a general purpose simulator*. Paper presented at the Proc. of the ICRA.
- Kwoh, Y. S., Hou, J., Jonckheere, E. A., & Hayati, S. (1988). A robot with improved absolute positioning accuracy for CT guided stereotactic brain surgery. *IEEE Transactions on Biomedical Engineering*, *35*(2), 153-160.
- Labadie, R. F., Davis, B. M., & Fitzpatrick, J. M. (2005). Image-guided surgery: what is the accuracy? *Current opinion in otolaryngology & head and neck surgery*, *13*(1), 27-31.
- Lasso, A., Heffter, T., Rankin, A., Pinter, C., Ungi, T., & Fichtinger, G. (2014). PLUS: open-source toolkit for ultrasound-guided intervention systems. *IEEE Transactions on Biomedical Engineering*, *61*(10), 2527-2537.
- Le Roux, P. D., Das, H., Esquenazi, S., & J. Kelly, P. (2001). Robot-assisted microsurgery: a feasibility study in the rat. *Neurosurgery*, *48*(3), 584-589.

- Lefranc, M., Capel, C., Pruvot-Ocean, A.-S., Fichten, A., Desenclos, C., Toussaint, P., Peltier, J. (2015). Frameless robotic stereotactic biopsies: a consecutive series of 100 cases. *Journal of neurosurgery*, 122(2), 342-352.
- Lefranc, M., Capel, C., Pruvot, A. S., Fichten, A., Desenclos, C., Toussaint, P., Peltier, J. (2014). The impact of the reference imaging modality, registration method and intraoperative flat-panel computed tomography on the accuracy of the ROSA® stereotactic robot. *Stereotactic and Functional Neurosurgery*, 92(4), 242-250.
- Lefranc, M., & Le Gars, D. (2012). Robotic implantation of deep brain stimulation leads, assisted by intra-operative, flat-panel CT. *Acta neurochirurgica*, 154(11), 2069-2074.
- Lemaignan, S., Garcia, F., Jacq, A., & Dillenbourg, P. (2016). *From real-time attention assessment to with-me-ness in human-robot interaction*. Paper presented at the The Eleventh ACM/IEEE International Conference on Human Robot Interaction.
- Li, Q. H., Zamorano, L., Pandya, A., & Gong, J. (2012). *The application accuracy of the NeuroMate robot—a quantitative comparison with frameless and frame-based surgical localization systems*. Paper presented at the CARS 2002 Computer Assisted Radiology and Surgery: Proceedings of the 16th International Congress and Exhibition Paris, June 26–29, 2002.
- Li, Q. H., Zamorano, L., Pandya, A., Perez, R., Gong, J., & Diaz, F. (2002). The application accuracy of the NeuroMate robot—A quantitative comparison with frameless and frame - based surgical localization systems. *Computer Aided Surgery*, 7(2), 90-98.
- Lieberman, I. H., Togawa, D., Kayanja, M. M., Reinhardt, M. K., Friedlander, A., Knoller, N., & Benzel, E. C. (2006). Bone-mounted miniature robotic guidance for pedicle screw and translaminar facet screw placement: Part I—Technical development and a test case result. *Neurosurgery*, 59(3), 641-650.
- Louw, D. F., Fielding, T., McBeth, P. B., Gregoris, D., Newhook, P., & Sutherland, G. R. (2004). Surgical robotics: a review and neurosurgical prototype development. *Neurosurgery*, 54(3), 525-537.
- Mani, V. R. S., & rivazhagan, D. S. (2013). Survey of Medical Image Registration. *Journal of Biomedical Engineering and Technology*, 1(2), 8-25.
- Martínez Verdú, J., María Sabater Navarro, J., José González Penella, V., Manuel García Aracil, N., & Miguel López Buendía, Á. (2013). Rapid design and synthesis of robots using standard computer tools. *Industrial Robot: An International Journal*, 40(4), 363-381.
- Matias, C. M., Frizon, L. A., Nagel, S. J., Lobel, D. A., & Machado, A. G. (2018). Deep brain stimulation outcomes in patients implanted under general anesthesia with frame-based stereotaxy and intraoperative MRI. *Journal of neurosurgery*, 1-7.
- Mazor Robotics Ltd. Renaissance. (2018). Retrieved from <https://mazorrobotics.com/index.php/mazor-product-portfolio/renaissance-guidance-system>

- Medtech, S. (2010). Premarket notification 510 (K) submission rosa surgical device. *Montpellier, France*, 6-10.
- Meli, L., Pacchierotti, C., & Prattichizzo, D. (2014). Sensory subtraction in robot-assisted surgery: fingertip skin deformation feedback to ensure safety and improve transparency in bimanual haptic interaction. *IEEE Transactions on Biomedical Engineering*, 61(4), 1318-1327.
- Mitsuishi, M., Morita, A., Sugita, N., Sora, S., Mochizuki, R., Tanimoto, K., Harada, K. (2013). Master-slave robotic platform and its feasibility study for micro - neurosurgery. *The International Journal of Medical Robotics and Computer Assisted Surgery*, 9(2), 180-189.
- MODUS V, Fully-automated, robotic digital microscope. Retrieved from <https://www.synaptivemedical.com/products/modus-v/>
- Mohammadi, A. M., & Schroeder, J. L. (2014). Laser interstitial thermal therapy in treatment of brain tumors—the NeuroBlate System. *Expert review of medical devices*, 11(2), 109-119.
- Morelli, L., Guadagni, S., Di Franco, G., Palmeri, M., Di Candio, G., & Mosca, F. (2016). Da Vinci single site© surgical platform in clinical practice: a systematic review. *The International Journal of Medical Robotics and Computer Assisted Surgery*, 12(4), 724-734.
- Morgan, P. S., Carter, T., Davis, S., Sepehri, A., Punt, J., Byrne, P., Finlay, P. (2003). *The application accuracy of the Pathfinder neurosurgical robot*. Paper presented at the International congress series.
- Morita, A., Sora, S., Mitsuishi, M., Warisawa, S., Suruman, K., Asai, D., Mochizuki, R. (2005). Microsurgical robotic system for the deep surgical field: development of a prototype and feasibility studies in animal and cadaveric models. *Journal of neurosurgery*, 103(2), 320-327.
- Motkoski, J. W., & Sutherland, G. R. (2016). Why Robots Entered Neurosurgery. *Experimental Neurosurgery in Animal Models*, 85-105.
- Moveit. (2018). List of Robot compatible with Moveit framework Retrieved from <https://moveit.ros.org/robots/>
- . New surgical robots are about to enter the operating theatre. (Nov 16th 2017). *The Economist*.
- Nicolai, P., Raczowsky, J., & Wörn, H. (2015). A Novel 3D Camera Based Supervision System for Safe Human-Robot Interaction in the Operating Room. *Journal of Automation and Control Engineering Vol*, 3(5).
- Nimsky, C., Rachinger, J., Iro, H., & Fahlbusch, R. (2004). Adaptation of a hexapod-based robotic system for extended endoscope-assisted transsphenoidal skull base surgery. *min-Minimally Invasive Neurosurgery*, 47(01), 41-46.

- Nishiyama, K. (2017). From Exoscope into the Next Generation. *Journal of Korean Neurosurgical Society*, 60(3), 289.
- OpenCV, t. (2019). face recognition with open cv. https://docs.opencv.org/2.4.13.7/modules/contrib/doc/facerec/facerec_tutorial.html
- Pandya, S., Motkoski, J. W., Serrano-Almeida, C., Greer, A. D., Latour, I., & Sutherland, G. R. (2009). Advancing neurosurgery with image-guided robotics. *Journal of neurosurgery*, 111(6), 1141-1149.
- Paredis, C. J., Au, W., & Khosla, P. K. (1994). Kinematic design of fault tolerant manipulators. *Computers & electrical engineering*, 20(3), 211-220.
- Patel, S., & Sobh, T. (2015). Manipulator performance measures-a comprehensive literature survey. *Journal of Intelligent & Robotic Systems*, 77(3-4), 547-570.
- Patel, S. H., & Sobh, T. M. (2015). *Using task descriptions for designing optimal task specific manipulators*. Paper presented at the 2015 IEEE/RSJ International Conference on Intelligent Robots and Systems (IROS).
- Project, O. (2018). Orocos Kinematics and Dynamics. Retrieved from <http://www.orocos.org/kdl>
- Raabe, A., Krishnan, R., Wolff, R., Hermann, E., Zimmermann, M., & Seifert, V. (2002). Laser surface scanning for patient registration in intracranial image-guided surgery. *Neurosurgery*, 50(4), 797-803.
- Ringel, F., Stüer, C., Reinke, A., Preuss, A., Behr, M., Auer, F., Meyer, B. (2012). Accuracy of robot-assisted placement of lumbar and sacral pedicle screws: a prospective randomized comparison to conventional freehand screw implantation. *Spine*, 37(8), E496-E501.
- Robotic Assistant for Transcranial Magnetic Stimulation (TMS). Retrieved from <http://www.axilumrobotics.com/en/tms-robot/>
- Robotis. (2017). Robotis Manipulator H manual. Retrieved from http://support.robotis.com/en/techsupport_eng.htm#product/manipulator.htm
- Robotis. (2018). Dynamixel servo motors manual Retrieved from http://support.robotis.com/en/product/actuator/dynamixel_pro.htm
- ROSA., M. Retrieved from <http://www.medtech.fr>
- Rosen, J., Brown, J. D., Barreca, M., Chang, L., Hannaford, B., & Sinanan, M. (2002). The blue dragon-a system for monitoring the kinematics and the dynamics of endoscopic tools in minimally invasive surgery for objective laparoscopic skill assessment. *Studies in health technology and informatics*, 412-418.
- Rosen, J., & Hannaford, B. (2006). Doc at a distance. *IEEE spectrum*, 43(10), 34-39.

- Rybicki, F. J., & Grant, G. T. (2017). *3d Printing in Medicine: A Practical Guide for Medical Professionals*: Springer.
- Sagonas, C., Antonakos, E., Tzimiropoulos, G., Zafeiriou, S., & Pantic, M. (2016). 300 faces in-the-wild challenge: Database and results. *Image and vision computing*, 47, 3-18.
- Salma, A., Makiese, O., Sammet, S., & Ammirati, M. (2012). Effect of registration mode on neuronavigation precision: an exploration of the role of random error. *Computer Aided Surgery*, 17(4), 172-178. doi:10.3109/10929088.2012.691992
- Sameer, A., Keir, M., & Others. Ceres Solver. Retrieved from <http://ceres-solver.org>
- Serletis, D., Bulacio, J., Bingaman, W., Najm, I., & González-Martínez, J. (2014). The stereotactic approach for mapping epileptic networks: a prospective study of 200 patients. *Journal of neurosurgery*, 121(5), 1239-1246.
- Shamir, R., Freiman, M., Joskowicz, L., Shoham, M., Zehavi, E., & Shoshan, Y. (2005). *Robot-assisted image-guided targeting for minimally invasive neurosurgery: planning, registration, and in-vitro experiment*. Paper presented at the International Conference on Medical Image Computing and Computer-Assisted Intervention.
- Shamir, R., Freiman, M., Joskowicz, L., Shoham, M., Zehavi, E., & Shoshan, Y. (2006). *Robot-assisted image-guided targeting for minimally invasive neurosurgery: intraoperative robot positioning and targeting experiment*. Paper presented at the MICCAI 2006 Workshop Proceedings.
- Shen, J. (2014). Tools for NIFTI and ANALYZE image. Retrieved from <http://www.mathworks.com/matlabcentral/fileexchange/8797-tools-for-nifti-and-analyze-image>
- Shiakolas, P., Koladiya, D., & Kebrle, J. (2002). Optimum robot design based on task specifications using evolutionary techniques and kinematic, dynamic, and structural constraints. *Inverse Problems in Engineering*, 10(4), 359-375.
- Sipos, E. P., & Heisey, J. (2015). Intraoperative CT Scanner Combined With Image-Guided Neurosurgery. *Journal of Radiology Nursing*, 34(2), 73-79. doi:<http://dx.doi.org/10.1016/j.jradnu.2014.11.009>
- Sivakumar, G., Smith, S., Morgan, P., & Byrne, P. (2003). The bionic surgeon: Initial experience with the pathfinder robot: Nottingham.
- Sloan, A. E., Ahluwalia, M. S., Valerio-Pascua, J., Manjila, S., Torchia, M. G., Jones, S. E., . . . Clampitt, M. (2013). Results of the NeuroBlate System first-in-humans Phase I clinical trial for recurrent glioblastoma: clinical article. *Journal of neurosurgery*, 118(6), 1202-1219.
- Smith, J. A., Jivraj, J., Wong, R., & Yang, V. (2016). 30 Years of neurosurgical robots: Review and trends for manipulators and associated navigational systems. *Annals of biomedical engineering*, 44(4), 836-846.

- Steady-Hand Eye Robot. Retrieved from <https://ciis.lcsr.jhu.edu/dokuwiki/doku.php?id=research.eyerobots>
- Stelter, K., Ledderose, G., Hempel, J. M., Morhard, D. F., Flatz, W., Krause, E., & Mueller, J. (2012). Image guided navigation by intraoperative CT scan for cochlear implantation. *Computer Aided Surgery*, 17(3), 153-160.
- Sung, K.-S., Song, Y.-J., & Kim, K.-U. (2016). Novalis Stereotactic Radiosurgery for Spinal Dural Arteriovenous Fistula. *Journal of Korean Neurosurgical Society*, 59(4), 420.
- Sutherland, G. R., Latour, I., & Greer, A. D. (2008). Integrating an image-guided robot with intraoperative MRI. *IEEE engineering in medicine and biology magazine*, 27(3), 59-65.
- Sutherland, G. R., Latour, I., Greer, A. D., Fielding, T., Feil, G., & Newhook, P. (2008). An image-guided magnetic resonance-compatible surgical robot. *Neurosurgery*, 62(2), 286-293.
- Sutherland, G. R., Wolfsberger, S., Lama, S., & Zarei-nia, K. (2013). The evolution of neuroArm. *Neurosurgery*, 72(suppl_1), A27-A32.
- systems, I. (2019). iSYS1. Retrieved from <https://www.interventional-systems.com/global/technology/isys-1/>
- Takasuna, H., Goto, T., Kakizawa, Y., Miyahara, T., Koyama, J., Tanaka, Y., Hongo, K. (2012). Use of a micromanipulator system (NeuroBot) in endoscopic neurosurgery. *Journal of clinical neuroscience*, 19(11), 1553-1557.
- Taylor, R., Jensen, P., Whitcomb, L., Barnes, A., Kumar, R., Stoianovici, D., Kavoussi, L. (1999). A steady-hand robotic system for microsurgical augmentation. *The International Journal of Robotics Research*, 18(12), 1201-1210.
- Teh, B. S., Paulino, A. C., Lu, H. H., Chiu, J. K., Richardson, S., Chiang, S., Bloch, C. (2007). Versatility of the Novalis system to deliver image-guided stereotactic body radiation therapy (SBRT) for various anatomical sites. *Technology in cancer research & treatment*, 6(4), 347-354.
- The DG Information Society & Media, s. E. C. S. a. R. L. Active Constraints Technologies for Ill-defined or Volatile Environments. Retrieved from <http://www.active-fp7.eu/index.html>
- Tian, Z., Lu, W., Wang, T., Ma, B., Zhao, Q., & Zhang, G. (2008). Application of a robotic telemanipulation system in stereotactic surgery. *Stereotactic and Functional Neurosurgery*, 86(1), 54-61.
- Tokuda, J., Fischer, G. S., Papademetris, X., Yaniv, Z., Ibanez, L., Cheng, P., Golby, A. J. (2009). OpenIGTLink: an open network protocol for image - guided therapy environment. *The International Journal of Medical Robotics and Computer Assisted Surgery*, 5(4), 423-434.

- Trévilhot, V., Sobral, R., Dombre, E., Poignet, P., Herman, B., & Crampette, L. (2013). Innovative endoscopic sino-nasal and anterior skull base robotics. *International journal of computer assisted radiology and surgery*, 8(6), 977-987.
- Uhl, E., Zausinger, S., Morhard, D., Heigl, T., Scheder, B., Rachinger, W., Tonn, J.-C. (2009). Intraoperative computed tomography with integrated navigation system in a multidisciplinary operating suite. *Operative Neurosurgery*, 64(suppl_5), ons231-ons239.
- Ungi, T., Lasso, A., & Fichtinger, G. (2016). Open-source platforms for navigated image-guided interventions. *Medical Image Analysis*, 33, 181-186. doi:10.1016/j.media.2016.06.011
- University, D. o. C. S. R. (2018). The Open Motion Planning Library. Retrieved from <http://ompl.kavrakilab.org/>
- Van Henten, E., Van't Slot, D., Hol, C., & Van Willigenburg, L. (2009). Optimal manipulator design for a cucumber harvesting robot. *computers and electronics in agriculture*, 65(2), 247-257.
- Varma, T., & Eldridge, P. (2006). Use of the NeuroMate stereotactic robot in a frameless mode for functional neurosurgery. *The International Journal of Medical Robotics and Computer Assisted Surgery*, 2(2), 107-113.
- ve Pozisyonlandırıcı, H. K. E. T., & Sistem, R. (2015). A haptic guided robotic system for endoscope positioning and holding. *Turk Neurosurg*, 25(4), 601-607.
- Vercruyssen, M., Hultin, M., Van Assche, N., Svensson, K., Naert, I., & Quirynen, M. (2014). Guided surgery: accuracy and efficacy. *Periodontology 2000*, 66(1), 228-246.
- Villaret, A. B., Doglietto, F., Carobbio, A., Schreiber, A., Panni, C., Piantoni, E., Cassinis, R. (2017). Robotic transnasal endoscopic skull base surgery: systematic review of the literature and report of a novel prototype for a hybrid system (Brescia Endoscope Assistant Robotic Holder). *World neurosurgery*, 105, 875-883.
- Voigt, J. D., & Torchia, M. (2014). Laser interstitial thermal therapy with and without MRI guidance for treatment of brain neoplasms—A systematic review of the literature. *Photonics & Lasers in Medicine*, 3(2), 77-93.
- von Langsdorff, D., Paquis, P., & Fontaine, D. (2015). In vivo measurement of the frame-based application accuracy of the Neuromate neurosurgical robot. *Journal of neurosurgery*, 122(1), 191-194.
- Waqas, M., Enam, S. A., Hashmi, F. A., Mubarak, F., & Arain, F. (2017). Video Microscope Robotic Arm-Assisted, Neuronavigation-guided Glioma Resection and Regional Sampling. *Cureus*, 9(10).
- Waran, V., Devaraj, P., Chandran, T. H., Muthusamy, K., Rathinam, A. K., Balakrishnan, Y. K., . . . Rahman, Z. (2012). Three-dimensional anatomical accuracy of cranial models created by rapid prototyping techniques validated using a neuronavigation station. *Journal of Clinical Neuroscience*, 19(4), 574-577.

- Waran, V., Narayanan, V., Karuppiah, R., Owen, S. L., & Aziz, T. (2014). Utility of multimaterial 3D printers in creating models with pathological entities to enhance the training experience of neurosurgeons: Technical note. *Journal of neurosurgery*, *120*(2), 489-492.
- Waran, V., Narayanan, V., Karuppiah, R., Pancharatnam, D., Chandran, H., Raman, R., Aziz, T. Z. (2014). Injecting realism in surgical training—initial simulation experience with custom 3D models. *Journal of surgical education*, *71*(2), 193-197.
- Widmann, G., Stoffner, R., Schullian, P., Widmann, R., Keiler, M., Zangerl, A., Bale, R. J. (2010). Comparison of the accuracy of invasive and noninvasive registration methods for image-guided oral implant surgery. *International Journal of Oral & Maxillofacial Implants*, *25*(3).
- Wilson, P. I., & Fernandez, J. (2006). Facial feature detection using Haar classifiers. *J. Comput. Sci. Coll.*, *21*(4), 127-133.
- Woerdeman, P. A., Willems, P. W., Noordmans, H. J., Tulleken, C. A., & van der Sprenkel, J. W. B. (2007). Application accuracy in frameless image-guided neurosurgery: a comparison study of three patient-to-image registration methods. *Journal of neurosurgery*, *106*(6), 1012-1016.
- Wu, Z., Zhao, Q., Tian, Z., Zhang, J., Xiao, X., Lin, H., Wang, F. (2014). Efficacy and safety of a new robot-assisted stereotactic system for radiofrequency thermocoagulation in patients with temporal lobe epilepsy. *Experimental and therapeutic medicine*, *7*(6), 1728-1732.
- Xia, T., Baird, C., Jallo, G., Hayes, K., Nakajima, N., Hata, N., & Kazanzides, P. (2008). An integrated system for planning, navigation and robotic assistance for skull base surgery. *The International Journal of Medical Robotics and Computer Assisted Surgery*, *4*(4), 321-330.
- Zhou, C., Anschuetz, L., Weder, S., Xie, L., Caversaccio, M., Weber, S., & Williamson, T. (2016). Surface matching for high-accuracy registration of the lateral skull base. *International journal of computer assisted radiology and surgery*, *11*(11), 2097-2103. doi:10.1007/s11548-016-1394-3
- Zhu, Q., Yeh, M.-C., Cheng, K.-T., & Avidan, S. (2006). *Fast human detection using a cascade of histograms of oriented gradients*. Paper presented at the Computer Vision and Pattern Recognition, 2006 IEEE Computer Society Conference on.
- Zimmermann, M., Krishnan, R., Raabe, A., & Seifert, V. (2004). Robot-assisted navigated endoscopic ventriculostomy: implementation of a new technology and first clinical results. *Acta neurochirurgica*, *146*(7), 697-704.

LIST OF PUBLICATIONS AND PAPERS PRESENTED

Published:

Mehbodniya, A. H., Moghavvemi, M., Narayanan, V., & Waran, V. (2019). Frequency and Causes of Line of Sight Issues During Neurosurgical Procedures Using Optical Image-Guided Systems. *World neurosurgery*, 122, e449-e454.

Mehbodniya, A., Moghavvemi, M., Narayanan, V., Muthusamy, K. A., Hamdi, M., & Waran, V. (2020). Identifying the sources of error when using 3-dimensional printed head models with surgical navigation. *World neurosurgery*, 134, e379-e386.

Under review:

Amirhossein Mehbodniya, Mahmoud Moghavvemi, Thangaraj Munusamy & vicknes waran (2019). Towards developing an open source robotic platform for general neurosurgical tasks. *International Journal of Computer Assisted Radiology and Surgery*.

Conferences:

Ganapathy, V., Sudhakara, P., Huesin, A., & Moghavvemi, M. (2018, January). A New Surgical Robotic System Model for Neuroendoscopic Surgery. In *International Conference on Communications and Cyber Physical Engineering 2018* (pp. 615-628). Springer, Singapore.

Mehbodniya, A. H., Moghavvemi, M., Almurib, H. A. F., & Waran, V. (2016, November). Using actual surgical navigation data to design or study the workspace of neurosurgical manipulators. In *2016 IEEE Industrial Electronics and Applications Conference (IEACon)* (pp. 287-290). IEEE.